Modification chimique de la cellulose nanofibrillée par les alcoxysilanes : application à l'élaboration de composites et mousses

Zheng Zhang

N° d'ordre : 4888

THESE

présentée à

L'UNIVERSITÉ BORDEAUX 1

ÉCOLE DOCTORALE DES SCIENCES CHIMIQUES

par

ZHENG ZHANG

POUR OBTENIR LE GRADE DE

DOCTEUR

SPÉCIALITÉ: POLYMÈRES

CHEMICAL FUNCTIONALIZATION OF NANOFIBRILLATED CELLULOSE BY ALKOXYSILANES: APPLICATION TO THE ELABORATION OF COMPOSITES AND FOAMS

Soutenue le 12 Novembre 2013

Après avis de :

MM.	**N. Belgacem**, *Professeur, INP-Pagora, Grenoble*	**Rapporteur**
	P. Navard, *Directeur de recherche, CEMEF, Nice*	**Rapporteur**

Devant la commission d'examen formée de:

MM.	**B. De Jéso**, *Professeur, Université Bordeaux, Bordeaux*	**Président**
	N. Belgacem, *Professeur, INP-Pagora, Grenoble*	**Rapporteur**
	P. Navard, *Directeur de recherche, CEMEF, Nice*	**Rapporteur**
	T. Zimmermann, *Dr., EMPA, Dübendorf*	**Examinateur**
	P. Tingaut, *Dr., EMPA, Dübendorf*	**Examinateur**
	G. Sèbe, *Maître de Conférences, Université Bordeaux, Bordeaux*	**Examinateur**

- 2013 -

Acknowledgements

I wish to express my most sincere gratitude to my supervisors, Dr. Gilles Sèbe of University Bordeaux and Dr. Philippe Tingaut of EMPA. Dr Gilles Sèbe gave me the most valuable advice, to guide me on the right way. Despite the distance between Bordeaux and Zurich, the communication with Dr. Sèbe and his feedbacks were always very fast, which I really appreciated. Dr. Philippe Tingaut has spent countless time and work in this project, and I deeply thank him for the discussions, helps, suggestions and feedbacks at any time. He was not only a great supervisor, but also a good colleague during my entire PhD study.

I would also like to express my special gratitude to our head of the lab, Dr. Tanja Zimmermann, who has greatly supported me, helped me during some difficult periods and shared her experience with me, as an experienced scientist, as well as a friend.

This work would not be possible without helps from many people and my few words of gratefulness could not be compared with the help and support these people gave me. I would like to thank my great and supportive colleagues, Margrit Conradin, Esther Strub, Dr. Houssine Sehaqui, Paola Orsolini, Franziska Grüneberger, Uxua Pérez de Larraya, Dr. Sebastien Josset, Anja Huch, Robert Widmann, Robert Jockwer and my students Julia Weiss, Vincent and Christoph. Many other people of the institute have also contributed very important parts to this book: Beatrice Fischer, Dr. Daniel Rentsch, Marcel Rees and Dr. James Eilertsen.

In the end, I wish to avail myself of this opportunity, to express a sense of appreciation and love to my mother and my deceased father for their unconditional love and support. Last but not least, my beloved husband deserves my most heartily thanks for his support, encouragement and understanding.

Ce travail de thèse s'inscrit dans le cadre d'un projet financé par la Commission pour la Technologie et l'Innovation (CTI) Suisse (projet « SICEPO », contrat CTI N° 9725.1) visant à développer une méthode de silylation de la Cellulose Nanofibrillée (CNF) en milieu aqueux afin d'améliorer ses propriétés intrinsèques et étendre son champs d'applications. Ce projet a été réalisé au Swiss Federal Laboratories for Materials Science and Technology (EMPA, Dübendorf, Suisse) en collaboration avec le Laboratoire de Chimie des Polymères Organiques (LCPO, Université de Bordeaux, France) et deux partenaires industriels : Falcone Chemical Specialities Ltd. (Siebnen, Suisse) et Jelu-Werk Josef Ehrler GmbH & Co. KG (Rosenberg, Allemagne).

Au cours de ce travail, la cellulose nanofibrillée (CNF) a été isolée à partir de fibres de paille d'avoine puis modifiée chimiquement par des alcoxysilanes en milieu aqueux. La CNF silylée a ensuite été utilisée pour élaborer de nouveaux matériaux composites et mousses bio-sourcés.

Après une introduction générale situant le contexte de cette thèse, une première partie bibliographique (Chapitre I) présente la composition chimique des plantes, les différentes méthodes de synthèse des nanocelluloses, et décrit les propriétés principales de la CNF (Figure 1) ainsi que ses applications dans le domaine des composites, aérogels et mousses. La CNF présentant certains inconvénients liés à sa structure chimique (en particulier son caractère hydrophile), un état de l'art des différentes approches de fonctionnalisation chimique permettant de limiter ses inconvénients est présenté. Au regard de cette étude bibliographique, il apparaît que la majorité des méthodes de modification chimique envisagées jusqu'à présent nécessitent des conditions anhydres et l'utilisation de solvants organiques. Il existe cependant une méthode à base d'alcoxysilanes, permettant de fonctionnaliser les substrats hydroxylés en milieu aqueux et dans des conditions douces. Cette méthode de silylation ayant été très peu appliquée à la CNF, il nous est apparu nécessaire de poursuivre et amplifier les recherches dans ce domaine, afin de mieux caractériser le matériau silylé et de bien maîtriser le procédé.

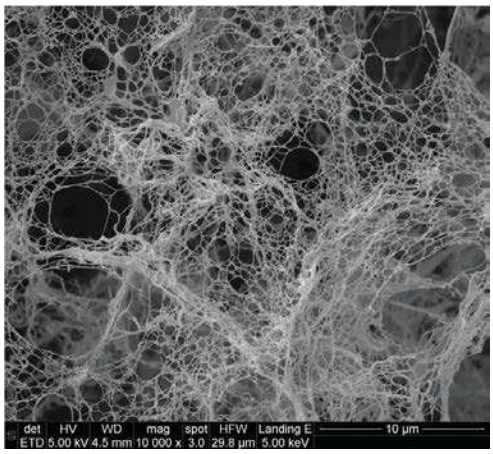

Figure 1 Photomicrographie de NFC isolée à partir de paille d'avoine, utilisée lors de ce travail de thèse.

Le chapitre II est consacré à la fonctionnalisation de la CNF par le méthyltriméthoxysilane (MTMS) – choisi comme alcoxysilane modèle – ainsi qu'à la caractérisation du matériau silylé. Plusieurs paramètres réactionnels (pH, temps de réaction, concentration initiale en MTMS) ont été étudiés et optimisés, à partir de deux protocoles expérimentaux distincts, nommés *Protocole 1* et *Protocole 2*. Les modifications ont été caractérisées à l'échelle moléculaire par différentes techniques physico-chimiques, en utilisant notamment la spectroscopie infra-rouge à transformée de Fourier (IRTF) et la Résonnance Magnétique Nucléaire en phase solide (RMN CP-MAS du ^{13}C et du ^{29}Si). Afin d'étudier de façon systématique l'impact des paramètres réactionnels sur la silylation de la CNF, une méthode rapide et efficace pour suivre l'évolution du taux de silane dans le matériau a d'abord été développée. A partir d'un nombre limité d'échantillons, une droite de calibration permettant de déterminer le pourcentage de silicum à l'intérieur des échantillons, directement à partir des spectre IRTF, a ainsi été élaborée.

Les résultats présentés dans ce chapitre ont montré qu'il était possible de silyler la CNF avec le MTMS en milieu aqueux. Les deux protocoles envisagés ont conduit à des matériaux très différents, tout en préservant la structure cristalline originale de la CNF. Le *Protocole 1* à conduit à un matériau constitué de particules de polysiloxane dispersées dans le réseau de CNF (Figure 2a), alors qu'avec le *Protocole 2* des nanofibrilles recouvertes d'une couche de polysiloxane ont été obtenues (Figure 2b). La taille des particules et l'épaisseur des couches de polysiloxanes ont pu être contrôlées en ajustant la concentration initiale en MTMS. Les tests de lessivages ont montré que seul le *Protocole 2* permettait une fixation durable du polysiloxane à la surface de la CNF. Des différences ont également été notées en termes de mouillabilité et de stabilité thermique. La CNF silylée issue du *Protocole 1* s'est avérée hydrophile,

alors que le *Protocole 2* a conduit à un matériau très hydrophobe. Une augmentation significative de la stabilité thermique a également été notée dans ce dernier cas.

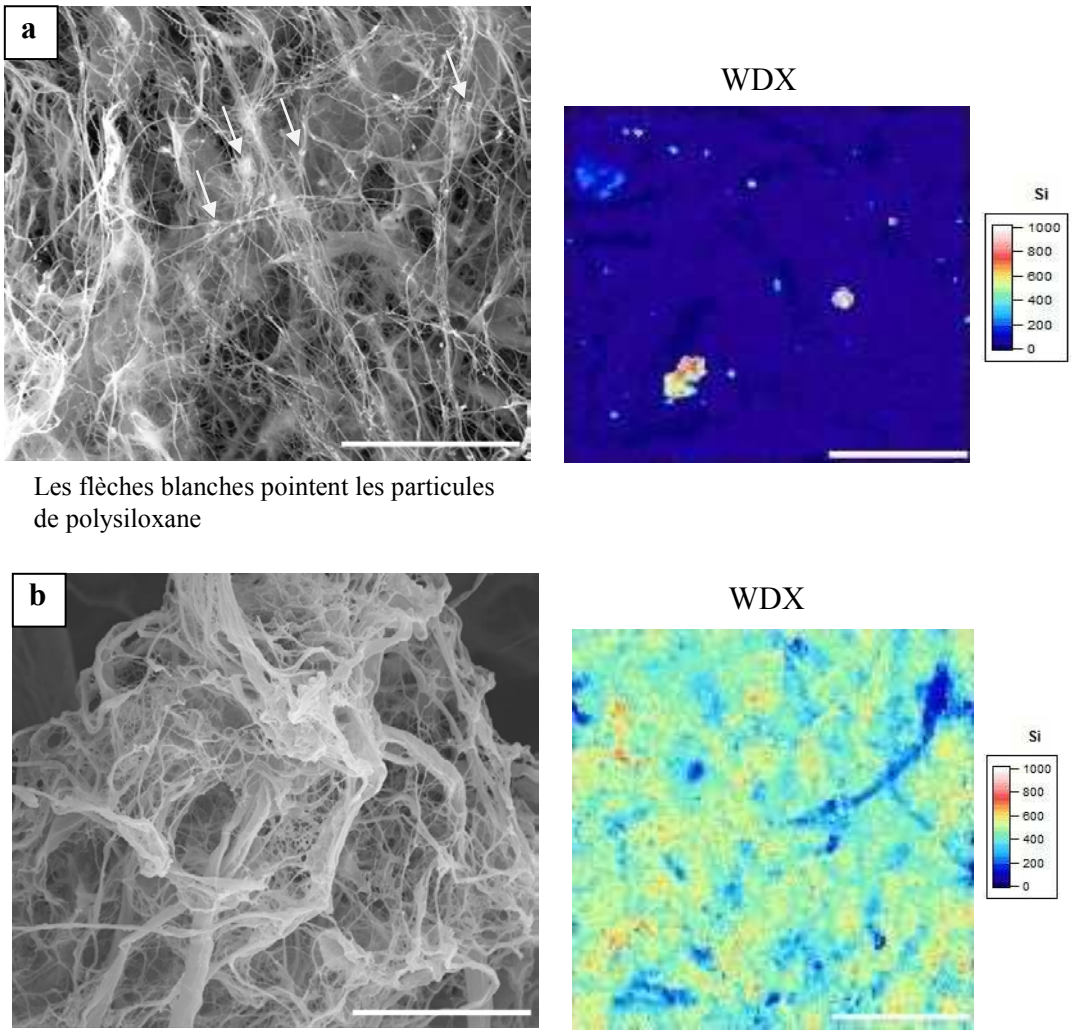

Figure 2 Photomicrographies de CNF traitée avec le MTMS selon le *Protocole 1* (a) ou le *Protocole 2* (b) (barre d'échelle : 10 µm). La distribution du silicium obtenue par analyse dispersive en longueur d'onde (WDX) est également reportée (barre d'échelle : 100 µm).

Dans le chapitre III, l'impact de la silylation sur les propriétés de composites à matrice acide poly(lactique) (PLA) ou polydiméthylsiloxane (PDMS) chargée en CNF a été évalué. Les propriétés mécaniques, la stabilité thermique et l'hygroscopicité des composites ont particulièrement été étudiées. Des résultats différents ont été obtenus en fonction de la matrice polymère utilisée.

Pour les composites à matrice PDMS chargés avec 1% de CNF, une augmentation du module de cisaillement (G'), du module d'Young (E) et de la résistance en traction ont été obtenues après silylation à partir du *Protocole 2* dans certaines conditions. Par contre, une diminution

de la déformation à la rupture a systématiquement été mesurée et le matériau s'est avéré plus hygroscopique que le PDMS seul (mais la prise en eau reste faible).
Pour les composites à matrice PLA chargés avec 10% de CNF, aucune amélioration notable des propriétés mécaniques a été notée après silylation, voire une détérioration. Une augmentation de l'hygroscopicité a été mesurée en présence de CNF (mais la silylation tend à réduire la prise en eau).
Une augmentation de la stabilité thermique des composites (PDMS et PLA) a été mise en évidence en présence de CNF silylée, mais aucune tendance n'a pu être établie ou corrélée avec le taux de silylation ou le type de protocole utilisé.

Dans le chapitre IV, la CNF silylée à partir du *Protocole 2* a été utilisée pour produire de nouveaux matériaux moussés hydrophobes et oléophiles. Des mousses ultra-légères (≤ 17.3 Kg/m^3), poreuses (≥ 99%) et possédant une faible surface spécifique (≤ 20 m^2/g) ont été synthétisées. L'analyse microscopique a montré que la structure interne des matériaux étant majoritairement composée d'un réseau 3D de feuillets et nanofilaments interconnectés.
Les propriétés mécaniques des mousses ont été évaluées sous compression. Une augmentation du module d'élasticité et de la résistance à 50% de déformation ont été notées avec l'augmentation du niveau de silylation. De façon remarquable, les mousses silylées ont présenté une très grande élasticité par rapport au matériau de référence non modifié, la déformation sous compression étant quasi réversible à partir d'un certain taux de silylation (Figure 3).

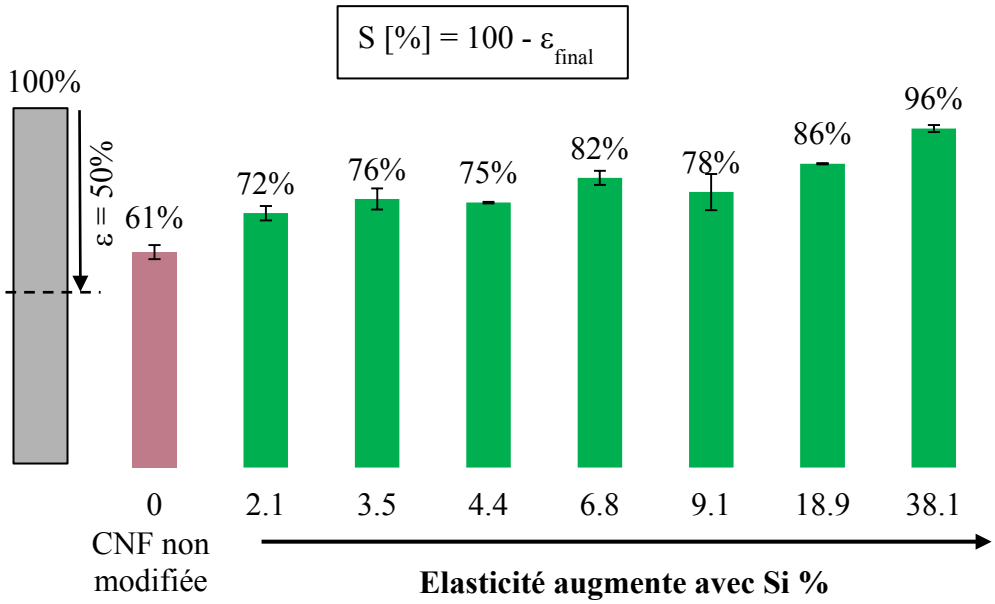

Figure 3 Schéma présentant la reprise en épaisseur (S) des mousses silylées après un test de compression réalisé à 50% de déformation (ε = 50%).

Les mousses silylées se sont avérées à la fois hydrophobes et oléophiles, et se sont montrées très efficaces pour absorber sélectivement une pollution de dodecane (choisi comme huile modèle) présente à la surface de l'eau (Figure 4). Par ailleurs, le matériau silylé a pu être recyclé plus de 10 fois sans modification notable de sa capacité d'absorption, et sans altération de son intégrité physique.

Une diminution de la conductivité thermique des mousses a également été mise en évidence après silylation.

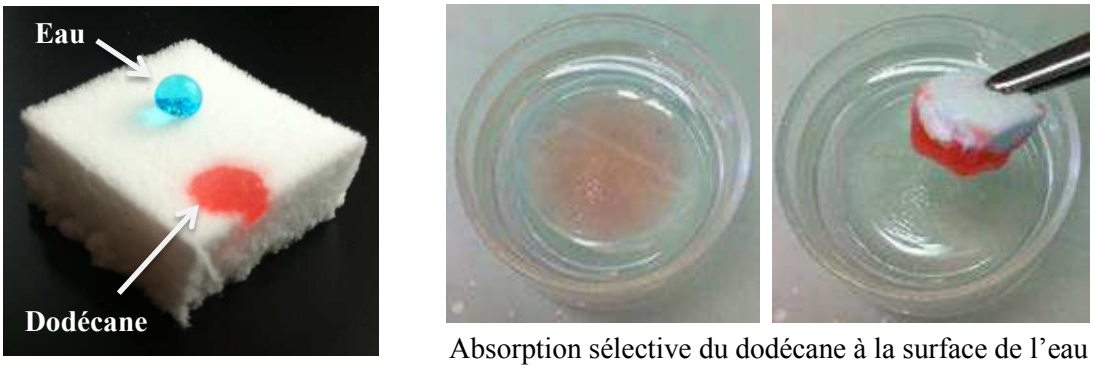

Absorption sélective du dodécane à la surface de l'eau

Figure 4 Démonstration des propriétés hydrophobes et oléophiles d'une mousse silylée à partir du MTMS. L'eau et le dodécane sont colorés en bleu et en rouge, respectivement.

Table of content

General introduction

This research project was founded by the Commission for Technology and Innovation (CTI) of Switzerland and was initiated in cooperation between the Swiss Federal Laboratories for Materials Science and Technology (Dübendorf, Switzerland), the University of Bordeaux 1 (Bordeaux, France) and two industrial partners, namely: Falcone Chemical Specialities Ltd. (Siebnen, Switzerland) and Jelu-Werk Josef Ehrler GmbH & Co. KG (Rosenberg, Germany).

In the context of petroleum resources depletion, new environmental regulations and spread of sustainability concerns, cellulose has increasingly drawn attention over the last three decades.[1] Cellulose is the most abundant polymer on the earth, representing about 1.5 x 10^{12} tons of the total annual biomass production,[2] and it presents very attractive properties. Cellulose fibres have low cost, are renewable, biodegradable, have high specific strength and modulus, low density,[3, 4] and can replace conventional inorganic or petroleum-based materials in composites applications.[5, 6]

In recent years, interest has been increasingly focused on nanocelluloses extracted from wood or plants, as exemplified by the increasing number of scientific publications and patents published since the beginning of the 21st century.[7] Nanocelluloses such as cellulose nanocrystals, nanofibrillated cellulose or electro-spinned cellulose nanofibres, possess highly interesting properties related to their high aspect ratio and specific surface area, as well as good mechanical properties.[8, 9] Hence, they have the potential to serve as building blocks for the elaboration of novel functional materials.[7, 10-12]

In particular, nanofibrillated cellulose (NFC) has been extensively considered as reinforcing agent in polymer matrices for composites application.[7, 12-14] More recently, promising lightweight, flexible and robust cellulosic foams have been successfully prepared using NFC as starting material.[10] However, the hydroxylated surface of these nanofibrils is often pointed out as a limiting factor for its use in commercial applications. In particular, NFC undergoes irreversible aggregation upon drying (hornification), which precludes any dry processes. Additionally, NFC fibrils cannot be ideally dispersed in non-polar solvents, monomers or polymers since the hydrophilic surface of the NFC is incompatible with hydrophobic environments (the NFC tends to aggregate by hydrogen bonding). Furthermore, the strong

tendency of NFC to absorb water is often undesirable in many composites and foams applications.

As most of these drawbacks and limitations are related to the chemical nature of the NFC surface, they can be suppressed or limited by chemical functionalization. For instance, hydrophobic functions can be grafted at the NFC surface to decrease the interfacial energy and increase their interaction with hydrophobic environments (physical or chemical interactions). A decrease in the hydrophilicity of the NFC composites and foams can also be obtained by this method.

As hydroxyl groups are the most reactive sites at the NFC surface, reactions based on alcohol chemistry have mostly been explored in the literature. The reactants conditions must be mild enough to limit cellulose degradation. A broad range of catalysts and solvents have been tested (in particular DMSO, DMF, toluene and hexane), but due to environmental concerns, green solvents are increasingly investigated (*i.e.* $scCO_2$, ionic liquids, and water). Energy saving procedures, such as microwave-assisted reaction,[15, 16] are also increasingly considered.

In this context, we envisaged monitoring the surface of NFC produced from oat straw, by developing an environmentally friendly method based on alkoxysilanes, which can be processed in water. Because a large variety of functional groups is available within commercial alkoxysilanes, it is anticipated that the method will open up opportunities to broaden the spectrum of application of NFC. In the current thesis, the potential of silylated NFC as reinforcing agents in composites and as building block for the elaboration of foams was particularly investigated.

The thesis is divided in six chapters:

Chapter I presents some general aspects about nanocelluloses – in particular NFC - and their use in composite materials and foams.

Chapter II is dedicated to the functionalization of NFC by methyltrimethoxysilane – chosen as a model silane – and to the comprehensive examination of the silylated materials. Reaction conditions such as pH, reaction time and initial silane concentration have been particularly investigated and optimized using two distinct experiment protocols. The modifications have been characterized at the molecular level by various physicochemical techniques. The

properties of the silylated nanofibres, *i.e.* the morphology, crystallinity, wettability, hygroscopicity and thermal stability have been subsequently examined.

Chapter III investigates the impact of silylation on the mechanical, thermal and hygroscopic properties of NFC-reinforced composites prepared with two distinct polymeric matrices: polydimethylsiloxane (PDMS) and poly(lactic acid) (PLA).

Chapter IV examines the impact of silylation on the properties of NFC-foams prepared by freeze drying, in particular the porosity, compressive properties, wettability, hygroscopicity, oleophilicity and thermal conductivity

A general conclusion is drawn in Chapter V and some outlooks are proposed.

Finally, the materials and methods that have been employed throughout this thesis are described in Chapter VI.

I. Generalities

I.1. Chemical composition of plant fibres

I.1.1. Macromolecular substances

I.1.1.1. Cellulose

Cellulose can be extracted from different plants and animals, for example, wood, cotton, bamboo, cereal straw (wheat, oat, rice etc.), algae, bacteria, animal tunicates, etc.[17, 18] This linear polymer is composed of D-anhydroglucopyranose units (AGU) which are linked by β-1,4-glucosidic linkages. The polymer chain contains one hemiacetal reducing end, and a non-reducing end with a hydroxyl group in the C4 position (Figure 1).[19, 20]

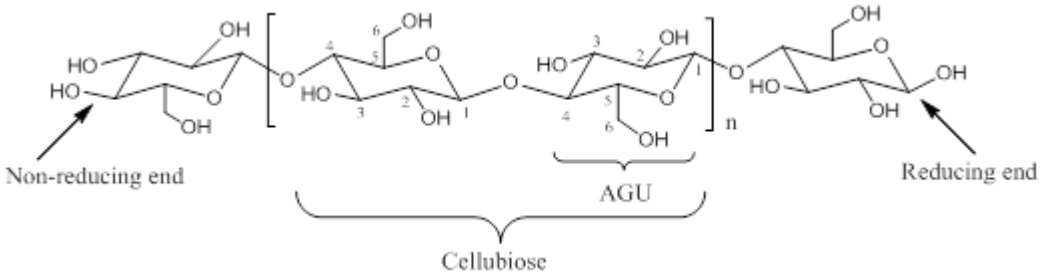

Figure 1: Molecular structure of cellulose highlighting the non-reducing end (free hydroxyl at the C4 position) and the reducing end with a hemiacetal group.

The degree of polymerization (DP) depends on the source and treatment used to isolate the polymer. In general, the DP of cellulose obtained from cotton fibres is 8,000-14,000, cotton linters 1,000-6,500, bagasse 700-900 and wood fibres 8,000-9,000.[21] To our knowledge, the value of DP of cellulose from oat straw (used in the present thesis) is not available in the literature.

In plant fibres, cellulose chains interact with each other through hydrogen bonds, forming bundles of fibrils (or microfibrillar aggregates), in which highly ordered regions (*i.e.* crystalline phases) alternate with disordered domains (*i.e.*, amorphous phases).[4] The formation of intra- and intermolecular hydrogen bonds have been the subject of many studies.[22-24] While there is only one possibility of hydrogen bonding between O3-H▪▪▪O5, there are different possibilities for O2-H and O6-H. An example of such hydrogen bonds network between two cellulose chains in Cellulose I is presented in Figure 2.[23]

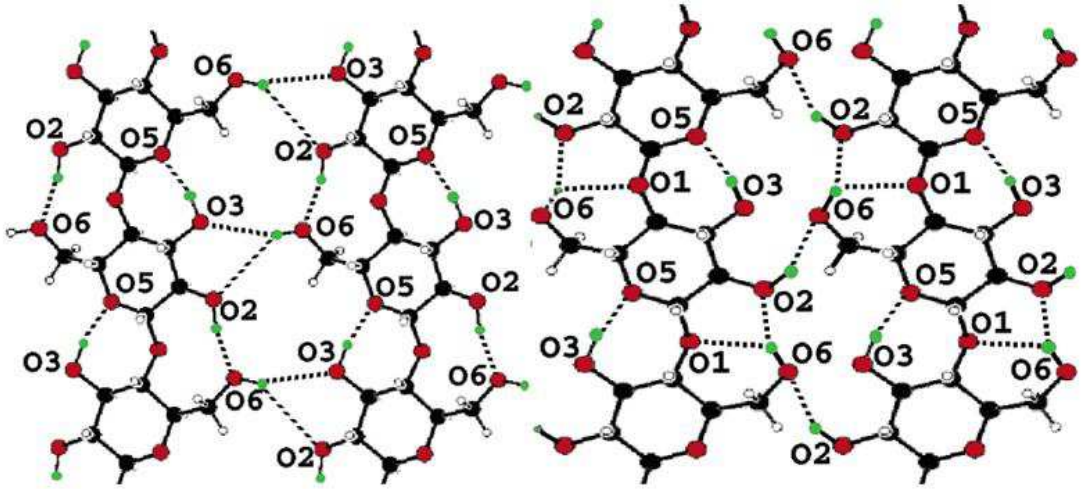

Figure 2: Schematic representation of hydrogen bonds in cellulose Iβ.[23] Black: Carbon, red: Oxygen, white: hydrogen of methyl group, green: hydrogen of hydroxyl group; dotted line: hydrogen bonds. Only the oxygen atoms involved in hydrogen bonding are labelled.

The crystallinity degree depends on the source and treatment of the materials. For example, the crystallinity degree of natural fibres such as cotton, ramie, flax, sisal, and banana is about 65%, while that of regenerated cellulose is about 35%. Four polymorphs of cellulose have been characterized so far in the literature.[25, 26] Cellulose I is the structure of native cellulose, while other polymorphs are obtained by different chemical treatments of Cellulose I. Cellulose II is usually obtained after regeneration of native cellulose, or by the mercerization process (treatment with sodium hydroxide). Cellulose III is formed when Cellulose I or II is

modified with organic amines or liquid ammonia, while Cellulose IV is obtained after a thermal treatment of Cellulose III.[19] Each polymorph is defined by its unit cell parameters.[25] Cellulose I has two polymorphs, Iα and Iβ, which coexist in different proportions depending on the sources – Iα is dominant in bacterial and algal celluloses, whereas Iβ is dominant in plants and tunicates.[27, 28] In the present study the cellulose source was oat straw, therefore the term "cellulose" refers to native cellulose, namely Cellulose I.

I.1.1.2. Hemicelluloses

Hemicelluloses are a heterogeneous group of branched matrix polymers of relatively low molecular weight. Whereas cellulose contains only glucose, hemicellulose contains a variety of sugars such as glucose, mannose, xylose, arabinose etc.[19] Hemicellulose molecules are tightly hydrogen bonded to the cellulose microfibrils, acting as a cross-linking matrix between cellulose and lignin.[17] The main monomers constitutive of hemicelluloses are presented in Figure 3.

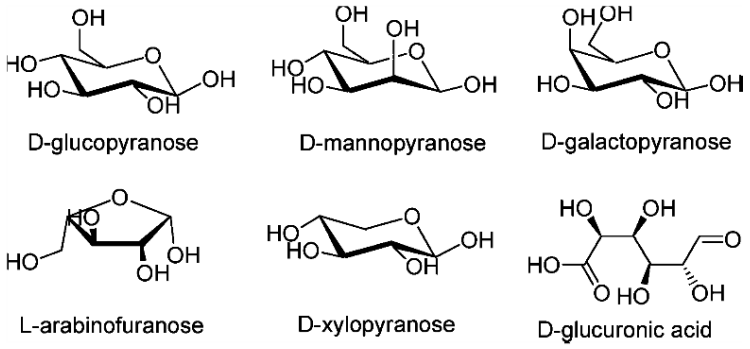

Figure 3: The main monomers constitutive of hemicelluloses.[20]

I.1.1.3. Lignin

Lignin is a very complex polymer composed of highly branched aromatic-aliphatic moieties.[20] In the plant, lignin is synthesized through dehydrogenative polymerization of three monolignol precursors: p-coumaryl alcohol, coniferyl alcohol and sinapyl alcohol. An example of lignin structure is presented in Figure 4.[29]

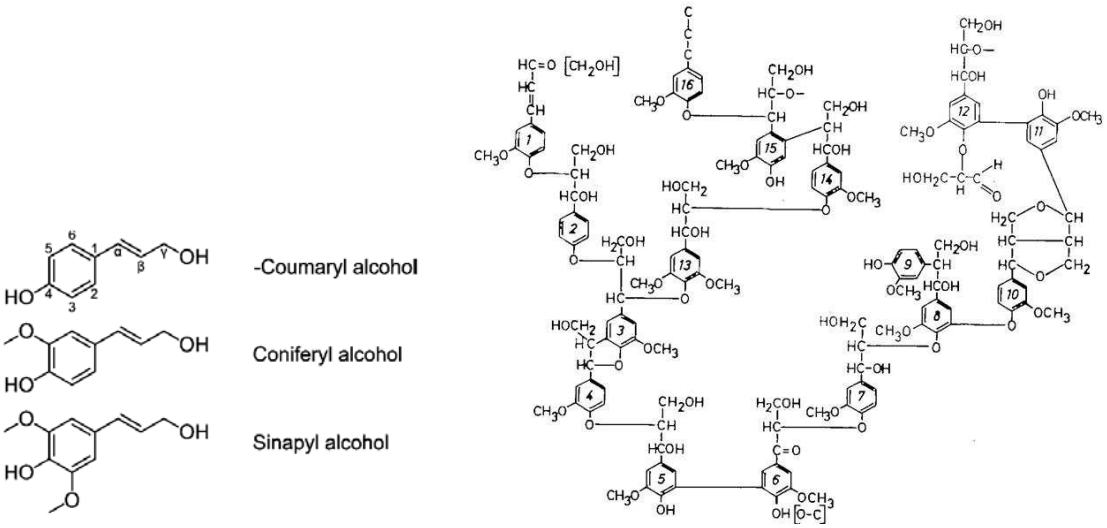

Figure 4: The three fundamental lignin monomer precursors[20] (left) and a model of lignin structure[29] (right).

Cellulose and hemicelluloses are closely bound by lignin, which provides rigidity and cohesion to the cell wall, and acts as barrier against moisture or microbial attacks.[30]

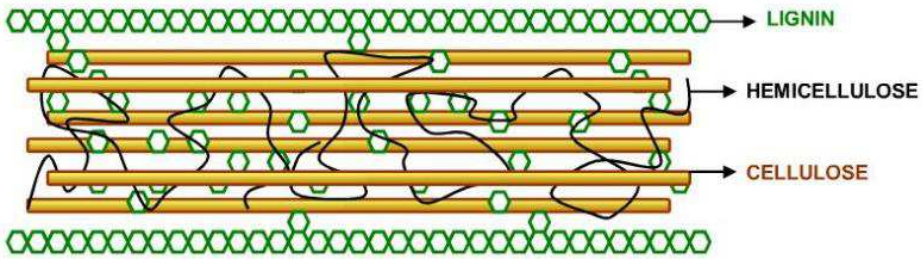

Figure 5: Representation of lignocellulose structure[31]

I.1.2. Low molecular weight substances

I.1.2.1. Extractives

The term extractives is related to a heterogeneous group of substances, which can be extracted from wood or plants using solvents like methanol, ethanol, acetone, toluene or dichloromethane.[32] Extractives in oat straw are mainly free fatty acids, resin, sterols and waxes.[32]

I.1.2.2. Mineral substances

Minerals are essential for the growth of plants.[32] They remain in the form of ash, after combustion of the lignocellulosic material. The main mineral in oat straw is SiO_2, which

represents 65-70% of the total mineral content. It has been reported to contribute to the plant growth and antimicrobial resistance,[32] as well as to the rigidity of the stem.[33] The other minerals are macro- and micronutrients, such as N, P, S, Ca, and Fe, Mn, Zn, Cu etc.[32]

I.1.3. Chemical composition of oat straw

The chemical composition of oat straw has been reported by different authors, with some variations (Table 1).

Table 1: Chemical composition of oat straw in literature (in w/w %):

Ref.	*Water solubles*	*Cellulose*	*Hemicelluloses*	*Lignin*	*Wax*	*Ash*
Sun[34]	4.6	38.5	31.7	16.8	2.2	6.1
Theander[35]	***Proteins***	***Cellulose***	***Hemicelluloses***	***Lignin***	***Extractives***	***Ash***
	4.5	33	31	18	7.4	6.0
Adapa[36]		***Cellulose***	***Hemicelluloses***	***Lignin***		
		25.4±1.0	21.7±0.9	19.6±0.6		

I.2. Structure of plant cell walls

The plant cell walls consist of cellulose microfibrils, which are embedded in a highly crosslinked amorphous hemicellulose-lignin matrix.[37] The structure of a natural fibre cell wall can be assimilated to a microscopic tube composed (from exterior to in interior) of a middle lamella, a primary wall, a secondary wall and finally the lumen (Figure 6).[17]

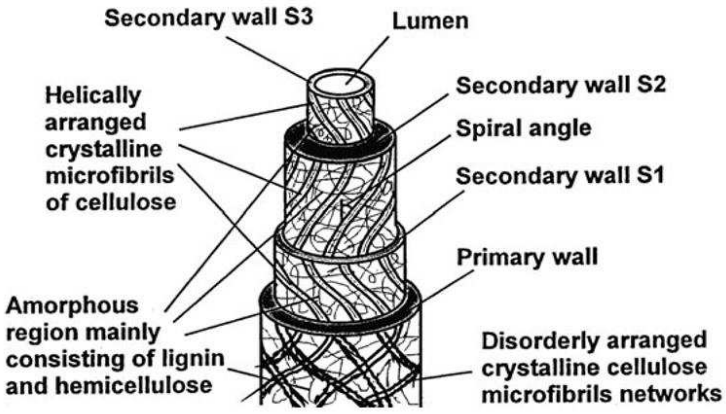

Figure 6: Structural constitution of a plant fibre cell.[18]

In the cell wall, elementary fibrils (Ø = 1.5 to 3.5 nm)[2] aggregate into microfibrils (Ø = 2 to 50 nm)[19], which further form microfibrillar bands (width in range of 100 nm)[2]. The microfibril angle (*i.e.* the angle between the direction of the helical windings of cellulose

microfibrils and the long axis of cell) plays a central role in determining the mechanical behaviour of the plant.[38]

I.2.1. Middle lamella and primary wall

The middle lamella is a thin layer composed of hemicellulose and lignin, which glues the cells together.[30] It has primary walls on both sides.

The primary wall is a thin layer of about 0.1-0.2 μm, consisting of cellulose, hemicellulose, pectin and protein, all embedded in lignin. In the primary wall, the microfibrils orient in random manner, building a netlike texture.[38]

The term "compound middle lamella" (CML) generally refers to the middle lamella plus adjacent primary walls.[30]

I.2.2. Secondary wall (S)

I.2.2.1. S1

The outer layer (S1) is thin (0.2-0.3 μm) and forms 10-20% of the total cell wall.[38] In the S1 layer, microfibrils are arranged in tightly wound helices, at a nearly transverse orientation (60-80° to the cell axis).[19]

I.2.2.2. S2

The middle layer (S2) is thick (1-5 μm) and forms 70-90% of the total cell wall.[38] In the S2 layer, the microfibrils are densely packed and orient helically at a relatively small angle (5-30°) to the cell axis.[19]

I.2.2.3. S3

The inner layer (S3) is the thinnest layer (about 0.1 μm), forming 2-8% of the total cell wall.[38] In the S3 layer, the microfibrils are arranged again in tightly wound helices, at a nearly perpendicular orientation (60-90° to the cell axis).[19]

I.3. Nanofibrillated cellulose (NFC): isolation and morphological characteristics

I.3.1. Nomenclature

The nomenclature concerning micro- and nanomaterials from natural resources has not been standardized yet. Different terms are used according to recent review papers:[7, 39]

- "Microcrystalline cellulose (MCC)" refers to commercial cellulose materials, applied mainly in pharmaceutical and food industry. The diameter of this material is generally greater than 1 μm;[7, 39]
- "Microfibril" refers to fibrous cellulose structures formed during the biosynthesis in higher plants. Synonyms which can be found in the literature are nanofibril, nanofibre;[7]
- "Microfibrillated cellulose (MFC)" or "Nanofibrillated cellulose (NFC)" refers to microfibril aggregates produced by mechanical refining of plant fibres.[39] In the present work, only the term "nanofibrillated cellulose (NFC)" was used;
- "Cellulose nanocrystals (CNC)" refers to rod-like shaped cellulose nanoparticles obtained after acid hydrolysis of pulp, MCC or NFC. Synonyms which can be found are cellulose whiskers, nanowhiskers, rod-like cellulose crystals.[7, 39]

The average dimensions that have been reported for each type of cellulosic material are presented in Table 2:

Table 2: Dimensions of the micro- and nano-scaled cellulose materials, isolated from natural fibres

Type	*Diameter d [nm]*	*Length L [μm]*	*Aspect ratio (L/d)*
MCC[7]	>1,000	>1	~1
Microfibril[7]	2-10	>10	>1,000
MFC/NFC[7, 39]	4-40	5-10's	100-150
CNC[7, 39]	3-5	0.1-0.6	10-100

I.3.2. Isolation methods

The processes for the isolation of nano-celluloses have been reviewed comprehensively by Moon et al.[39] They are produced from purified fibres, after elimination of hemicelluloses, lignin, etc. Different approaches have been used separately, in sequence or in combination.

I.3.2.1. Isolation of cellulose nanocrystals (CNC)

CNC can be produced by acidic hydrolysis of the starting cellulosic material. This simple process usually involves a partial acid hydrolysis of cellulose using concentrated sulfuric acid (H_2SO_4), which removes disordered or paracrystalline regions of cellulose and leaves crystalline regions intact. After this treatment, rod-like shaped cellulose nanocrystals bearing anionic sulfate ester groups at their surface are produced. Their geometrical dimensions generally depend on the starting cellulose source, resulting in values varying from 5 to 20 nm in width, and from 100 nm to 1-2 μm in length (Figure 7).[40, 41]

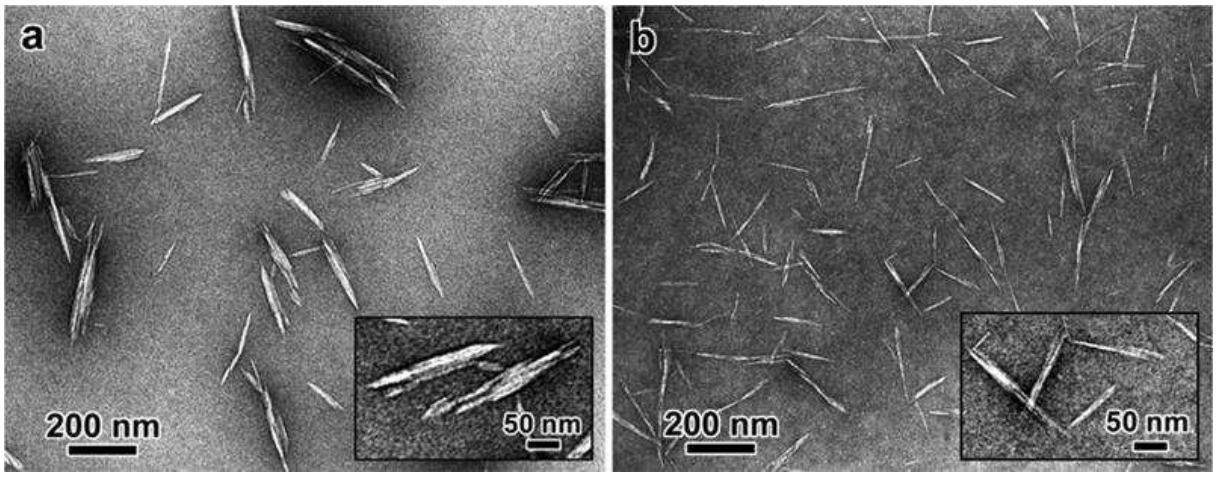

Figure 7: TEM micrographs of CNC obtained by sulfuric acid hydrolysis of cotton (a), and MCC (b).[40]

I.3.2.2. Isolation of nanofibrillated cellulose (NFC)

Nanofibrillated cellulose (NFC) is generally produced by mechanical disintegration. This process generally involves a refining step followed by a high-pressure homogenization step,[42, 43] but cryocrushing and grinding methods have been also reported.[44, 45] The mechanical treatments produce a network of interconnected cellulose microfibrils, with diameters from 10 to 100 nm and aspect ratios from 50 to 100[46-48] (Figure 8).

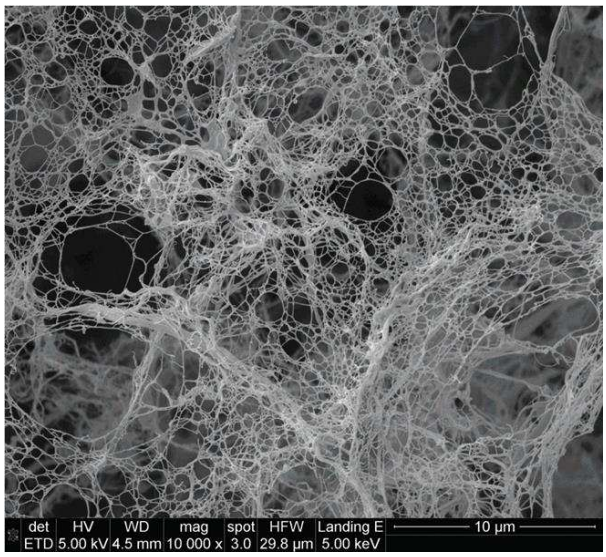

Figure 8: SEM micrograph of NFC, mechanically isolated from oat straw cellulose powder[12]

In order to decrease the high energy consumption associated with these processes, chemical pre-treatments of the cellulose raw material have been also envisaged: TEMPO,[49-53] carboxymethylation,[54-56] periodate oxidation,[57] and enzymatic[58-60] modifications.

I.3.3. Properties of NFC

I.3.3.1. Mechanical properties of isolated NFC

The mechanical properties of isolated NFC cannot be easily evaluated because of the variability of the NFC material. Only information about single plant fibers or crystalline regions could be found in the literature. For single plant fibres, E modulus in the range of 5-45 GPa and tensile strength in the range of 0.3-0.8 GPa have been reported, based on Raman techniques.[14, 61, 62] For the crystalline regions, E modulus between 124 and 155 GPa[63] and tensile strength up to 7 GPa[39] have been reported (evaluated experimentally or using modelling).

I.3.3.2. Properties of NFC films

One of the most interesting features of NFC stems from its excellent film forming properties. NFC films are mainly obtained through solution casting, a process during which the solvent (mostly water) is removed by evaporation, vacuum filtration, pressing, or a combination of these processes.[59, 64] The nanofibrils in the dried films cannot be re-dispersed in water, due to the irreversible agglomeration of cellulose nanofibres upon drying. This phenomenon is

called hornification and is explained by the formation of additional hydrogen bonds between amorphous parts of the cellulose fibrils during drying.[65, 66]

a) Mechanical properties

Excellent mechanical properties in tension mode have been reported in the literature for NFC films, with values in the range of 1-17.5 GPa and of 20-240 MPa for E-modulus and tensile strength, respectively.[39] These values are lower than those obtained for crystalline cellulose, because of the presence of amorphous regions in NFC and because of the random in-plane nanofibril orientation within the film.[39] Nevertheless, if the density of cellulose (1500 kg/m^3)[67] is taken into consideration, the mechanical properties of NFC films are comparable with metals and ceramics.[39]

b) Optical properties

NFC films are generally characterized by their medium to low transparency, which is associated to the light scattering caused by different phenomena: high fraction of air in the films (porosity ~20-40%); difference of refractive index between air and cellulose (air: ~1.0; NFC: 1.618 along the fibril, 1.544 in the transverse direction[68]), nanofibrils sizes, film thickness and surface roughness.[39]

c) Barrier properties

Concerning barrier properties, significant water sorption (15 % at 90 % RH)[59] and water permeability values (321 ± 46 g m^{-2} day^{-1})[69] have been measured, because of the highly hydrophilic nature of cellulose. But excellent barrier properties towards oxygen have been often reported, with oxygen transmission rate (OTR) values down to 17.8 ml m^{-2} day^{-1} measured for NFC films with a thickness of 20-30 μm.[70]

I.4. Applications of NFC

As mentioned above, NFC has many interesting properties related to its nano-size dimensions and chemical structure, which makes it an interesting candidate for various applications. In particular, NFC has been extensively studied as reinforcing agent in polymer matrices for composites application.[7, 12-14] More recently, promising lightweight, flexible and robust cellulosic foams have been prepared using NFC as starting material.[10] These two applications will be developed in the next paragraph.

I.4.1. NFC as reinforcing agents in composites

A wide range of polymer matrices have been reinforced with NFC, but the majority of the studies involved hydrophilic matrices, because of the good compatibility with the hydrophilic NFC. An overview of the most popular matrices reinforced with NFC can be found in the classification below (Figure 9).[7]

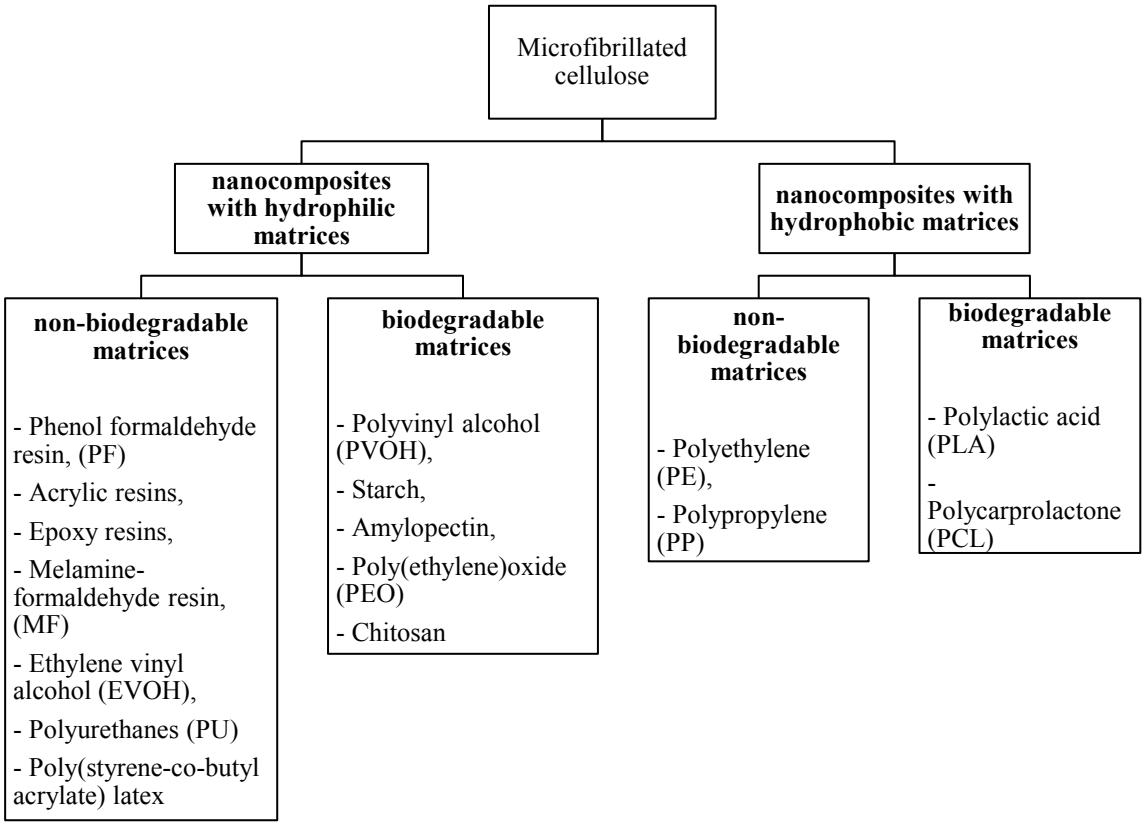

Figure 9: Classification of nanocelluloses reinforced polymer composites, summarized by Siró et al.[7]

I.4.1.1. Methods for the processing of NFC composites

Several preparation methods have been envisaged to elaborate NFC-reinforced polymer composite materials. In the most popular approaches, NFC is dispersed in a solvent containing the dissolved polymer, and is subsequently processed by techniques such as solution casting,[47, 71-74] melt compounding[75, 76] or electrospinning.[77] These methods are limited by the amount of NFC that can be incorporated in the suspension, which cannot exceed 30 wt %.[39]

In order to increase the NFC ratio in the composite material, a three steps process can be envisaged, which consists in: i) elaborating a NFC film through a solvent casting process, ii)

impregnating the dried film with the desired resin and iii) oven drying the film with or without hot pressing.[59, 64] Composite materials with NFC contents above 70 wt % have been reported with this technique.[39]

Another technique based on a wet-laid process (papermaking-like) has been also reported, and allowed the preparation of NFC/PLA composites with NFC weight fraction up to 90 %.[78]

The incorporation of NFC in the polymer melt[73] or the polymerization of the monomer "in-situ"[79] have been also proposed in two recent studies.

I.4.1.2. Mechanical properties of NFC composites

As compared with neat polymer matrices, an increase of both E modulus and tensile strength, with a concomitant decrease of the strain at break, have been reported with composites prepared from hydrophilic polymers such as PVOH[47], HPC[47], PF[80], MF[59], poly(styrene-co-butyl acrylate)latex[81] and PU.[82]

The reinforcing effect of NFC in composites with hydrophobic matrices has shown mixed results. Wang and Sain,[83, 84] incorporated NFC into molten PE and PP, using acrylic oligomers as dispersant, but the mechanical properties of these composites did not show significant improvement. The most studied hydrophobic matrix is PLA, because of its 100 % renewable nature.[7] PLA has some shortcomings, such as brittleness and low thermal stability.[7] Several attempts have been made to reinforce PLA by NFC using different processing methods, such as solution casting[72, 85], extrusion[86, 87] or wet-laid processing[78]. A slight increase in modulus and tensile strength has been noted,[78, 85, 86] but aggregation occurs during processing and poor mechanical properties are still displayed by the composite.[87]

I.4.1.3. Optical properties of NFC composites

Optically transparent NFC composites were prepared by Iwamoto et al.[44, 64] by impregnating a dry NFC film with acrylic resins, followed by UV curing. Light transmittance between 70 and 85 % was obtained, with up to 70 wt % NFC dispersed in the matrix. The transmittance in such composites depends on refractive index match, film thickness, nanocelluloses dimensions and volume fraction (Figure 10).[39]

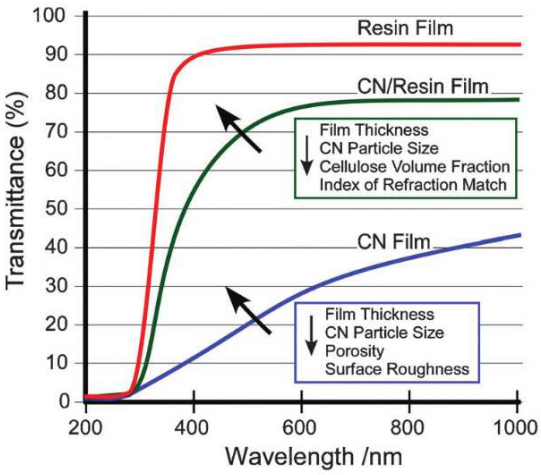

Figure 10: Factors impacting the light transmittance of CN/resin composites.[39] (CN refers to different types of nanocelluloses, such as NFC and CNC)

I.4.1.4. Thermal properties of NFC composites

In general, the thermal stability of the NFC-reinforced composites tend to increase with increasing weight fraction of NFC, as demonstrated with matrices such as PLA,[74, 88, 89] cellulose acetate,[90] melamine formaldehyde resin[59] or amylopectin.[91] This is particularly the case in the temperature range higher than glass-transition temperature (T_g).[39]

The coefficient of thermal expansion (CTE) is another important parameter for applications such as flexible transparent displays.[92] Iwamoto et al.[44, 64] found that a significant decrease in CTE could be obtained when NFC were incorporated into acrylic matrices. The CTE tended to decrease with increasing crystallinity of NFC.[93]

I.4.1.5. Barrier properties of NFC composites

The barrier properties to oxygen have been improved by addition of NFC in amylopectin films.[94] The oxygen transmission rate (OTR) was found to decrease with increasing NFC content.

Water sorption is regarded as one of the major issues that limits the application of NFC-polymer composites, due to the hydrophilic nature of cellulose. Hence, when hydrophobic polymer matrices are used, the water sorption of the composites is generally higher than that of the neat polymer.[72] Water sorption has been shown to decrease in some rare cases, as

demonstrated by Henriksson et al. with melamine formaldehyde matrices.[59] But if hydrophilic matrices such as starch are used, a reduction in water sorption can be measured.[95-97]

To obtain better barrier properties, some authors have envisaged incorporating nanoclays in combination with NFC and obtained a reduction in both water sorption and oxygen permeability.[98, 99]

I.4.2. NFC as matrix for the elaboration of aerogels or foams

I.4.2.1. Definitions

Aerogels and foams are ultra-light weight and highly porous materials that are prepared by the replacement of a liquid solvent in a gel by air. The term "aerogels" is generally employed to name materials in which the typical structure of the pores and the network is mostly maintained, *i.e.* the gel structure does not change after replacement of the liquid by air (shrinkage phenomena are minimized).[100] If the network structure has changed, the more general term "foam" is preferred. In present study, the term "foam" will be used for any porous material prepared from NFC.

Brought to light in 1931,[101] these porous materials are mostly elaborated through the Sol-gel® polymerisation of inorganic metal oxides, such as silica, alumina, titania, zirconia or tin oxides.[100, 102] The interest in such materials lies in their low density (typically between 0.004 and 0.500 g/cm^3), high porosity (typically greater than 80%), high specific surface area, low thermal conductivity, excellent shock absorption and low dielectric permittivity.[100, 102, 103] Hence, aerogel materials have been used in various applications including thermal and acoustic insulation, paints, electrical applications, life science, catalysis or optical applications.[102]

But these materials generally suffer from their brittleness. To overcome this problem, alternative lightweight, flexible and robust cellulosic aerogels or foams have been proposed using NFC as starting material.[104-106] Since aqueous NFC suspensions have gel-like properties, due to the presence of long and interconnected hydrophilic cellulose nanofibrils, replacing water with air results in an aerogel or foam with long entangled cellulose nanofibres.

I.4.2.2. Methods for the processing of NFC foams

NFC foams can be prepared by freeze-drying or supercritical CO_2 drying:

- With the freeze-drying method, the NFC suspension is frozen in a mould and water is eliminated by sublimation (Figure 11).[106-109] Alternatives consist in first solvent-exchanging water with t-butanol, and then freeze-drying the alcoholic suspension.[104, 108] In that case, the foam obtained is more homogeneous and displays a higher specific surface area.
- The supercritical CO_2 drying method ($scCO_2$ drying) is performed in two steps: i) water is solvent exchanged with organic solvents miscible with CO_2, such as ethanol or acetone; ii) the organic solvent is solvent-exchange with CO_2. The disadvantage of this process is that it is time consuming.[110]

Figure 11: Image of NFC foam prepared by the freeze-drying method.[104]

I.4.2.3. Morphology of NFC foam

With the freeze-drying method, different morphologies can be obtained depending on the speed with which the freezing step is performed. If the NFC suspension forms a thin layer in the mould (1-3mm), the freezing is so fast that that a porous structure composed mostly of nanofilaments is obtained (Figure 12a).[108, 109, 111] When the thickness of the NFC gel exceeds this range, aggregation of nanofibrils starts to occur and two types layers are formed: i) the bottom layer, which freezes quickly, is composed of nanofilaments (Figure 12c); ii) the layer above, which freezes slowly, is composed of cell wall sheet structures (Figure 12b), resulting from the agglomeration of cellulose nanofibres during freezing.[104, 108] This phenomenon arises because the ice crystals formed during slow freezing tend to push the cellulose nanofibres into the interstitial regions of the crystals.[112]

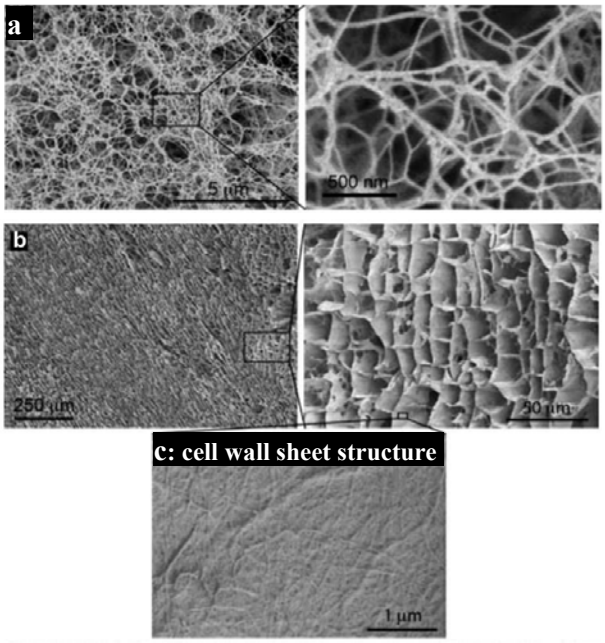

Figure 12: SEM images of NFC foams obtained by freeze-drying: a) Fast freezing (bottom layer); b-c) Slow freezing (layer > 3 mm).[111]

With both the t-butanol freeze-drying and $scCO_2$ drying methods, a porous structure composed mainly of nanofilaments is obtained (Figure 13).[104, 113] As t-butanol has a much lower expansion coefficient than water, the cellulose nanofibrils are not squeezed during freezing.[100] In the case of the $scCO_2$ method, no freezing step is involved.

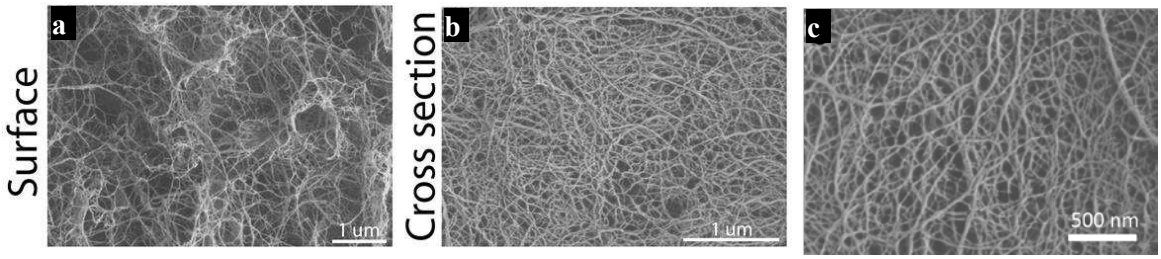

Figure 13: SEM micrographs of NFC aerogels prepared by t-butanol freeze drying (a and b)[104] and supercritical CO_2 drying (c)[113]

I.4.2.4. Density, porosity and specific surface area

The density, porosity and specific surface area are directly impacted by the method of processing (*i.e.* the nature of the fibrillar network) and the concentration of NFC in the original suspension, as demonstrated by the data presented in Table 3:

Table 3: Density (ρ), porosity and BET surface area of various NFC foams produced by different methods

Ref.	Drying process	NFC concentration [wt%]	ρ [kg/m^3]	porosity [%]	BET surface area [m^2/g]
Pääkkö[109]	Vacuum pumping freeze drying	2	30	95-98	20
	Cryogenic freeze drying	2	20	98	66
Sehaqui[113]	t-BuOH freeze drying	~15	380	74	117
	$scCO_2$ drying	~15	205	86	304
Sehaqui[106]	Cryogenic freeze drying	0.7	7	99.5	44
		6.0	61	95.9	~15
		10	103	93.1	15

I.4.2.5. Mechanical properties of NFC foams

Besides the high porosity and specific surface area, NFC foams provide interesting mechanical characteristics compared with other foams. The E modulus and compressive yield strength of the foams increases with increasing density, which can be controlled by varying the concentration of NFC in the original suspension.[106] The energy of absorption in compression of NFC foams is generally higher than that of polymer foams such as expanded polystyrene foams.[111] Nevertheless, NFC foams have been reported to have limited shape recovery after compression.[105] Table 4 presents the mechanical properties of some NFC foams prepared with the freeze-drying method:

Table 4: Mechanical properties of NFC foams prepared with the freeze drying method[111]

NFC concentration [wt%]	0.7	2.2	4.2	10
Density [kg/m^3]	7	22	43	103
Porosity [%]	99.5	98.5	97.2	93.1
E Modulus [kPa]	56	435	1510	5310
Yield stress [kPa]	7.8	31.9	135.1	515.6
Energy absorption [kJ/m^3]	8.4	55.5	210	927.7

I.4.2.6. Application of NFC foams

For the time being, NFC foams have been mostly tested as reinforcing agents in composites or as porous templates. Amylopectin and PVOH reinforced NFC foams have been shown to display an increase in E modulus of up to 40%.[97, 112]. Conducting foams have been prepared by dipping the NFC foams in a solution of polyaniline.[109] Photoswitchable or magnetic NFC aerogels have been produced by chemical vapour deposition of TiO_2,[114] or precipitation of magnetic nanoparticles,[115] respectively.

I.5. Chemical functionalization of NFC

I.5.1. Context

NFC possesses many interesting properties, but its hydroxylated surface is often pointed out as a limiting factor for its use in commercial applications. In particular, NFC undergoes irreversible aggregation upon drying (hornification), which precludes any dry processes. Hence, NFC is generally processed in the form of water suspensions (max. solid content 30 %), which causes high transport and storage costs, and favours microbial degradation. Additionally, NFC fibrils cannot be ideally dispersed in non-polar solvents, monomers or polymers since the hydrophilic surface of the NFC is incompatible with hydrophobic environments (the NFC tends to aggregate by hydrogen bonding). Furthermore, the strong tendency of NFC to absorb water is often undesirable in many composites and foams applications.

As most of these drawbacks and limitations are related to the chemical nature of the NFC surface, they can be suppressed or limited by chemical functionalization. For instance, the introduction of surface charge by oxidation can be a successful pathway to limit the aggregation of the nanofibres upon drying and subsequently reduce the shipping cost of NFC. In another approach, hydrophobic functions can be grafted at the NFC surface to decrease the interfacial energy and improve their interaction with hydrophobic environments (physical or chemical interactions). A decrease in the hydrophilicity of the NFC composites and foams can be also obtained by this method.

As hydroxyl group is the most reactive sites at the NFC surface, reactions based on alcohol chemistry have mostly been explored in the literature. A broad range of catalysts and solvents have been tested (in particular DMSO, DMF, Toluene and hexane), but due to environmental concerns, green solvents are increasingly investigated (*i.e.* $scCO_2$, ionic liquids, and water).

Energy saving procedures, such as microwave-assisted reaction,[15, 16] are also increasingly considered.

A broad range of chemical modifications have been reported with microcrystalline cellulose, pulp or paper,[116, 117] but we will focus here on literature related to NFC.

I.5.2. Oxidation

I.5.2.1. TEMPO-oxidation

2,2,6,6-tetramethylpiperidine-1-oxyl (TEMPO) mediated oxidation is used to produce negatively charged NFC at the surface. The reaction is selective to the primary alcohol at the C6 position of the anhydroglucose unit (Scheme 1).[51] This reaction was performed in aqueous system.

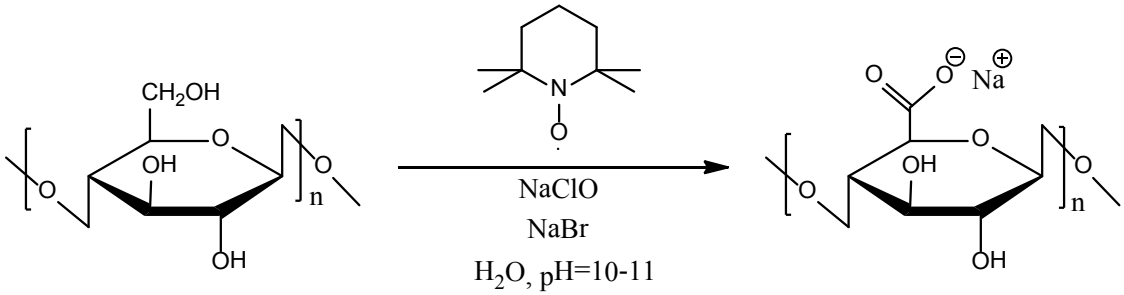

Scheme 1: TEMPO oxidation of NFC surface

The utilisation of this method as a pre-treatment before mechanical disintegration of cellulose pulp proved to be very efficient in reducing the energy consumption associated with the production of NFC.[49-53]

In addition, TEMPO-oxidation of NFC led to films displaying high light transmittance, good mechanical properties, low thermal expansion and excellent oxygen barrier property.[50, 113, 118] But the thermal stability was poor and the film was very hydrophilic.[50]

Recently, TEMPO-oxidized NFC has been used as template to prepare hybrid organic-ceramic aerogels with TiO_2 or TiO_2/SiO_2, which showed high adsorption towards organic molecules and photocatalytic activity.[119]

I.5.2.2. Other oxidation routes

By pre-treating cellulose pulp with periodate and sodium bisulfite before mechanical disintegration, Liimatainen at el. obtained a similar effect than with the TEMPO-oxidation method (Scheme 2).[57]

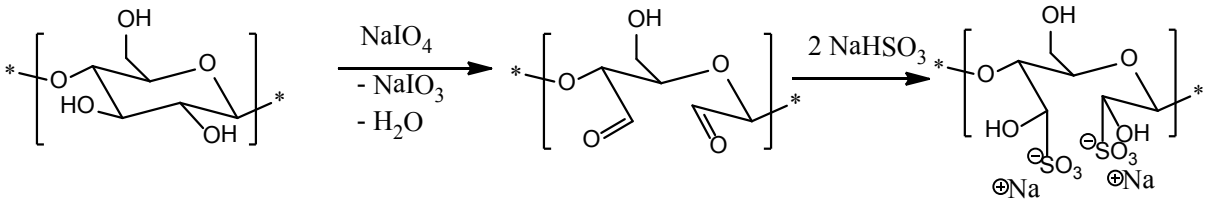

Scheme 2: Regioselective periodate oxidation and sulfonation of cellulose pulp[57]

Stenstad et al.[120] used ammonium cerium(IV) nitrate as a powerful oxidation agent for the post-oxidation of NFC, with the objective to further react the oxidized NFC with glycidyl methacrylate (Scheme 3).

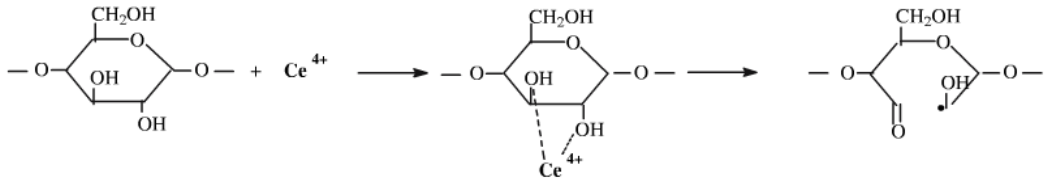

Scheme 3: Oxidation of 1,2-glycol groups of cellulose by Ce^{4+}.[120]

I.5.3. Esterification

Among the different methods that have been studied so far, the NFC esterification with anhydride molecules has received the most attention (Scheme 4).

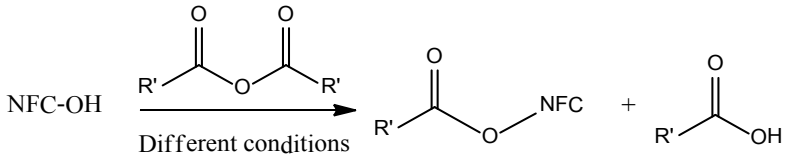

Scheme 4: Esterification of NFC with anhydrides

The most commonly used anhydride is acetic anhydride, which has been employed either as a fibrillation pre-treatment[121-123], or for the post-modification of NFC.[72, 124-126] Catalyst such as pyridine,[72, 123], or perchloric acid in combination with acetic acid,[121, 122, 125] have been reported,

but the reaction could be also performed without catalyst.[124, 126] Other anhydrides, such as trifluoroacetic anhydride, have been also envisaged.[127]

In comparison with neat NFC, acetylated NFC (ac-NFC) can be more easily dispersed in organic solvents of low polarity such as chloroform.[72] It is also more hydrophobic[123, 127] and displays a low coefficient of thermal expansions (CTE).[124, 125] But slightly poorer mechanical properties have been also noted in film[124] or aerogels,[126] probably because of weaker fibre-fibre interactions. Regarding the barrier properties, oxygen permeation was found to increase after acetylation, but water sorption decreased.[72, 124, 126]

Ac-NFC has been incorporated in polymer matrices, such as PLA[72, 122, 123] or acrylic resins[121, 124, 125], but mixed results were found regarding the mechanical performances. In some studies, a reinforcing effect was measured,[72, 121] but in other ones, no significant improvement was noted.[123] Thermomechanical properties[72, 122, 123] and transmittance [121, 122, 124, 125] were generally improved after acetylation.

I.5.4. Etherification

Etherification is an important method for the industrial production of cellulose derivatives. Since the first production of methylcellulose at the beginning of last century, cellulose ethers such as methylcellulose, carboxymethylcellulose and hydroxyethylcellulose have become one of the most important commercial cellulose derivatives.[116]

The etherification of NFC has been mostly conducted using halogenated or epoxy-based reactants, through nucleophilic substitutions and ring-opening reactions, respectively.

I.5.4.1. Reaction with halogenated molecules

The carboxymethylation reaction has been used to introduce negative charges at the NFC surface (Scheme 5).[54-56] In contrast to TEMPO oxidation, this reaction is not selective to primary alcohols.

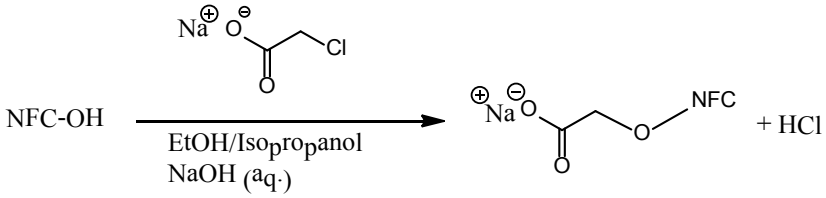

Scheme 5: Carboxymethylation of NFC with chloroacetic acid sodium salt

Similarly to TEMPO oxidation, this reaction has been applied as a pre-treatment before mechanical disintegration, to decrease the energy consumption in NFC production.[54-56] The post-carboxymethylation of NFC has been also envisaged in some papers.[56, 128]

Films prepared from carboxymethylated NFC (cm-NFC) displayed a high transparency,[55, 129] improved mechanical properties[130] and excellent oxygen barrier properties[129]. The dried cm-NFC can be easily re-dispersed in water, indicating that the treatment prevents fiber hornification.[56] But like in the case of TEMPO-oxidized NFC, the thermal-stability of NFC decreases after carboxymethylation,[56] while the hydrophilicity increases.[129]

Different application fields have been reported for cm-NFC. They have been shown to reinforce hydroxypropyl cellulose matrices.[128] They have been also used to prepare polyelectrolyte multilayers for sensor applications, taking advantage of the strong interactions existing between the negatively charged cm-NFC and positively charged polyelectrolytes.[54, 55] Aerogels of cm-NFC have been investigated, with the objective to prepare porous materials with tuneable oleophobicity.[131] By coating paper with cm-NFC, an increase in oil resistance and air permeability was also obtained.[129]

Etherification can be also used to introduce positive charges at the NFC surface, by reacting NFC with choline chloride (Scheme 6):[132]

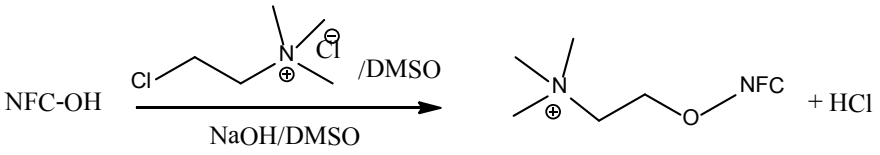

Scheme 6: Cationic functionalization of NFC with choline chloride.[132]

These cationic nanofibres have been used in combination with anionic clays to produce functional films with oxygen and water barrier properties, for packaging applications.[69, 98, 99]

I.5.4.2. Reaction with epoxides

Pei et al.[133] used another etherification route to prepare cationic NFC: they first modified cellulose pulp with glycidyltrimethylammonium chloride (Scheme 7), then subsequently passed the etherified material in a microfluidizor. The quaternized NFC obtained was able to adsorb anionic dyes from aqueous systems.

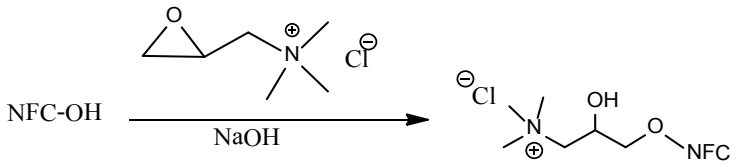

Scheme 7: Etherification of NFC with glycidyltrimethylammonium chloride

In another study, ring-opening etherification was used to introduce azidealkyne groups (Scheme 8), which were further grafted by click chemistry (Scheme 12).[134]

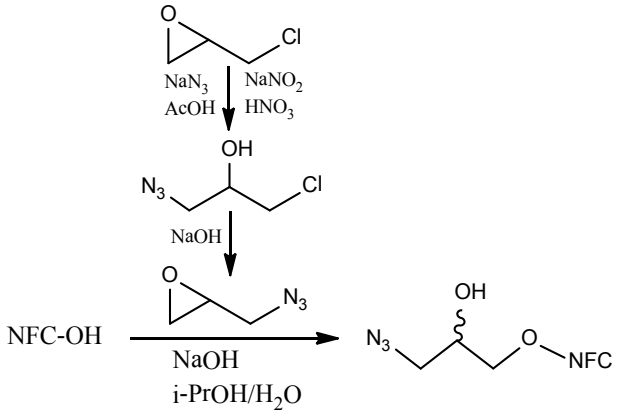

Scheme 8: Etherification of NFC with 1-azido-2,3-epoxypropane.[134]

I.5.5. Carbamylation reactions

Carbamylation with isocyantes is another route to covalently bond organic functions on the surface of NFC (Scheme 9).

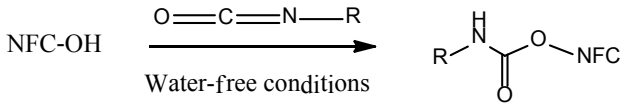

Scheme 9: Carbamylation of NFC with isocyanates

Siqueira et al.[135, 136] have used this functionalization pathway to introduce hydrophobic n-octadecyl chains at the NFC surface and to reinforce poly(ε-caprolactone) matrices. This carbamylation process was further studied by Missoum et al.,[137] to better understand the influence of degree of substitution on final properties. Stenstad et al.[120] grafted hexamethylene diisocyanate at the NFC surface, which they further cross-linked into a hydrophobic polymer layer, or reacted with amines to introduce positive charge at the NFC surface.

I.5.6. Silylation

I.5.6.1. Reaction with chlorosilane

Chlorosilanes can react with NFC hydroxyl groups according to Scheme 10. This reaction liberates HCl as a by-product, which is generally trapped by amine-based molecules.[138]

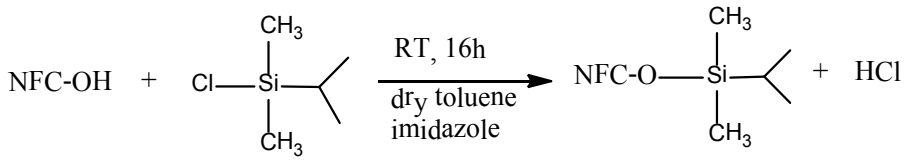

Scheme 10: Silylation of NFC with isopropyldimethyl-chlorosilane[138]

The reaction with isopropyldimethylchlorosilane (IPDMSiCl) in anhydrous toluene allowed producing highly hydrophobic nanofibres, which could be dispersed in THF, toluene, diethyl ether, chloroform, dichlormethane and rapeseed oil.[138, 139] The silylated NFC were shown to be very effective at stabilizing water-in-toluene emulsions, via a "Pickering" process.[140, 141]

Chemical vapour deposition (CDV) has been also envisaged, to graft various chlorosilanes on NFC foams.[131, 142-144] The main purpose and achievement of these works was to create super-hydrophobic materials with tunable oleophilicity/oleophobicity, which could float on the water surface and show selective absorption of non-polar solvents and oil.

I.5.6.2. Reactions with trialkoxysilanes

Alkoxysilanes react with hydroxylated substrates such as cellulose, according to the sol-gel process presented in Scheme 11. Compared with the chlorosilane silylation, the grafted silane structure is rather complex and depends on reaction conditions. Alcohol/water mixtures are generally used as solvent.

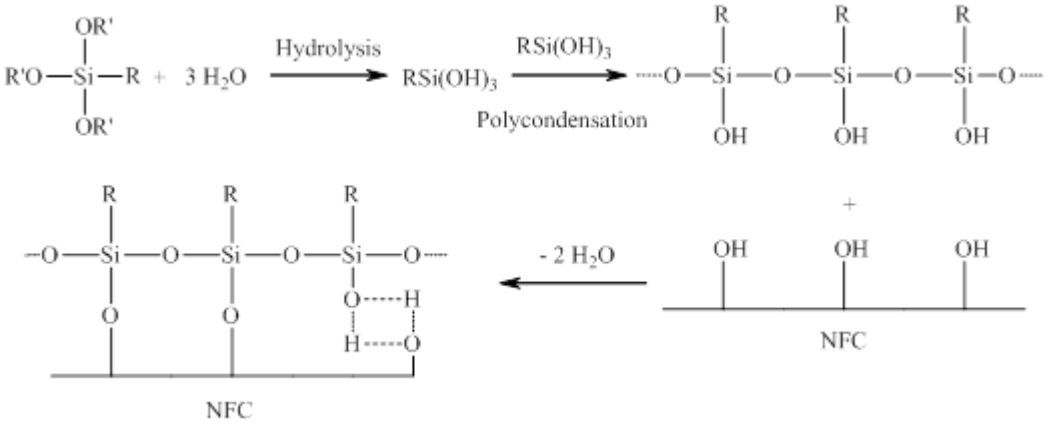

Scheme 11: Silylation of NFC with trialkoxysilanes[145]

With this method, Andresen et al.[146] prepared silylated NFC films which showed antibacterial activity on the surface, using octadecyldimethyl(3-trimethoxysilylpropyl)ammoniumchloride (ODDMAC) in methanol/water (90/10).

Tingaut et al.[147] performed silylation with vinyltrimethoxysilane (MeOSiVi) or 3-mercaptopropyltrimethoxysilane (MeOSiSH) to introduce vinyl or thiol group at the NFC surface for further thiol-ene coupling with click chemistry (Scheme 14).

Qu et al.[145] performed the mechanical disintegration of cellulose pulp in ethanol to produce an NFC suspension which was further modified with 3-methacryloxypropyltrimethoxysilane (MEMO). Polylactic acid (PLA) nanocomposites reinforced with the MEMO-modified NFC displayed improved mechanical properties, but the thermal stability of the NFC decreased after silylation.

Lu et al.[148] modified NFC with (3-aminopropyl)triethoxysilane (APS) and 3-glycidoxypropyl-trimethoxysilane (GLYMO) in acetone, and incorporated the silylated NFC in epoxy resins. They observed an increase in storage modulus of the epoxide composites when NFC was modified with the aminosilane.

Frone et al.[149] modified NFC with APS in ethanol/water mixture prepared PLA composites which displayed better interfacial adhesion after silylation.

Qua et al.[150] performed the GLYMO silylation during the disintegration process, when preparing the NFC. This is the only work reporting silylation in a 100% water system. The nanofibrils obtained were thinner, as the silylation treatment prevented the re-agglomeration

of nanofibrils. The GLYMO-modified NFC was also found to be more thermally stable than the unmodified one.

I.5.7. Other reactions

I.5.7.1. "Click" reactions

The "Click chemistry" concept was firstly introduced by Kolb et al.,[151] who defined a set of criteria that a process must fulfil, such as very high yields, inoffensive by-products, simple reaction conditions, the use of easily removable solvents, or water or no solvent. This concept has been applied to the functionalization of NFC by a few authors. A preliminary functionalization of the substrate is usually required in order to introduce a reactive site (azide, alkene, alkyne group, etc.) that will be later reacted with appropriate molecules.

The Copper-Catalyzed Azide Alkyne Cycloaddition (CuAAC) "click" reaction has been recently used by Pahimanolis et al. to graft 1,2,3-triazole-4-methanamine (route A) or 5-(dimethylamino)-N-(2-propyl)-1-naphthalenesulfonamide (route B) at the NFC surface, in water medium (Scheme 12).[134] The functionalized nanofibrils obtained were pH-responsive and fluorescent, respectively.

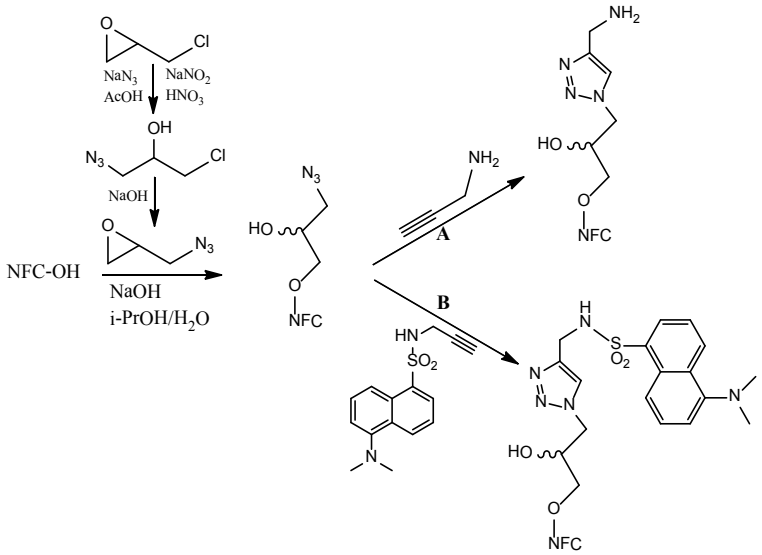

Scheme 12: Functionalization of NFC by Copper-Catalyzed Azide Alkyne Cycloaddition.[134]

Thiol-Ene coupling reactions have also been recently envisaged as an alternative to the azide-alkyne method. These reactions can be catalysed by acids or bases, or photochemically.[147]

Nielsen et al.[152] used methacrylic acid to introduce ene entities at the surface of cellulose nanocrystals, which further underwent thiol-ene reaction with cysteamine (Scheme 13). The objective was to prepare fluorescent labelled nanocelluloses.

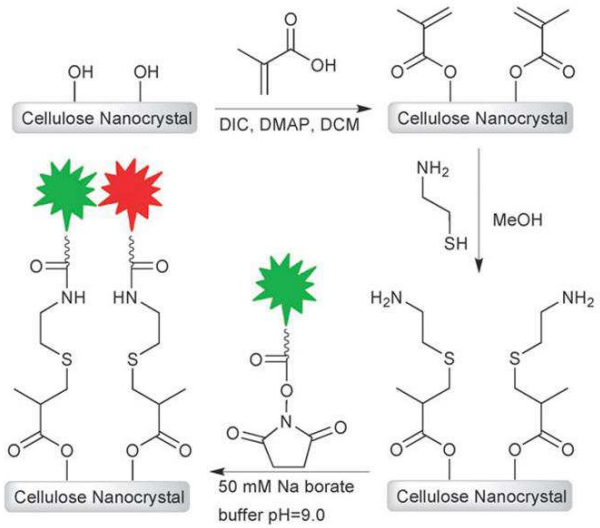

Scheme 13: Fluorescent labelling of cellulose nanocrystals by thiol-ene reaction[152]

In the work of Tingaut et al.,[147] ene or thiol groups were first introduced at the surface of the NFC films by silylation with MeOSiVi or MeOSiSH, respectively (Scheme 14, routes 1 and 2, respectively). The resulting films were subsequently coupled with thiol or ene-functionalized molecules, under UV irradiation and at room temperature, leading to materials with tuneable surface properties.

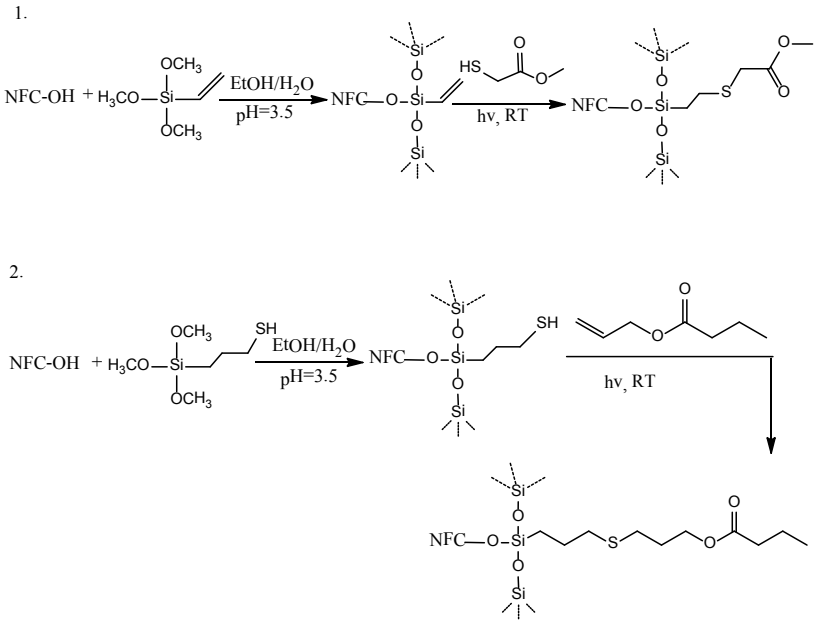

Scheme 14: Functionalization of NFC by silylation and subsequent thiol-ene coupling.[147]

I.5.7.2. Grafting of polymers

It is also possible to graft polymer chains directly at the NFC surface by applying the *graft-from* method. Poly(ε-caprolactone) (PCL) has been accordingly grafted at the surface of NFC by ring opening polymerization and the polymer chain length was controlled by adding different initiator/monomer ratio [153, 154] (Scheme 15). The grafted NFC could be dispersed in low polarity solvents such as THF.

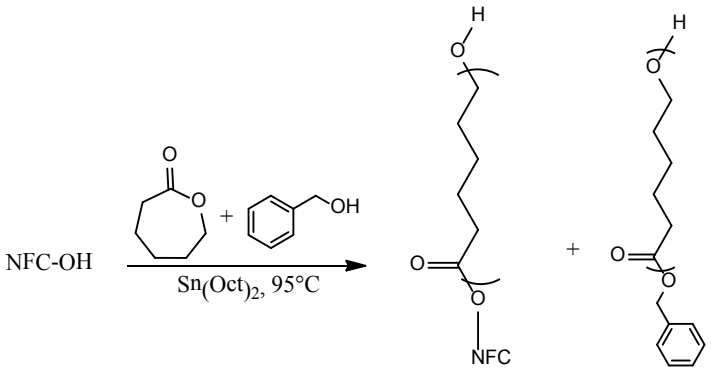

Scheme 15: Grafting of PCL on NFC by ring-opening polymerization.[153]

I.5.8. Concluding remarks and objectives of the thesis

Among all the modification methods discussed above, most of them must be carried out in organic solvents and anhydrous conditions. Hence, time-consuming solvent-exchange steps have to be applied before modification, to disperse the NFC in the reaction medium. This is one of the main drawbacks of the methods, which currently limit their use in industrial applications.

Oxidation reactions, presented in I.5.2, can be carried out in aqueous medium, but the products of negatively charged NFC are more hydrophilic than unmodified NFC, which again limits its applications. Azide-alkyne click chemistry in water medium could be an alternative,[134] but this type of treatment involves many steps and requires the utilization of toxic metal catalysts.

The approach that retained the most of our attention is the silylation method with alkoxysilanes. This reaction involves mild conditions and can be processed in water medium. Moreover, the large variety of functional groups available within commercial alkoxysilanes offers great opportunities to tailor the NFC surface and broaden the spectrum of application of NFC. The rare existing studies on the subject have demonstrated the potential of silylated NFC in composite applications, but the silylation process is not yet totally controlled or

optimized. Moreover, the characterization of the silylated material at the molecular level has not been thoroughly performed. So far, six types of alkoxysilane molecules have been investigated and most of the experimental works involved organic solvents (the only treatment in 100% water was performed during the disintegration process[150]).

In theory, existing knowledge on reactions involving trialkoxysilanes and cellulose (pulp, paper, natural fibres, etc.[155-159]) could be directly applied to the functionalization of NFC. However, preliminary studies performed at the beginning of this thesis highlighted the difficulty to chemically modify the nanofibers when published experimental conditions were adapted to our material. NFC has much higher surface area than macrofibres, which means that more OH groups are accessible at the NFC surface. As a consequence, NFC suffers from irreversible aggregation upon drying, which is not critical for macrofibres. Moreover, interfibrillar interactions must be avoided during silylation, to preserve the nanostructure of the NFC.

In this context, the objective of this thesis was to develop a method based on alkoxysilanes allowing the efficient silylation of NFC in water, while keeping intact the nanofibre structure during modification. The potential of silylated NFC as reinforcing agents in composites or as building block for the elaboration of foams was subsequently investigated.

II. Silylation of NFC with methyltrimethoxysilane: optimization of the treatment and characterization of the silylated material

As introduced in Chapter I, the silylation method with trialkoxysilanes has diverse advantages such as mild reaction conditions, the possibility of using water as reaction medium and the large variety of available functional silanes. Despite the promising potential of this reaction route, studies on the functionalization of NFC with alkoxysilanes are rare, particularly in water. And when this method is envisaged, there is generally a lack of control in the reaction process and in the characterization at the molecular level.

In this chapter, the chemical functionalization of NFC with alkoxysilanes in water medium has been envisaged. Methyltrimethoxysilane (MTMS) has been selected as a model trialkoxysilane molecule for the whole study. The reaction parameters (pH, reaction time and initial silane concentration) have been comprehensively studied and optimized, using two different protocols (*Protocols 1 & 2* described in paragraphs VI.3.1 and VI.3.2, respectively). Furthermore, the modifications have been characterized at the molecular level using appropriate physicochemical techniques.

Before the results are presented and discussed, a brief overview of the main parameters influencing the hydrolysis and condensation of trialkoxysilane is given in the first paragraph.

II.1. Preliminary investigations

II.1.1. Brief overview on the reactivity of trialkoxysilanes

II.1.1.1. Hydrolysis and condensation reactions

Alkoxysilanes are silicon based molecules with the general formula $R'_nSi(OR)_{4-n}$, where n=0, 1, 2 or 3. Due to their hydrolysable Si-OR functions, these molecules have been widely used for the modification of hydroxylated substrates (mostly inorganic), *via* the Sol-gel® process.[160] This process involves i) the hydrolysis of alkoxysilanes into silanols, ii) the polycondensation of silanols into polysiloxanes and iii) the condensation of polysiloxanes

with the hydroxylated substrate (see Scheme 11 in I.5.6.2). Although studies on di-and monoalkoxysilanes also exist,[161-163] trialkoxysilanes are the most used molecules.[164]

The hydrolysis of trialkoxysilanes proceeds step-wise, and the first step is generally slower than subsequent steps (Scheme 16).[165]

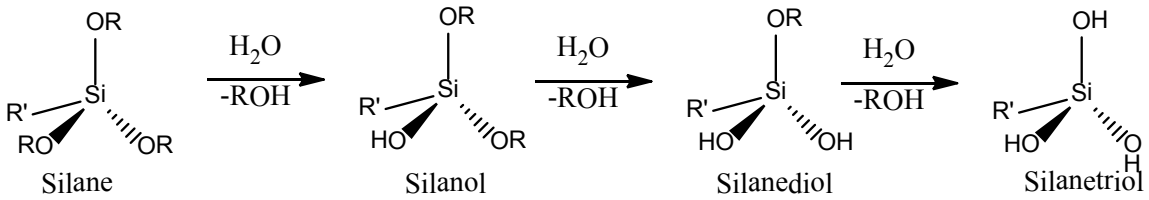

Scheme 16: Step-wise hydrolysis of trialkoxysilanes.[166]

It is a reversible process, but in large excess of water, the equilibrium is shifted towards the silanol formation.[160]

The condensation process is more complex due to numerous sequential and parallel competing reactions.[164] Nevertheless, the formation of siloxane linkages is also a reversible process and can be either obtained through the condensation of two silanol groups (Scheme 17a), or the condensation of an alkoxy group and a silanol function (Scheme 17b).[160]

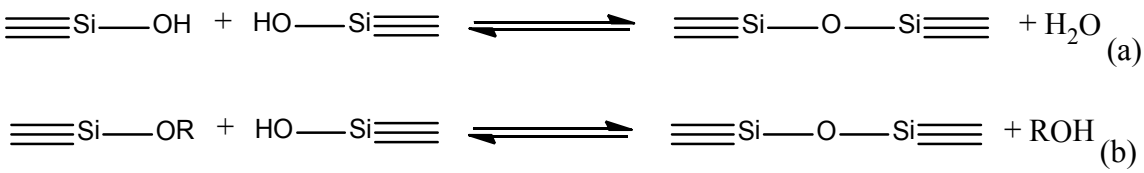

Scheme 17: Formation of siloxane linkages by condensation reactions[160]

In practice, condensation can start before the hydrolysis is completed (Scheme 18a).[167] As products, a series of species can be formed, such as cage-like structures,[168, 169] ledder structures,[170] less organized structures,[169] etc. Some examples are shown in Scheme 18b.

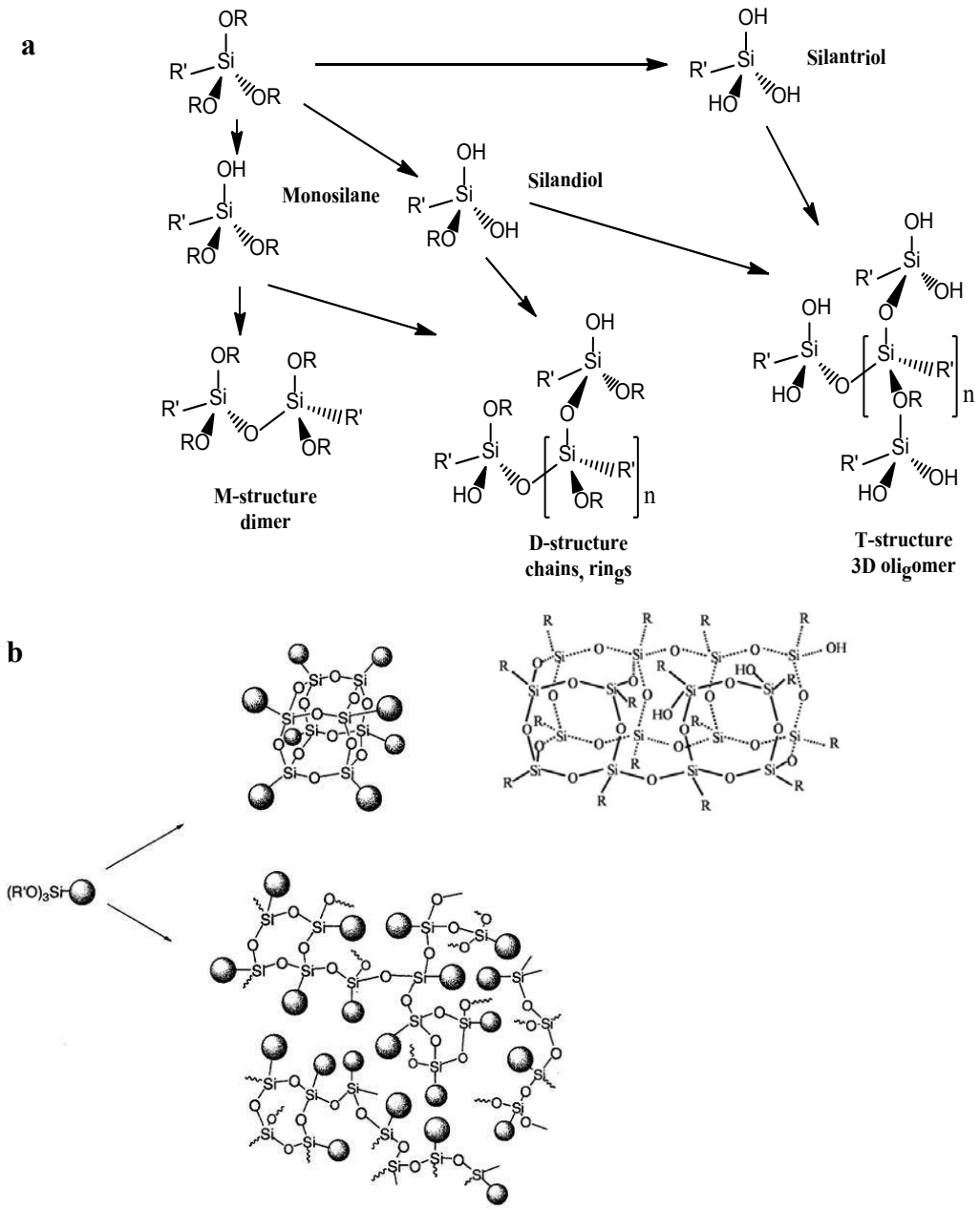

Scheme 18: (a) Oligomers formed during hydrolysis and condensation.[167] (b) Examples of oligomer structures: cage-like structures (upper)[168, 169] and various amorphous species (lower) [169]

II.1.1.2. Impact of pH

a) Hydrolysis

The hydrolysis of alkoxysilane molecules can be catalyzed by both acids and bases, such as HCl, H_2SO_4, acetic acid, ammonia, organotin esters, tirethylamine, KOH, KF, KH, etc.[160, 171, 172] A relationship exists between the rate of hydrolysis and pH: the reaction is slow at pH 7,[164, 165, 173] but each unit change in pH (in both directions), causes at least a 10-fold acceleration of the hydrolysis rate.[164]

b) Condensation

Condensation reactions are catalysed by both acids and bases, but also by neutral salts or metal alkoxydes.[160] A pH dependance profile has been highlighted by many researchers:[160, 165, 167, 171, 174, 175] condensation is fast at high and low pH, but the rate is minimum at pH 4, considered as isoelectric point of trialkoxysilanes.[160, 174]

In acidic conditions, hydrolysis is much faster than condensation, whereas in basic conditions, condensation occurs before all the alkoxy groups are hydrolysed.[164]

II.1.1.3. Impact of silane-to-water ratio

Silane-to-water ratio has been shown to play an important role in the kinetics of hydrolysis and condensation of trialkoxysilanes molecules. In agreement with the reversible mechanisms of the hydrolysis and condensation reactions, an increase in silane concentration has been shown to provoke a decrease in hydrolysis rate,[171] while the concentration of polymerized species increased.[160, 167, 171]

II.1.1.4. Impact of steric and inductive effects

The steric hindrance of alkoxyl groups (OR) tend to retard the kinetics of hydrolysis and condensation reactions.[160] Accordingly, hydrolysis and condensation reactions are generally faster for methoxysilanes. The reaction rates decrease in the order: methoxysilane>ethoxysilane>n-propoxysilane>n-butoxysilane>i-butoxysilane.[166, 176]

The steric hindrance of the alkyl substituent (R') also impacts both hydrolysis and condensation reactions. It has been shown that the rate constant of hydrolysis decreased several orders, when the chain length of R' increased form methyl to propyl.[177] In the same way, a decrease in the condensation rate is usually noted when the length and branching of the alkyl chain increase.[178]

Concerning the inductive effects, differences are noted depending on the pH. The hydrolysis rate increases with the electron-providing capacity of the alkyl substituent (R') in acidic medium, while it is the opposite under basic conditions (electron-withdrawing groups accelerate the reaction).[160]

Condensation is also impacted by inductive effects since OSi is more electron-withdrawing than OR, but steric effects are increasingly dominant as the reaction proceeds.[160]

II.1.1.5. Impact of reaction time

The structure of the species formed during the hydrolysis/condensation process depends strongly on the reaction time. In general, hydrolysis occurs very rapidly in acidic conditions (within minutes).[179] For condensation, an increase in reaction time generally leads to the formation of oligomers of higher molecular weight,[176] while di- and tri-condensed structures are favoured.[179]

II.1.2. Calibration chart for the evaluation of the Si content from IR spectra

To comprehensively study the impact of reaction parameters on NFC silylation, we needed a method to follow the evolution of silane content as a function of pH, reaction time or silane concentration. One method was to measure the silicon content in silylated NFC by elemental analysis (EA), as already reported by several authors for silylated cellulose fibres.[158, 159, 180, 181] But this characterization method turned out to be very expensive and could not be used to characterize all our samples. In this context, we decided to build a calibration chart based on a limited number of samples (15 samples), which we analysed by both EA and FTIR spectroscopy. In the chart, the Si wt% was correlated with a ratio measured by FTIR spectroscopy and characteristic of the grafted silane. This chart was later used to deduce the Si wt% based only on FTIR spectra.

II.1.2.1. FT-IR characterization of silylated NFC

15 samples of silylated NFC were characterized by both EA and FTIR spectroscopy. For a given sample, three spectra were recorded and averaged. An example of spectra obtained before and after silylation is presented in Figure 14.

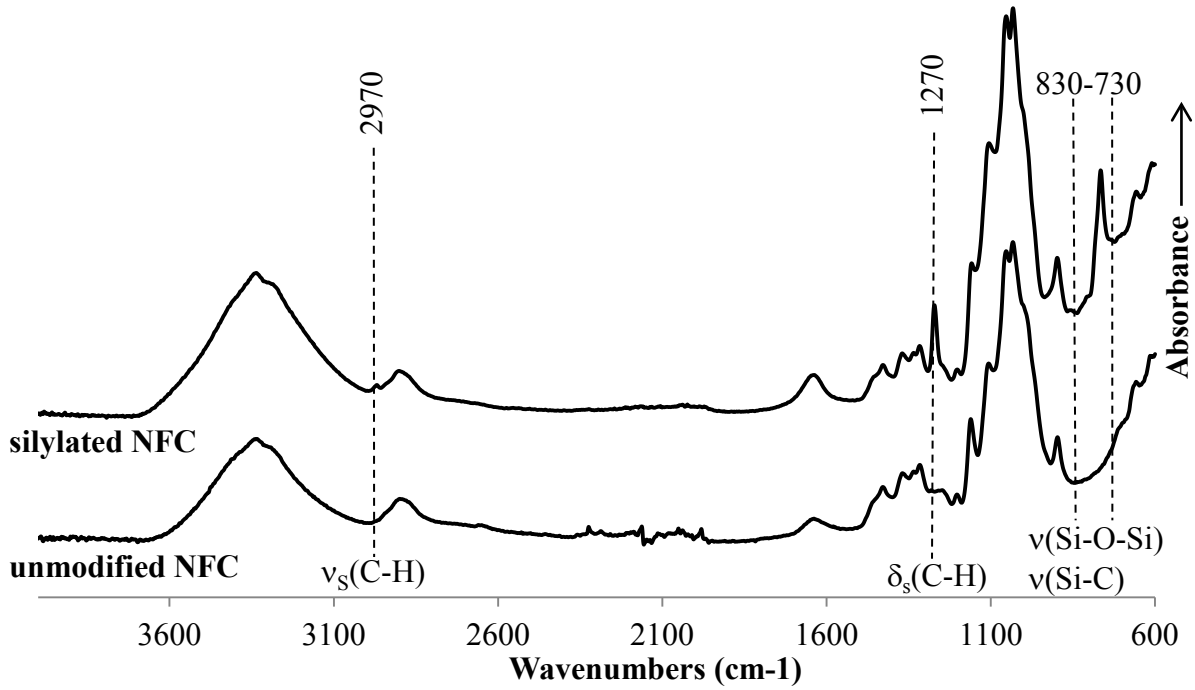

Figure 14: Example of FTIR spectra obtained after analysis of unmodified and MTMS-treated NFC (*Protocol 1*) samples. ν, stretching vibration; δ, in-plane bending, γ, out-of-plane bending.

In the spectrum of unmodified NFC, the characteristic vibrations of cellulose emerge at 3300 cm^{-1} (ν_{OH}), 2870cm^{-1} (ν_{CH}), 1426cm^{-1} (δ_{CH}), 1367cm^{-1} (δ_{CH}), 1332 cm^{-1} (δ_{OH}), 1317 cm^{-1} (δ_{CH}), 1200 cm^{-1} (δ_{CH} and δ_{OH}), 1157-893 cm^{-1} (ν_{C-O} and ν_{C-C}) and 651 cm^{-1} (γ_{O-H}).[182]

After modification with MTMS, the vibrations of the grafted groups were easily identified at 2970 cm^{-1} (ν_{C-H} of the methyl group), 1270 cm^{-1} (δ_{C-H} of the methyl group),[183] and between 830 and 730 cm^{-1} (ν_{Si-C} and/or ν_{Si-O}).[184]

II.1.2.2. Calibration chart

In preliminary experiments, we observed that the C-H in-plane bending vibration at 1270 cm^{-1} seemed to increase linearly with increasing silane content. Accordingly, this vibration was chosen to estimate the silane content from the IR spectra. The vibration at 1270 cm^{-1} was normalized to the intensity of the C-H in-plane bending of cellulose at 1317cm^{-1}, through the calculation of the H_{1270}/H_{1317} peak heights ratio. The vibration of cellulose at 1317 cm^{-1} was selected as an internal standard because it was not affected by the modification with MTMS. The calibration chart was then obtained by plotting the Si percentage determined by elemental

analysis as a function of the H_{1270}/H_{1317} ratio (Figure 15). The correlation coefficient of the calibration curve was 0.96. The scattering of the experimental points was assigned to inhomogeneity in the distribution of silane within the NFC network, leading to samples with slightly varying Si content. Although this calibration chart is not suitable for an exact evaluation of the Si content at the NFC surface, it turned out to be accurate enough to follow the evolution of Si content in our various experiments. For a given silylated sample, the Si content was accordingly estimated from its FTIR spectrum, by simply calculating the H_{1270}/H_{1317} ratio and reporting the value on the calibration chart.

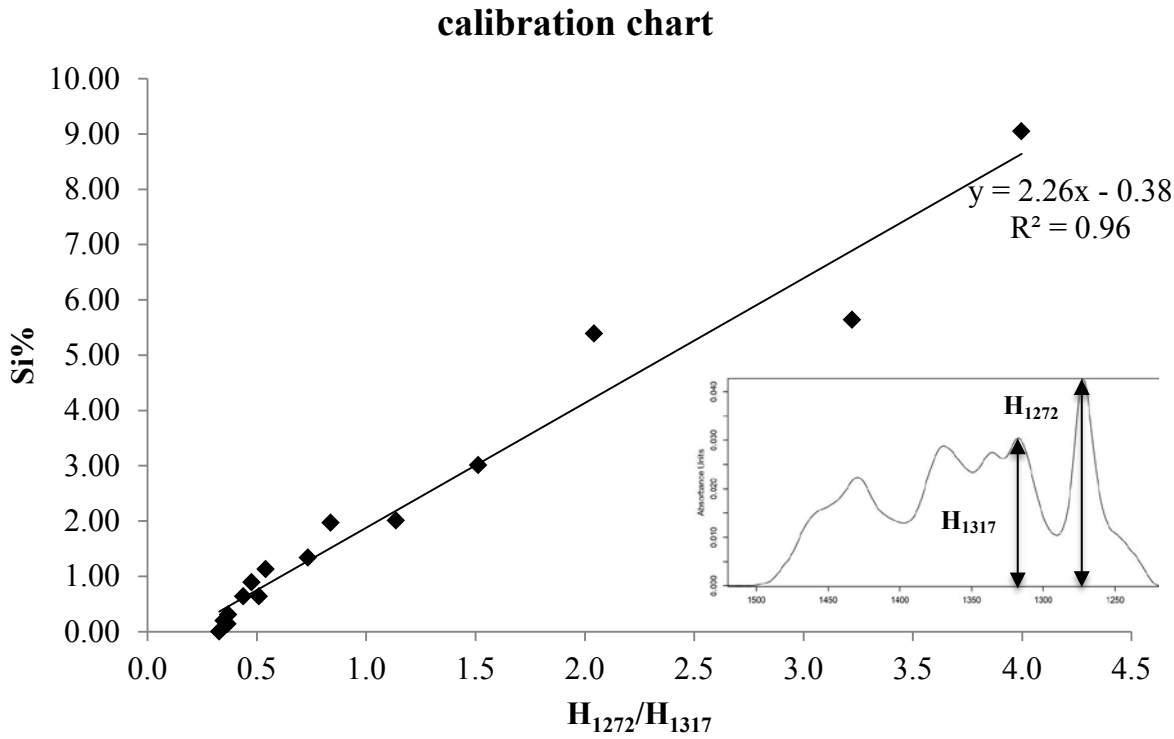

Figure 15: Calibration chart for the estimation of silane content from FTIR data.

II.2. Impact of reaction parameters

Three reaction parameters have been comprehensively studied and optimized: pH, reaction time and silane concentration. The evolution of Si content in the silylated material was estimated from the calibration chart in Figure 15. All the samples were characterized by solid-state NMR spectroscopy (^{13}C and ^{29}Si), SEM and WDX microscopy.

II.2.1. Experimental protocols

Two different protocols were envisaged depending on the experiments (*Protocols 1 & 2* described in paragraphs VI.3.1 and VI.3.2, respectively).

With *Protocol 1*, reactions were performed by i) stirring the NFC silane solution for a given reaction time, ii) washing the cellulosic substrate with water, iii) eliminating water by freeze-drying. Hence, with this protocol, any excess of acid or base, which may detrimentally impact the cellulose chains, was concurrently eliminated. This protocol was selected when studying the impact of pH on NFC silylation, because it could limit cellulose degradation, when high or low pH was investigated. We reasoned any silane that was bonded to the cellulosic substrate during the stirring step would remain attached during the washing step.

The same conditions were used with *Protocol 2* except that the silylated material was not washed before freeze-drying. As a consequence, all chemicals introduced in the reaction vessel, *i.e*. the silane (bonded or not) and the catalyst, remained in the dry material after freeze-drying. To favour the condensation between the hydrolysed MTMS and cellulose, the silane solution was adjusted to a single pH of 4, since the silanol concentration is expected to be maximal at this pH (see Chapter II.1.1.2). High and low pH were avoided to limit cellulose degradation.

II.2.2. Impact of pH (*Protocol 1*)

Reactions were performed at room temperature, for 2h, using an initial MTMS concentration of 7.4 mmol/g_{NFC}. The pH was varied between 0 and 11 by adding hydrochloride acid for the acidic range and sodium hydroxide for the basic range.

II.2.2.1. Evolution of Si content

The evolution of Si content as function of pH is presented in Figure 16. No silane was found in the material at pH above 2, but below this value, the silane content tended to increase with decreasing pH. The sample treated at pH 0.2 displayed an unexpected low Si wt% value (0.8%), which was assigned to inhomogeneities in the distribution of silane within the NFC network, and also to the low resolution of the calibration chart method used to evaluate the Si content.

After hydrolysis of MTMS, the silanols formed can homopolymerize by polycondensation and/or condense with the NFC surface (Scheme 11 in I.5.6.2). Both reactions are in

competition, and there was no guaranty at this stage of the study that the silane found in the samples (when pH < 2) was covalently bonded to the cellulosic substrate. In general, the rate of condensation decreases with increasing pH and is minimal at pH 4, where silanol concentration is maximal (see Chapter II.1.1.2).[160, 174] Hence, high molecular weight polysiloxanes with low solubility in water could be favored at low pH, while low molecular weight species with high silanol content may prevail at pH above 2. The decrease in silane content with pH could then be explained by an increasing solubilisation of the polar silanol species in water during the washing step. The remaining high molecular weight species may then be bonded or not to the cellulosic substrate.

At basic pH, the hydrolysis of alkoxysilanes is generally much slower (see II.1.1.2),[164] and 2h may not be sufficient to hydrolyse the silane in our experimental conditions (reaction time = 2h; [MTMS] = 7.4 mmol/g_{NFC}). Additionally, the reverse reaction of condensation is favoured under basic conditions, leading to formation of more soluble species,[160] which could be removed as well by the washing step.

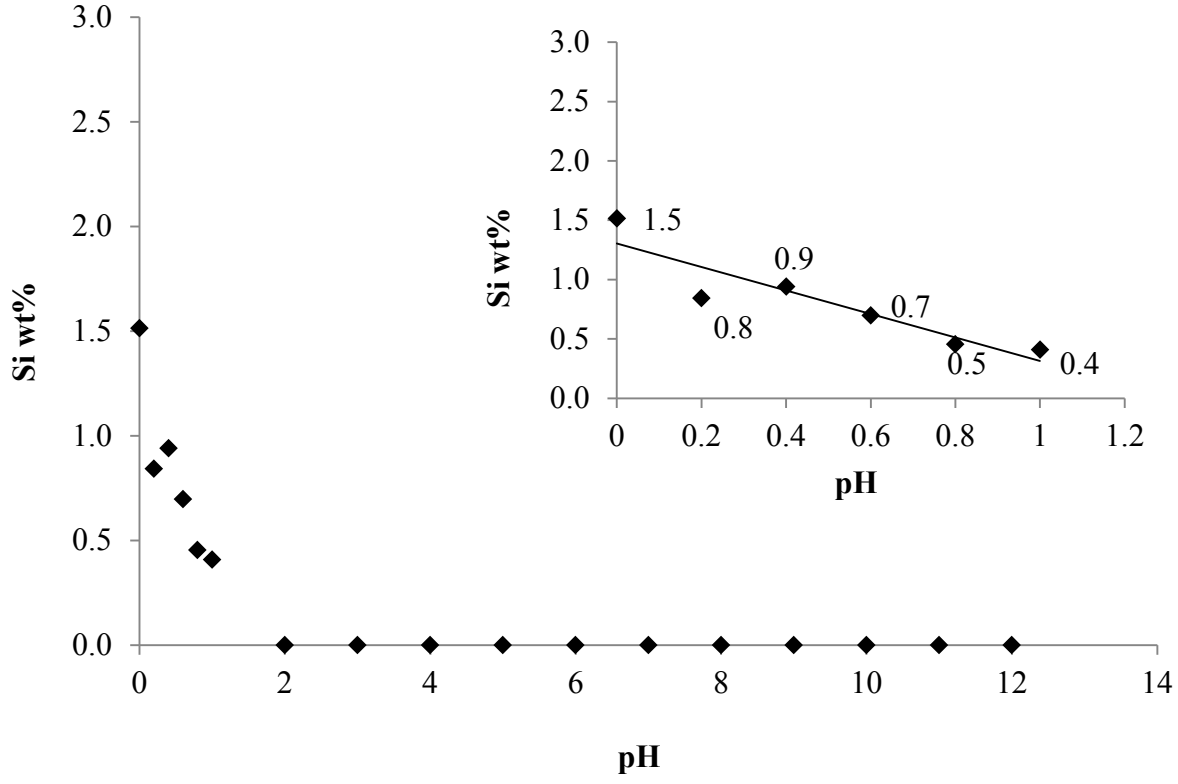

Figure 16: Evolution of the Si content as function of pH for NFC treated with MTMS according to *Protocol 1*. The insert plot presents the pH range 0-1.

II.2.2.2. Solid State NMR spectroscopy

The silylated samples were further characterized by ^{13}C and ^{29}Si CP-MAS NMR spectroscopy. Only the samples for which the Si wt% was significant were analysed (*i.e.* pH below 0.6).

a) ^{13}C CP-MAS NMR

The ^{13}C CP-MAS NMR spectra of unmodified and silylated NFC are presented in Figure 17. The spectrum of unmodified NFC displayed typical signals from cellulose that were assigned as follows: C_1 (105 ppm), C_4 crystalline (89 ppm), C_4 amorphous (83 ppm), $C_2/C_3/C_5$ (75 and 73 ppm), C_6 crystalline (65 ppm).[27]

After silylation with MTMS, the signal characteristic of the grafted methyl group emerged at around -3 ppm (C_α in Figure 17), confirming the presence of silane in the samples. The intensity of this peak was quite low for samples with Si content below 0.9 wt %, but it increased significantly at higher silylation level. No additional peak corresponding to the carbons of methoxyl groups were detected at 50 ppm, indicating that most of these groups were hydrolyzed during the treatment.

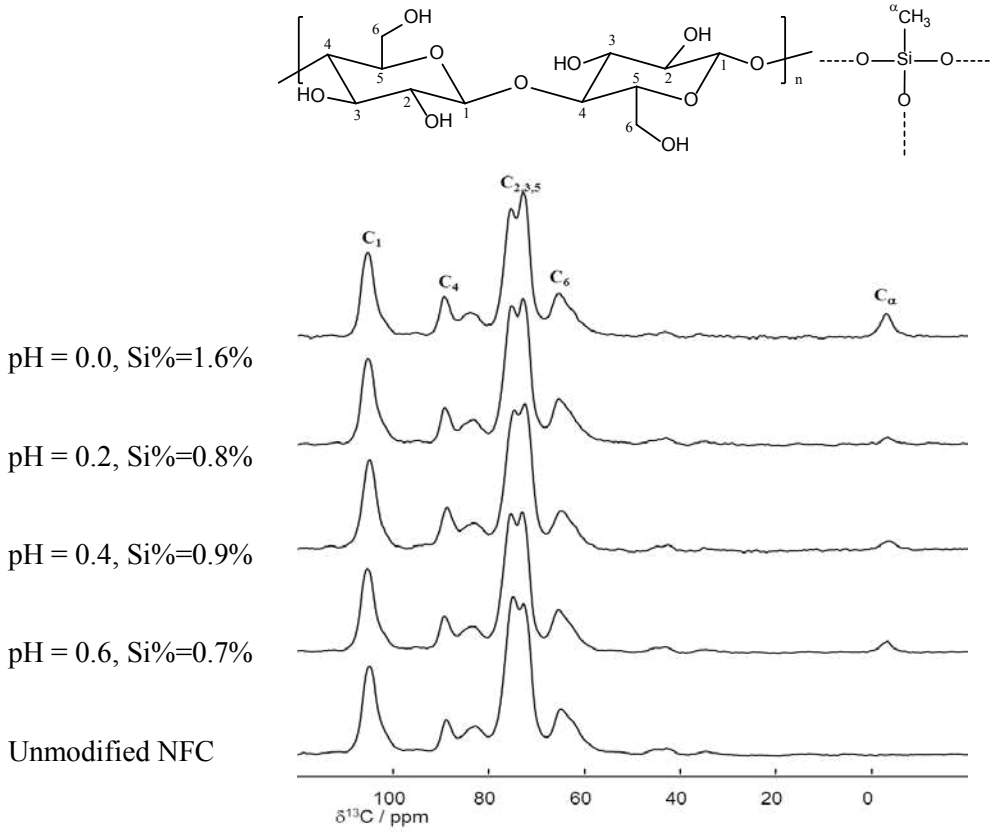

Figure 17: ^{13}C CP-MAS NMR spectra of unmodified and MTMS-modified NFC prepared at different pH

b) ^{29}Si solid state NMR

The chemical shift of ^{29}Si is sensitive to its local electronic environment and chemical changes about the silicon have been shown to provide significant shifts in the ^{29}Si NMR spectrum.[185, 186] In the following discussion, each silicon signal was assigned according to its chemical environment and was noted T_i or T_{ij}, where T is the trifunctional alkoxysilane; i the number of siloxane bridges (–OSi) attached to the site; j the number of hydroxyl groups (–OH) attached to the site. In this conventional nomenclature system, the $–Si(OSi)_1(OMe)_2$ moety is a T_{10} site, $–Si(OSi)_2(OMe)$ a T_{20} site, $–Si(OSi)_2(OH)$ a T_{21} site, etc..

The ^{29}Si CP-MAS NMR spectra of silylated NFC in Figure 18, confirm the presence of polysiloxane at the NFC surface. After silylation, two different environments were found for the silicon atom at -56 and -65 ppm. Before hydrolysis/condensation, the signal of silicon in MTMS is expected at -40 ppm, as was confirmed by liquid-state ^{29}Si NMR analysis (results not shown). It has been reported that the condensation of Si-OR into Si-OSi linkage results in an upfield shift of about 8-9 ppm for the silicon, when hydrolysis of the Si-OR linkage to Si-OH results in a downfield shift of 1-2 ppm.[186] Accordingly, the chemical shifts at -56 and -65 can be assigned to T_2 and T_{30} sites respectively, which can form after the di- and tri-condensation of MTMS. These assignments are in agreement with literature data.[169] The high intensity noted for the T_{30} signal indicates that significant homopolymerisation occurred during the treatment. T_{30} sites have no available functions, which can potentially covalent or hydrogen bond with the cellulosic substrate. As a consequence, the polysiloxane detected by NMR spectroscopy can be attached (if attached) only via the di-condensed species (*i.e.* T_2 sites). T_2 sites can carry alkoxyl groups (T_{20}) and/or silanol functions (T_{21}), which cannot be differentiated by the ^{29}Si CP-MAS technique. If T_{20} sites are present, a covalent bond with cellulose can be proposed (cellulose-O-Si) since most methoxyl groups have been cleaved during the hydrolysis process (the signal of methoxyl is expected at 50 ppm in the ^{13}C and at -40 ppm in the ^{29}Si CP-MAS spectrum). If uncondensed T_{21} sites subsist, the polysiloxane could be bonded to the cellulosic substrate by hydrogen bonding. But the absence of bonding at the cellulose surface cannot be ruled out, and the siloxane polymer could be simply adsorbed or entangled in the cellulose network (as will be demonstrated later, in Chapter II.3.1).

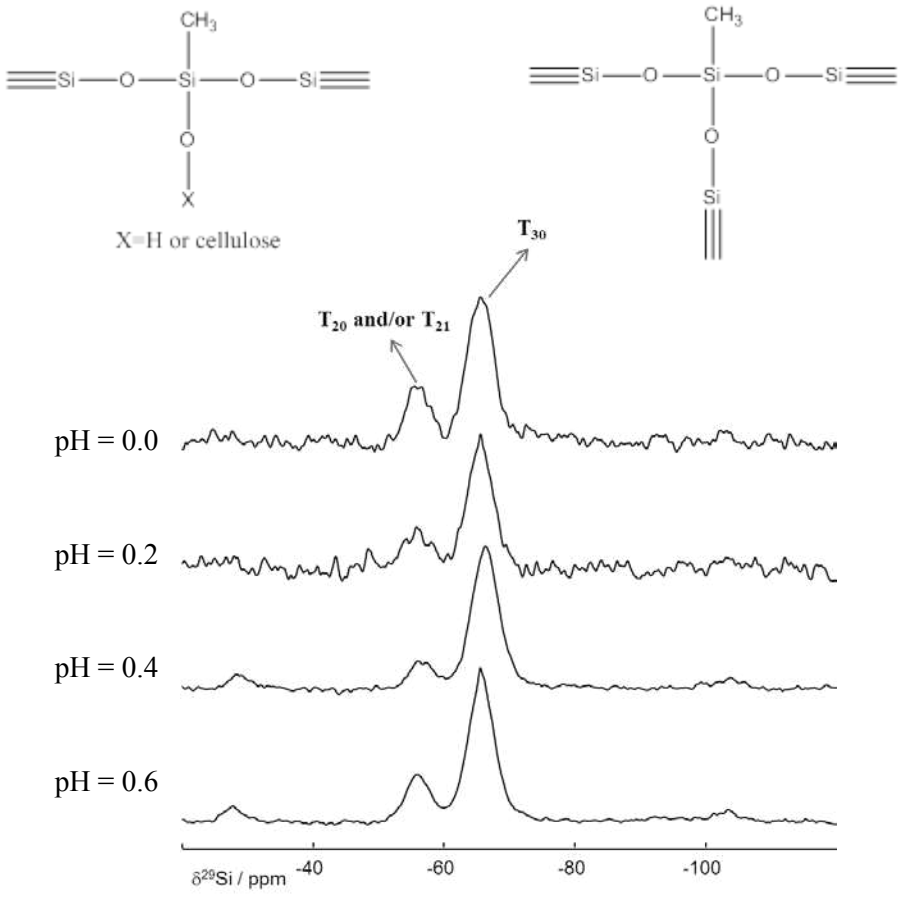

Figure 18: ^{29}Si CP-MAS NMR spectra of MTMS-treated NFC prepared at different pH. The signals at -28 and -104 ppm correspond to the spinning side bands of T_{30} at -65 ppm.

In order to evaluate the evolution of di- and tri-condensed structures in the modified NFC, each spectrum was deconvoluted and the ratio of the peaks area at -56 and -65 ppm (T_2/T_3 ratio) was calculated and plotted as a function of pH (Figure 19).

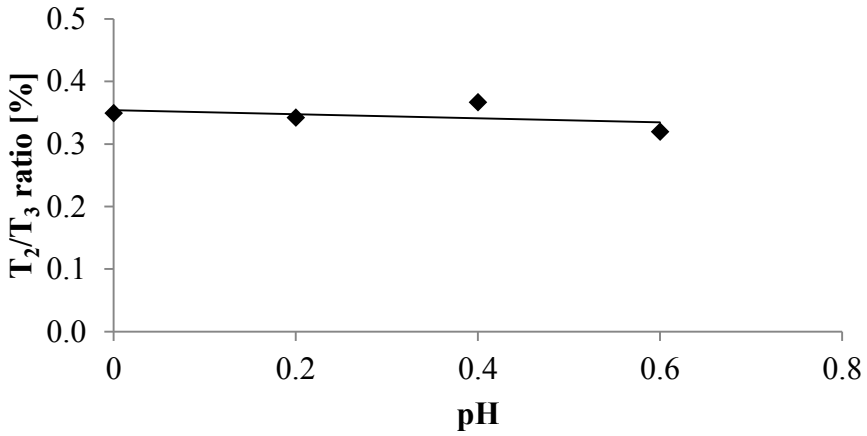

Figure 19: Evolution of the ratio of the peaks area at -56 and -65 ppm (T_2/T_3 ratio), as a function of pH.

The T_2/T_3 ratio was almost constant in all samples, indicating that the pH variations in the conditions used (reaction time = 2 h; $[MTMS]_i$ = 7.4 mmol/g_{NFC}) did not impact the structure of the polysiloxane on the NFC surface. Only the polymer content was impacted.

II.2.2.3. SEM and WDX Microscopy

The evolution of the NFC morphology upon silylation was examined using Scanning Electron Microscopy (SEM) and the resulting micrographs are presented in (Figure 20).

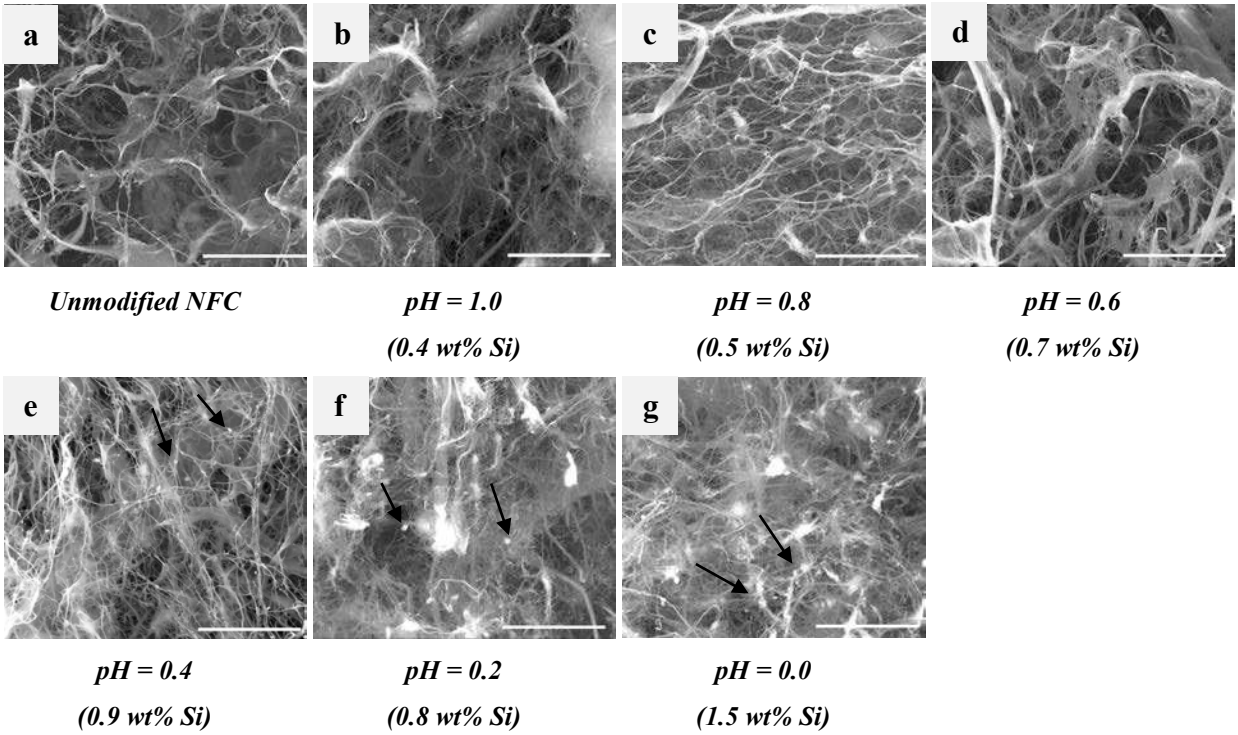

Figure 20: SEM micrographs of unmodified NFC (a) and NFC treated with MTMS (*Protocol 1*) in the pH range 1-0 (b-g). (Scale bar is 10 μm).

The SEM image of unmodified MFC (Figure 20-a) confirmed the presence of a 3-D network of nanofibrils with diameters in the range of 50 to 200 nm, with few visible aggregates. This result is in agreement with the literature and confirms that the freeze-drying process used in *Protocol 1* (fast freezing) maintained the nanofibrillar structure of NFC upon drying.

After silylation, the nanofibrillar structure prevailed in all samples, regardless of the pH (Figure 20- b-g). The presence of silane was detected in the form of white particles or clusters within the cellulose substrate (see arrows in Figure 20), which are most probably constituted of homopolymerized MTMS. Their number tended to increase with decreasing pH, *i.e.* when the Si content increased in the sample.

In order to validate this assumption, the various cellulosic substrates were further analysed by WDX (Wavelength Dispersive X-ray) microscopy (Figure 21). The micrographs provide a mapping of the Si element on flat surfaces, and give information about the presence and size of eventual clusters. A scale bar with arbitrary units is presented next to the map and the quantity of Si detected by X-ray is materialized with a colour. The images have to be compared with caution, because the morphology, surface roughness and sample inhomogeneity can impact the colour of the mapping.

The unmodified and silylated NFC samples produced in the pH range 1-0 were accordingly compressed to flat films and analysed with this technique. The results are presented in Figure 21.

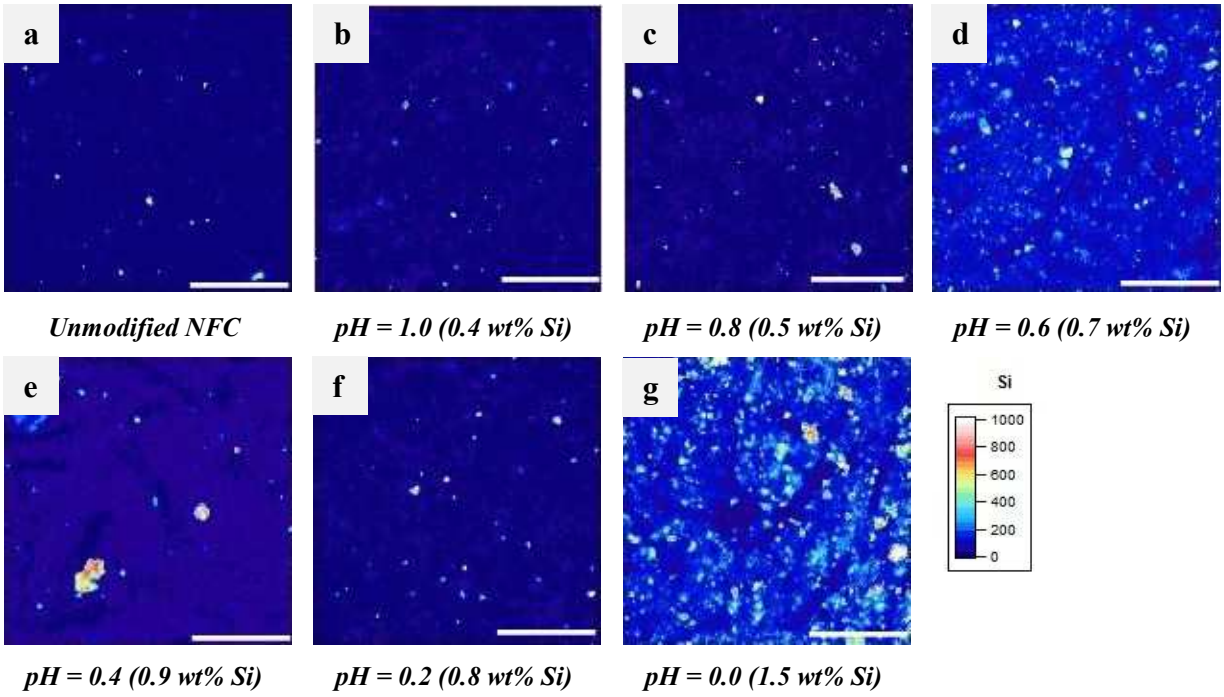

Figure 21: WDX Si mapping of unmodified NFC (a) and NFC treated with MTMS in the pH range 1-0. (Scale bar is 100 μm).

The silicon mapping of unmodified NFC displayed a dark and uniform blue color with few white spots, which were associated with impurities in the sample. In the starting cellulose pulp material, traces of Si have been confirmed. After silylation, the brightness of the image as well as the proportion of Si aggregates tended to increase with increasing polysiloxane content, confirming the SEM results. But the polysiloxane is not homogeneously dispersed within the NFC material, since more Si is detected in Figure 21d (0.7 wt% Si), compared with Figures 25e (0.9 wt% Si) or 25f (0.8 wt% Si).

When *Protocol 1* was used in further experiments, pH 0.4 was selected, to limit cellulose degradation as much as possible.

II.2.3. Impact of reaction time (*Protocol 1 & 2*)

Both *Protocol 1* (with washing step, pH 0.4) and *Protocol 2* (without washing step, pH 4) were investigaed. Reactions were performed at room temperature, using an initial MTMS concentration of 7.4 mmol/g_{NFC}. The reaction time was varied from 0.5 to 72 h.

II.2.3.1. Evolution of Si content

The evolution of Si content as function of reaction time is presented in Figure 22, for samples treated according to *Protocol 1* or *Protocol 2*.

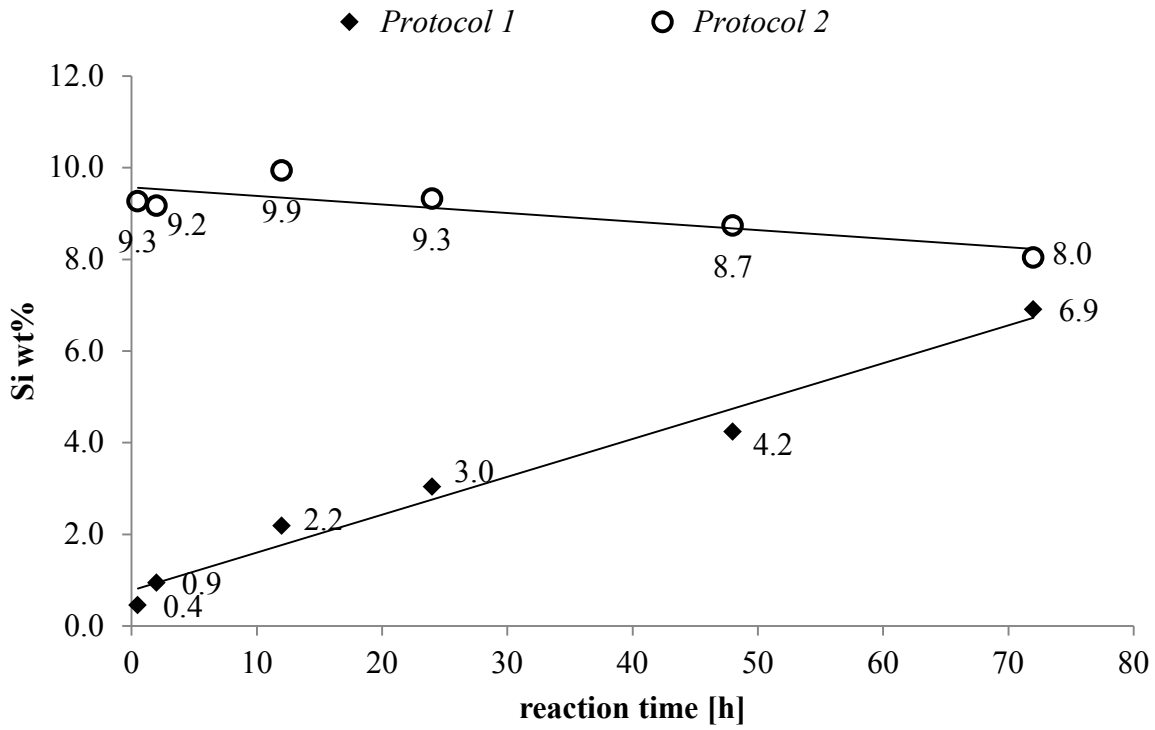

Figure 22: Evolution of Si content as function of reaction time for NFC treated with MTMS according to *Protocol 1* (pH 0.4) or *Protocol 2* (pH 4).

With *Protocol 1*, a gradual increase in Si content was noted with increasing reaction time. Since the washing step removed all non-bonded water-soluble compounds, this increase could be explained by the formation of an increasing number of oligomers or polymers insoluble in water. Another possibility would be that silane condensation at the NFC surface increased with reaction time, but leaching experiments performed in Chapter II.3.1 seem to contradict this interpretation.

With *Protocol 2*, the silylated material was not washed during the process and all the silane introduced in the reaction vessel remained in the dry material after freeze-drying. Consequently, the Si content in the samples remained constant with time, as observed in Figure 22.

II.2.3.2. Solid State NMR spectroscopy

a) ^{13}C CP-MAS NMR

The ^{13}C CP-MAS NMR spectra of NFC silylated at different reaction times are presented in Figure 23. Regardless of the protocol, the carbon of the MTMS methyl moiety was detected at -3 ppm in most of the spectra (carbons α according to the nomenclature in Figure 17). The intensity of the C_α peak increased steadily with reaction time in the case of *Protocol 1*, while it remained quasi constant with *Protocol 2*, confirming further the results of Figure 22.

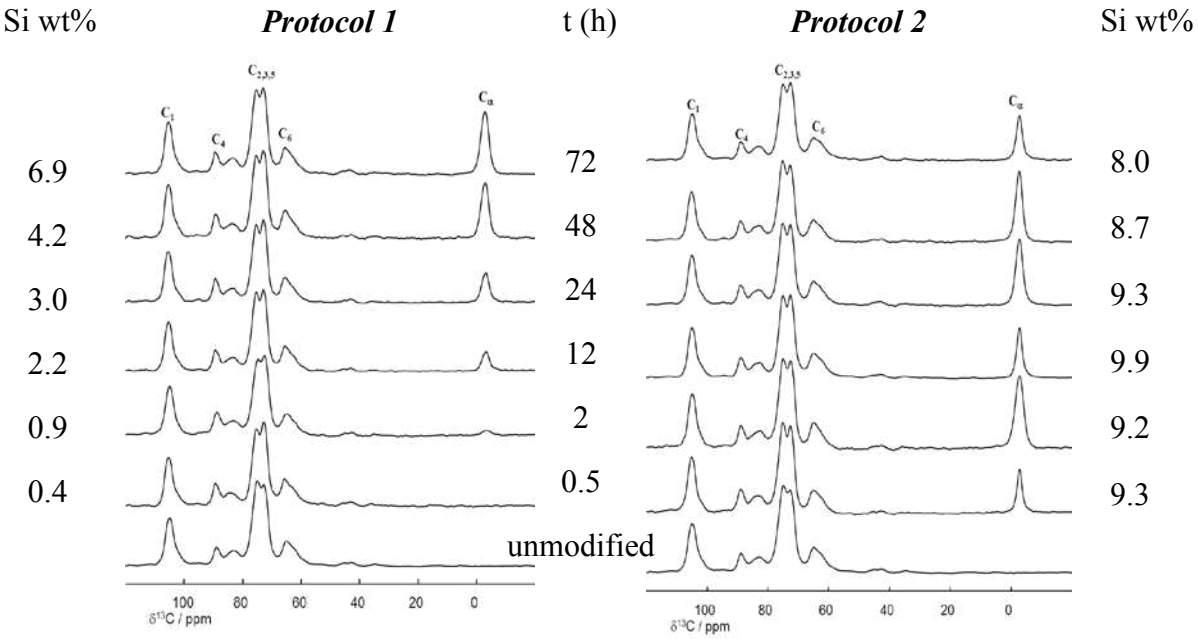

Figure 23: ^{13}C solid state NMR spectra of unmodified and MTMS-treated NFC prepared at different reaction times (*Protocol 1 & 2*).

b) ^{29}Si solid state NMR

The ^{29}Si CP-MAS NMR spectra of NFC silylated at different reaction times are presented in Figure 24.

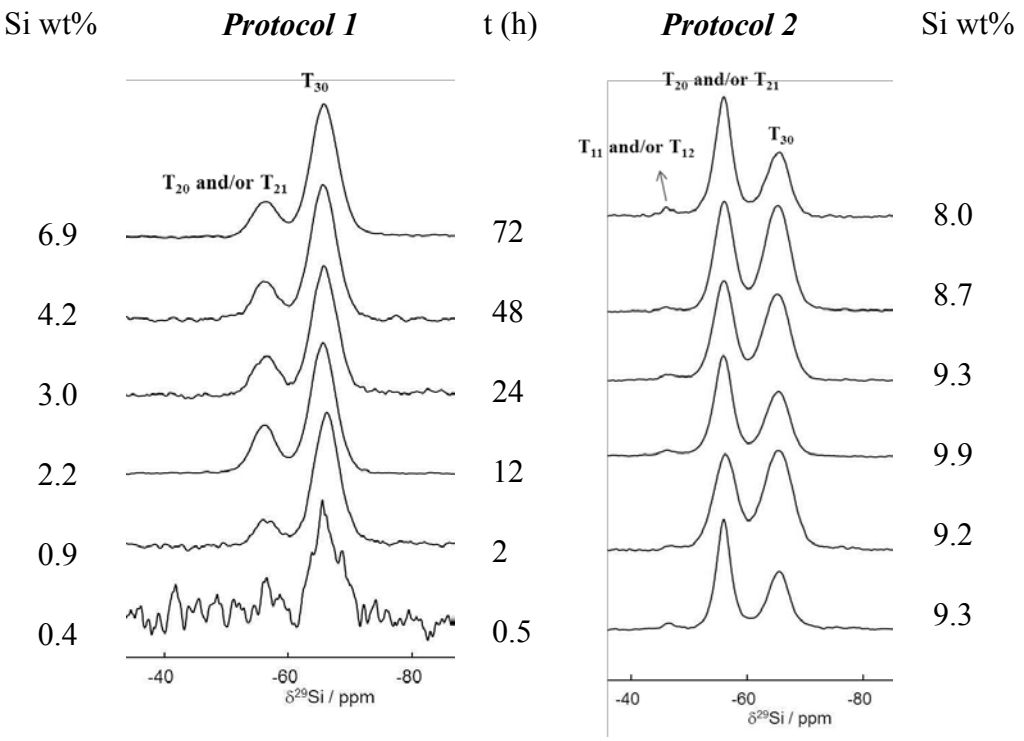

Figure 24: ^{29}Si CP-MAS solid state NMR spectra of MTMS-treated NFC prepared at different reaction times (*Protocol 1 & 2)*.

Once again, two different signals were detected at -56 and -65 ppm, regardless of the protocol, but the relative intensity of the peaks was significantly different depending on the method. These two signals were again assigned to di-condensed (T_{20} and/or T_{21}) and tri-condensed (T_{30}) structures, respectively, which can form after hydrolysis and condensation of MTMS. As previously argued (II.2.2.2b), the polysiloxane detected could be attached via the di-condensed sites, or could be also simply adsorbed or entangled in the cellulose network. With *Protocol 2*, a small additional signal was detected at -46 ppm and was assigned to residual T_1 structures bearing Si-OH moieties (T_{11} or T_{12}). These moieties may arise from the chain ends or from monocondensed species present in the substrate.[168] Since this signal was not observed in the spectra of samples prepared according to *Protocol 1*, they are probably eliminated in water during the washing step.

After deconvolution of the spectra, the ratio of the peaks area at -56 and -65 ppm (T_2/T_3 ratio) was calculated and plotted as a function of reaction time (Figure 25). The T_1 structures detected -46 ppm (*Protocol 2*) were not taken into consideration due to their negligible contribution.

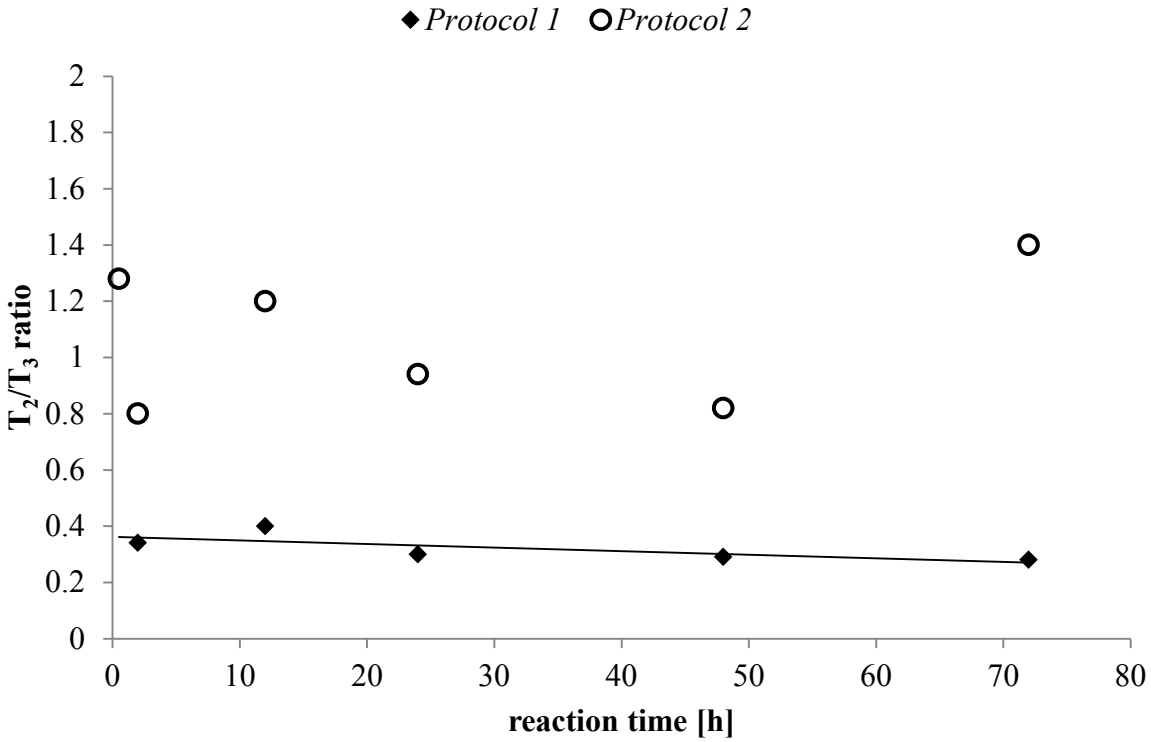

Figure 25: Evolution of the ratio of the peaks area at -56 and -65 ppm (T_2/T_3 ratio) as a function of reaction time.

With *Protocol 1*, the T_2/T_3 ratio was quasi constant in all samples ($T_2/T_3 \approx 0.3$), indicating that the reaction time in the conditions used did not significantly impact the chemical structure of the polysiloxanes bonded or dispersed in the NFC network.

In contrast, the T_2/T_3 ratio tended to fluctuate with reaction time, when *Protocol 2* was used, and more T_2 sites were found in that case. On average, there were quasi as may T_2 structures than T_3 structures in the silylated samples. With *Protocol 2*, reactions are performed at pH 4, which is considered as the isoelectric point of trialkoxysilanes.[160, 174] Homocondensation of alkoxysilanes is minimized at this pH and the concentration of silanol functions is maximal.[160, 174] Hence, the condensation or hydrogen bonding between the cellulosic substrate and the silanols was probably favoured, when water was progressively removed, leading to higher T_2/T_3 ratios (Scheme 19). This will be confirmed later by the leaching experiments in Chapter II.3.1, which showed that the fixation of polysiloxane was more favoured with *Protocol 2* than with *Protocol 1*.

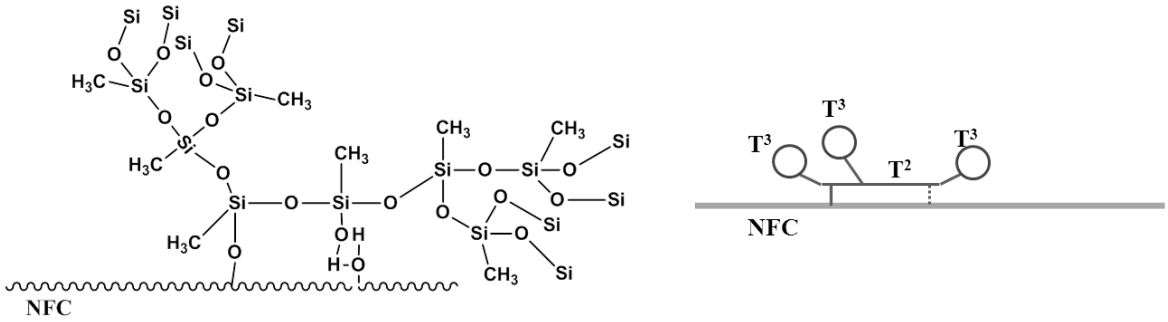

Scheme 19: Hypothesis for the bonding of polysiloxane at the NFC surface after silylation with *Protocol 2*

II.2.3.3. Microscopy

The evolution of the NFC morphology upon silylation was examined by SEM, and the resulting micrographs are presented in Figure 26.

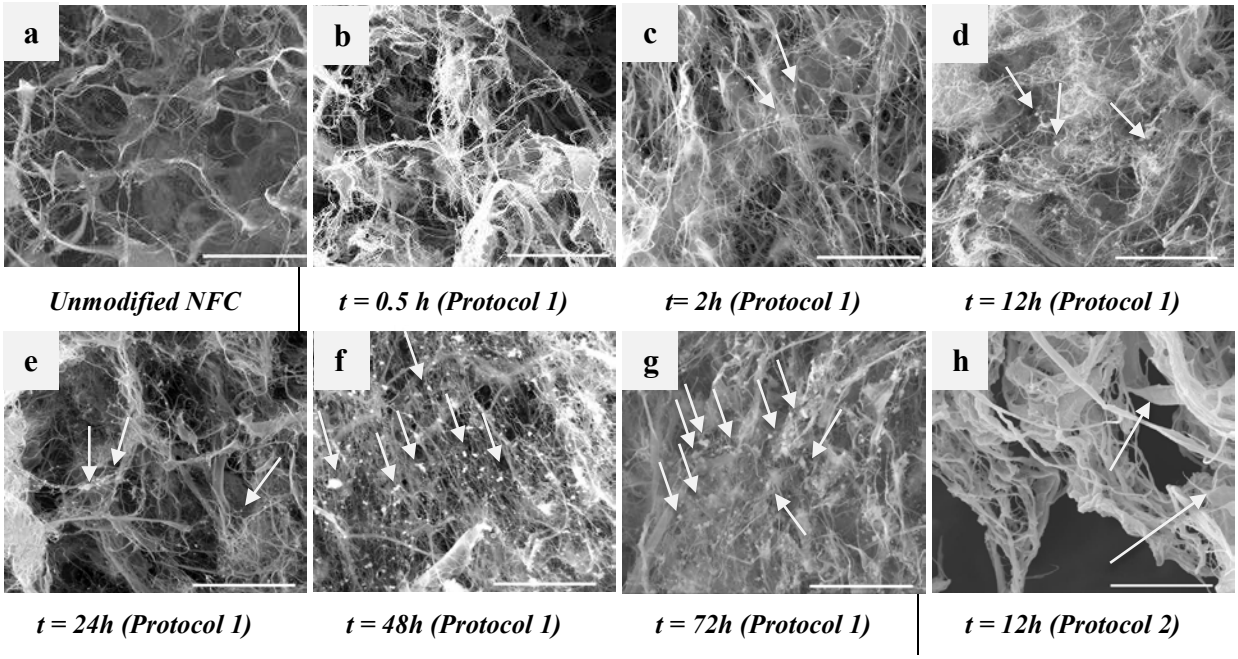

Figure 26: SEM micrographs of unmodified NFC (a) and NFC treated with MTMS according to *Protocol 1* (b-g) or *Protocol 2* (h) (Scale bar is 10 µm). Results with various reaction times are presented.

With *Protocol 1*, a 3D network of nanofilaments prevailed in all the samples, regardless of the reaction time. Above 2 h reaction, the presence of silane was detected in the form of white particles or clusters within the cellulosic substrate. These particles were constituted of homopolymerized MTMS, as will be later confirmed by WDX. Their number tended to increase with increasing reaction time, which was consistent with the results of Figure 22.

The morphology of NFC silylated according to *Protocol 2* was quite different, and did not vary significantly with reaction time (therefore, only 1 micrograph is present in Figure 26h). In this case, the fibrillar network was composed of filaments of increased diameters, which were connected to sheet structures. This sheet like morphology may be attributed to either hornified NFC covered with silane or to polysiloxane films. The increase in the filaments thickness was attributed to a full coverage of the nanofibres by the polysiloxane.

The WDX Si mapping of the samples compressed to flat films is presented in Figure 27.

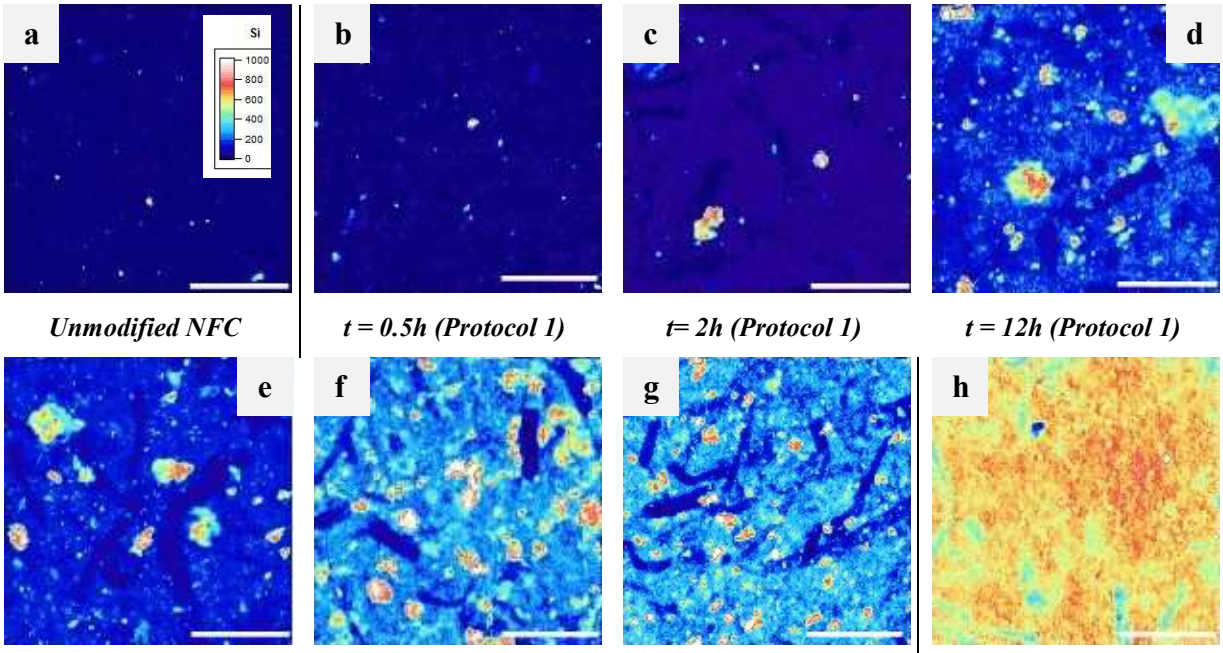

Figure 27: WDX Si mapping of unmodified NFC (a) and MTMS-treated NFC obtained according to *Protocol 1* (b-g) or *Protocol 2* (h) (Scale bar is 100 µm).

After silylation with *Protocol 1*, the brightness of the image as well as the proportion of Si aggregates progressively increased with reaction time, indicating that the NFC surface was increasingly covered by silane molecules, and also that polysiloxane particles were increasingly produced. These polymers, detected as white dots in the SEM micrographs, could be bonded or not to the substrate.

After silylation with *Protocol 2*, all the samples presented similar Si mappings, so only one example was presented (Figure 27h). In this case, a much brighter and more uniform colour was measured as compared with *Protocol 1*, confirming the full coverage of NFC by the polysiloxane.

II.2.4. Impact of initial silane concentration (*Protocol 1 & 2*)

Once again, both Protocol 1 (with washing step, pH 0.4) and Protocol 2 (without washing step, pH 4) were investigated. Reactions were performed for 2h at room temperature, using various concentrations of MTMS ($[MTMS]_i$) (Table 5).

Table 5: Initial concentrations of MTMS investigated

$[MTMS]_i$ [mmol/g]	*Protocol 1*	*Protocol 2*
1.2		✓
2.5		✓
3.7	✓	✓
4.9	✓	✓
7.4	✓	✓
9.9	✓	
12.4	✓	
14.8	✓	✓

II.2.4.1. Evolution of Si content

The evolution of Si content as function of $[MTMS]_i$ is presented in Figure 28.

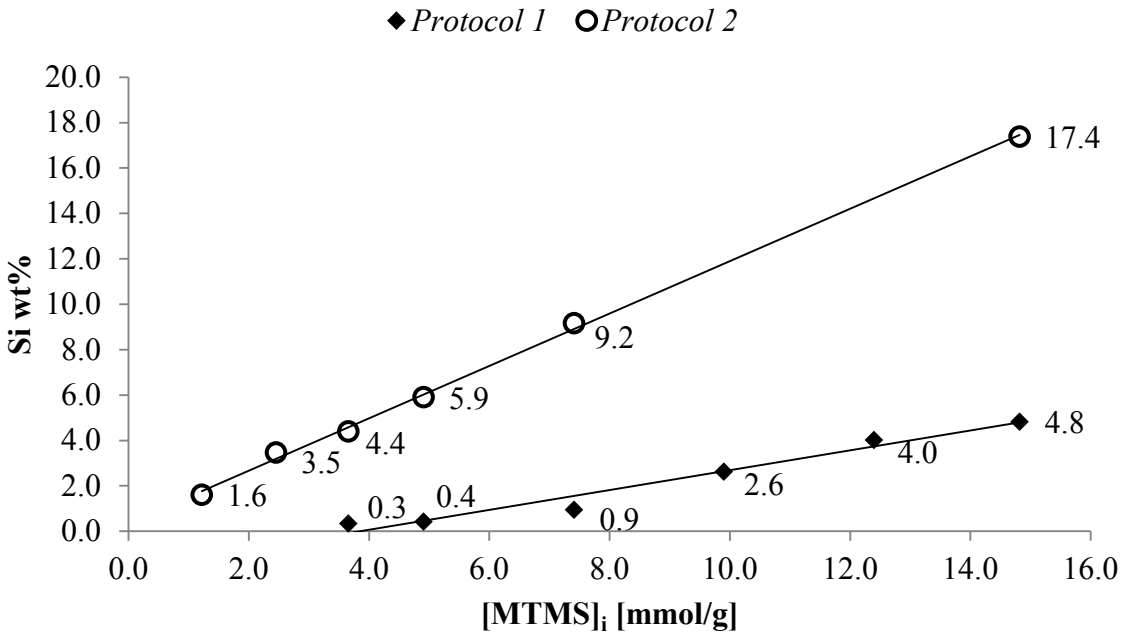

Figure 28: Evolution of Si content as a function of $[MTMS]_i$ for NFC treated with MTMS according to *Protocol 1* (pH 0.4) or *Protocol 2* (pH 4).

Regardless of the protocol used, a gradual increase in Si content was noted with increasing silane concentration. This increase is logical in the case of *Protocol 2*, since all the silane introduced remains within the NFC substrate after freeze-drying. With *Protocol 1*, the presence of silane was detected only when $[MTMS]_i$ was above 7.4 mmol/g. It is likely that below this concentration, most of the silane was leached out during the washing step with water. By increasing the silane concentration, homocondensation is increasingly favoured, and more insoluble polymers are probably produced. But the silane content remained low compared with the unwashed samples, which meant the major part of the silane introduced was leached out during the washing step.

II.2.4.2. Solid State NMR spectroscopy

a) ^{13}C CP-MAS NMR

The presence of silane at the NFC surface was confirmed by ^{13}C CP-MAS NMR (Figure 29). The carbon of the MTMS methyl moiety was detected at -3 ppm (C_α) in all spectra, except in the case of samples with low Si content (*Protocol 1*: $[MTMS]_i$ < 7.4 mmol/g). Regardless of the protocol, the intensity of the C_α peak increased gradually with $[MTMS]_i$, in agreement with the results of Figure 28.

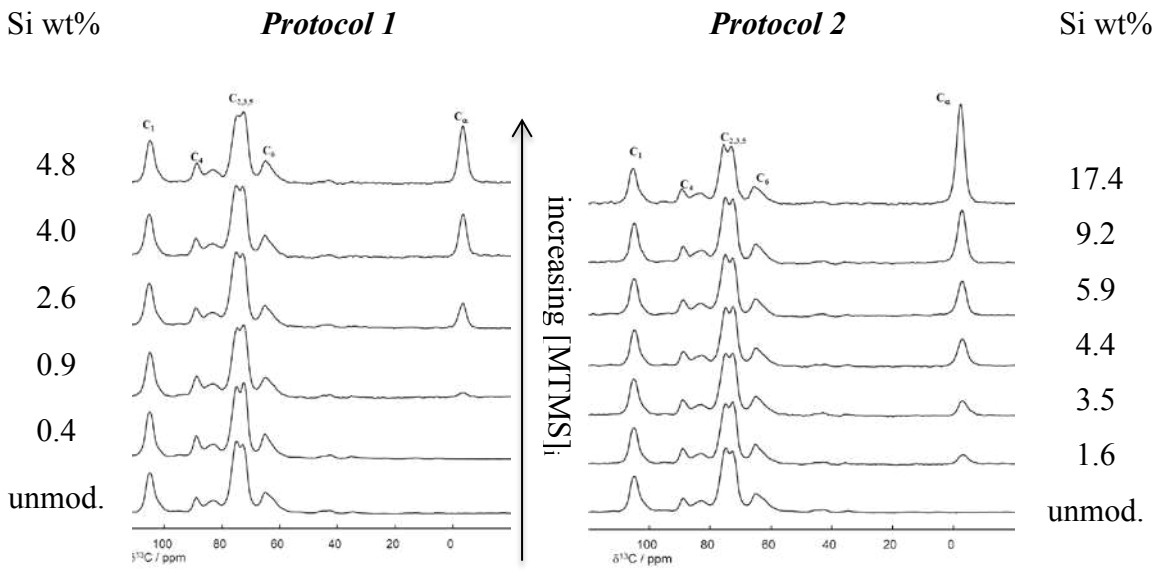

Figure 29: ^{13}C CP-MAS NMR spectra of MTMS-treated NFC prepared at different $[MTMS]_i$ (*Protocol 1 & 2*).

b) ^{29}Si CP-MAS NMR

The ^{29}Si CP-MAS NMR spectra of NFC treated at different $[MTMS]_i$ are presented in Figure 30.

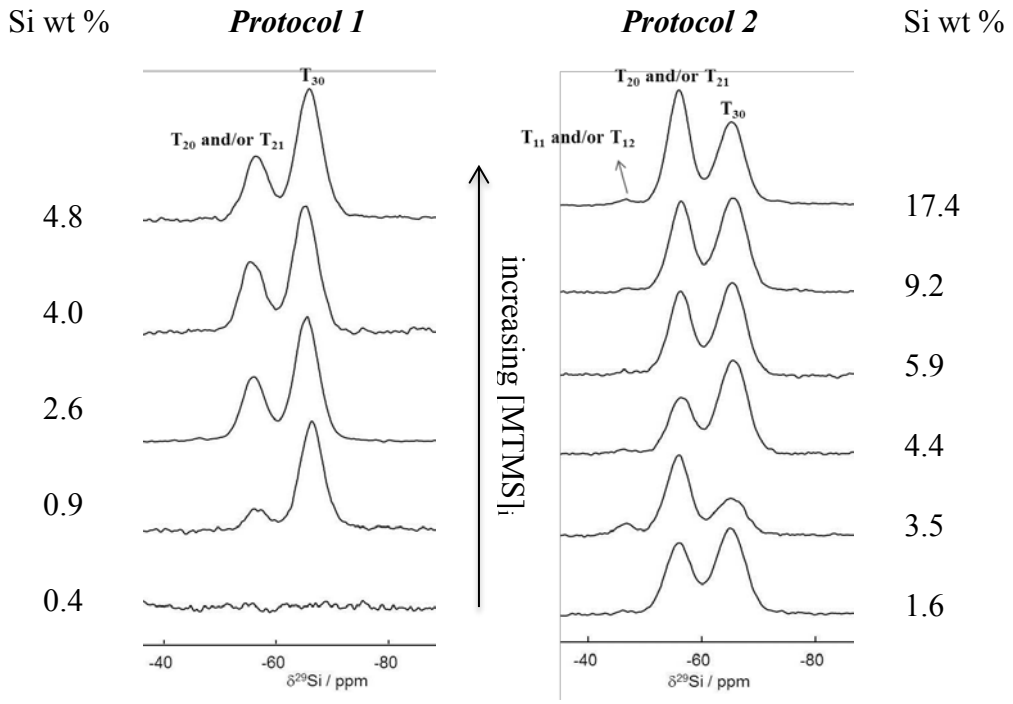

Figure 30: ^{29}Si CP-MAS solid state NMR spectra of MTMS-treated NFC prepared at different $[MTMS]_i$ (*Protocol 1 & 2*).

The two signals at -56 and -65 ppm were again detected, but the relative intensity of the peaks differed significantly depending on the method used and also on $[MTMS]_i$ in the case of *Protocol 2*. These two signals were again assigned to di-condensed (T_{20} and/or T_{21}) and tri-condensed (T_{30}) structures, respectively. A small additional signal, assigned to T_{11} and/or T_{12} structures, was again detected at -46 ppm in the case of *Protocol 2*.

After deconvolution of the spectra, the ratio of the peaks area at -56 and -65 ppm (T_2/T_3 ratio) was calculated and plotted as a function of $[MTMS]_i$ (Figure 31). The T_1 structures at -46 ppm were not taken into consideration due to their negligible contribution.

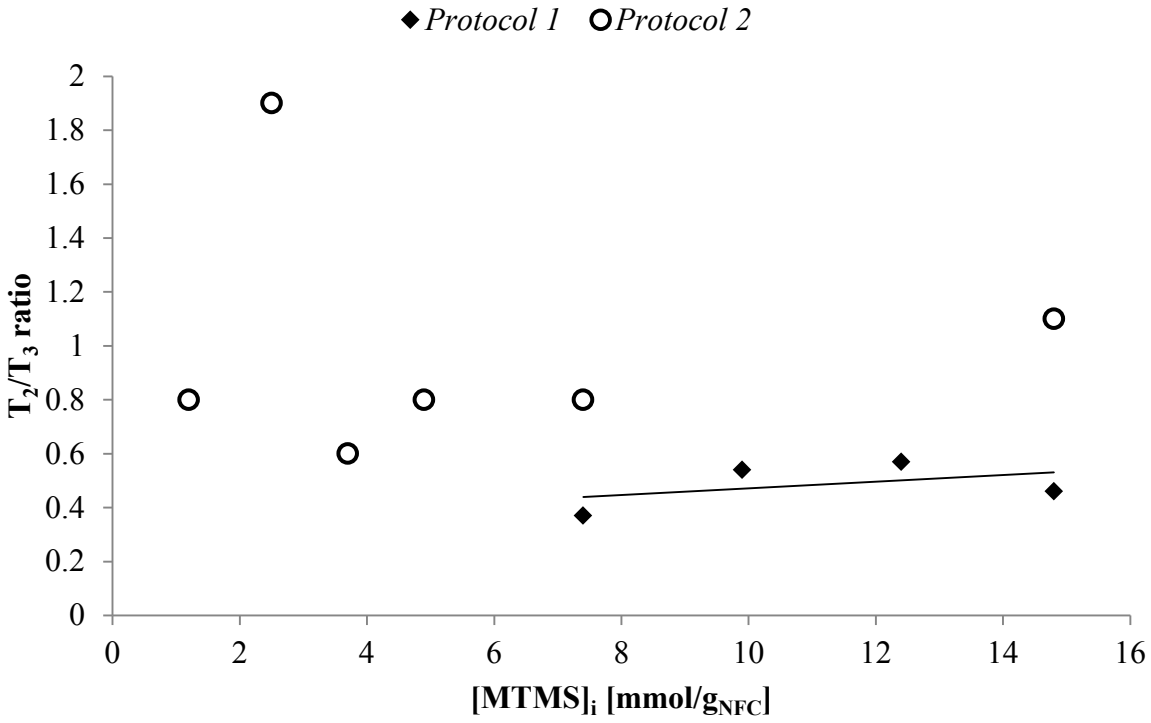

Figure 31: Evolution of the ratio of the peaks area at -56 and -65 ppm (T_2/T_3 ratio) as a function of $[MTMS]_i$.

With *Protocol 1*, the T_2/T_3 was quite stable when $[MTMS]_i$ was varied ($T_2/T_3 \approx 0.5$), as was already observed when pH and reaction time were varied (Figure 19 and Figure 25, respectively). Hence, the silane concentration did not significantly impact the structure of the polysiloxanes bonded or dispersed within the NFC network.

The samples prepared with *Protocol 2* contained more T_2 structures than the ones prepared with *Protocol 1* and the T_2/T_3 ratio fluctuated more, like in Figure 25. As was hypothesized in II.2.3.2.b, we believe that *Protocol 2* favoured the condensation between NFC and hydrolysed MTMS during freeze-drying, via T_2 sites (Scheme 19). It should be noted that the T_2/T_3 ratio obtained with 1.9 mmol/g $MTMS/g_{NFC}$ was unexpectedly higher than the ratios obtained with other $[MTMS]_i$. Maybe at this concentration, the respective rates of hydrolysis and condensation were in such a ratio that homocondensation was minimized. But additional work is required to clarify this point.

II.2.4.3. Microscopy

The evolution of the NFC morphology upon silylation was assessed using SEM and the resulting micrographs are presented in (Figure 32).

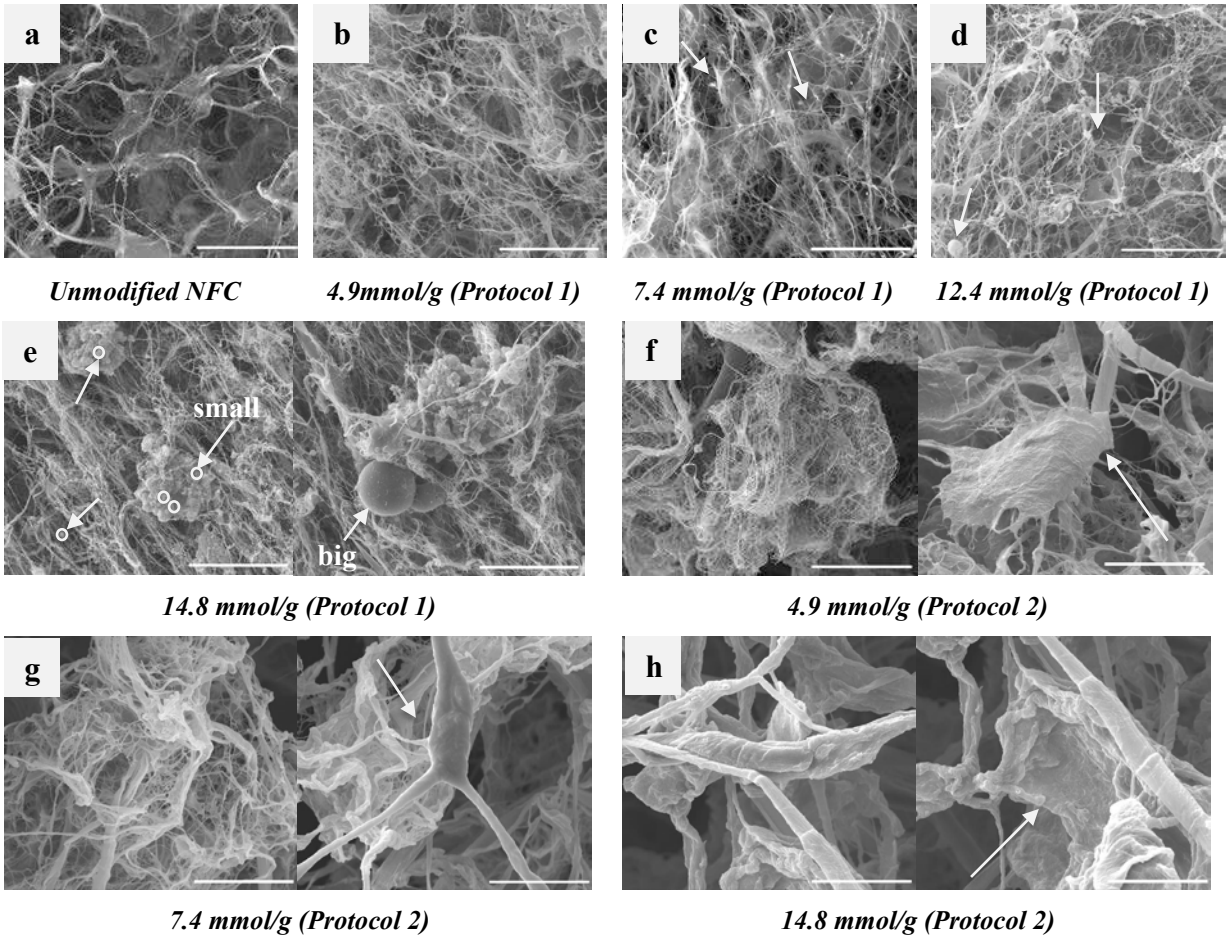

Figure 32: SEM micrographs of unmodified NFC (a) and NFC treated with MTMS, according to *Protocol 1* (b-e) or *Protocol 2* (f-h) (Scale bar is 10 μm). Results with various $[MTMS]_i$ are presented.

With *Protocol 1*, a 3D network of nanofilaments prevailed in all the samples, regardless of the reaction time. When $[MTMS]_i$ was 7.4 mmol/g_{NFC} or above, the presence of homopolymerized MTMS was detected in the form of white particles or clusters within the cellulose substrate (marked with arrows). Polysiloxane particles with diameters in the nanometer range (Φ ~ 200 - 400 nm) were observed when $[MTMS]_i$ was 7.4 mmol/g_{NFC} (Figure 32c), but aggregates consisting of both small particles (Φ ~ 0.5 μm, see circles with arrows in Figure 32e) and big particles (Φ ~ 6 μm, see arrows in Figure 32e) could be spotted above this concentration. This result is in agreement with our hypothesis that polymers of increasing molecular weight were formed when $[MTMS]_i$ was increased.

NFC silylated according to *Protocol 2* were composed of filaments which diameter tended to increase with increasing MTMS concentration (Figure 32f-h), suggesting an increasing decoration of the NFC surface by the polysiloxanes. Similar as what was observed in Figure 26h, sheet structures were also detected in these samples (marked with arrows in Figure 32f-h), which may correspond to hornified NFC covered with silane or to polysiloxane films.

The WDX Si mapping of the samples prepared according to *Protocol 1* confirmed the presence of polysiloxane particles of increasing size and number, when $[MTMS]_i$ was increased (Figure 33). An increase in overall image brightness was also noted with both *Protocol 1* and *Protocol 2*, indicating that the NFC surface was increasingly covered by the polysiloxane. But a brighter and more uniform colour was measured with *Protocol 2*, suggesting that the NFC were fully covered by the polymer in that case.

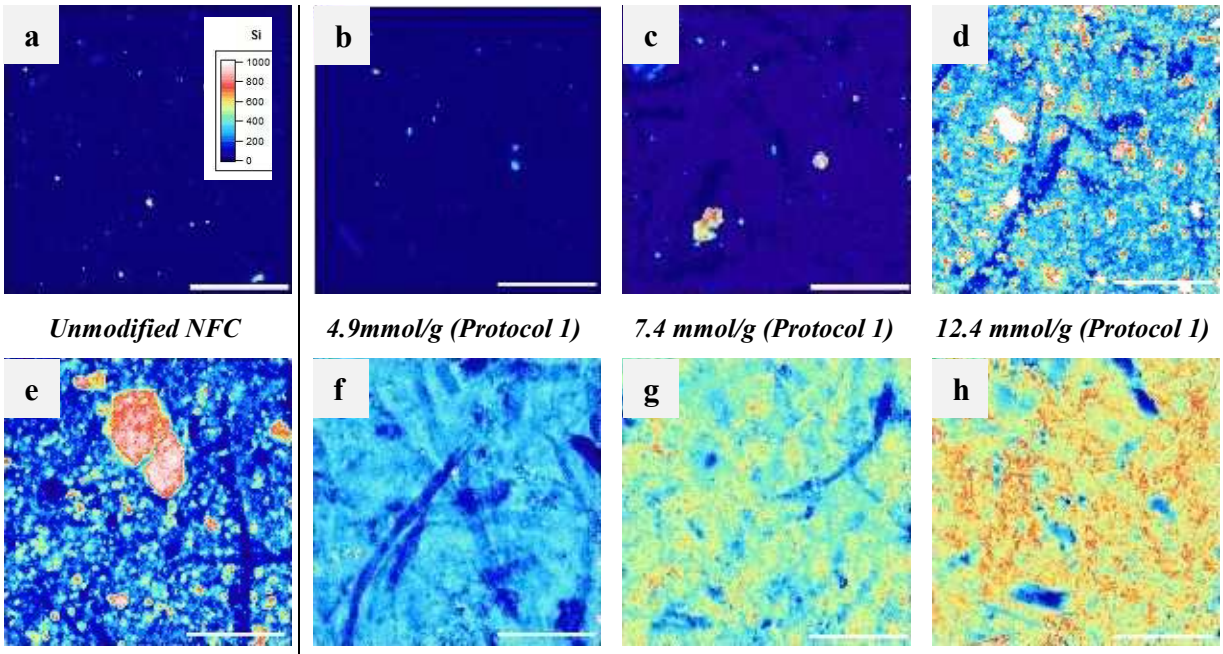

Figure 33: WDX Si mapping of unmodified NFC (a) and NFC treated at different $[MTMS]_i$, with *Protocol 1* (b-e) and *Protocol 2* (f-h). (Scale bar is 100 µm.)

II.3. Properties of silylated NFC

The properties of NFC produced according to *Protocol 1* or *Protocol 2*, were investigated and compared. Four different properties were investigated: resistance to leaching, crystallinity, wettability and thermal properties.

II.3.1. Resistance to leaching

The stability of the silylation adducts with regards to hydrolysis and leaching was evaluated by Soxhlet-extraction of the treated samples using different solvents. Only the samples prepared by varying the initial MTMS concentrations were tested (*Protocols 1 & 2* in II.2.4). Three solvents of different polarities were investigated, namely water (dielectric constant ε = 80 and dipole moment μ = 1.85 D), ethanol (ε = 25 and μ = 1.85 D) and chloroform (ε = 4.8 and μ = 1.04 D). Water was selected to test the stability to hydrolysis of the silane possibly condensed at the cellulose surface. Ethanol has been shown to be particularly efficient in removing any physically adsorbed silane species from the cellulose surface.[152, 153, 155] Chloroform is known to be a good solvent for polysiloxanes.[184]

After 20 h of soxhlet extraction with each solvent, the Si content of the samples was re-evaluated by FTIR spectroscopy using the calibration chart of Figure 15.

For samples prepared with *Protocol 1*, the Si content tended to decrease after soxhlet extraction and the leaching occurred in the order: water < chloroform < ethanol (Figure 34).

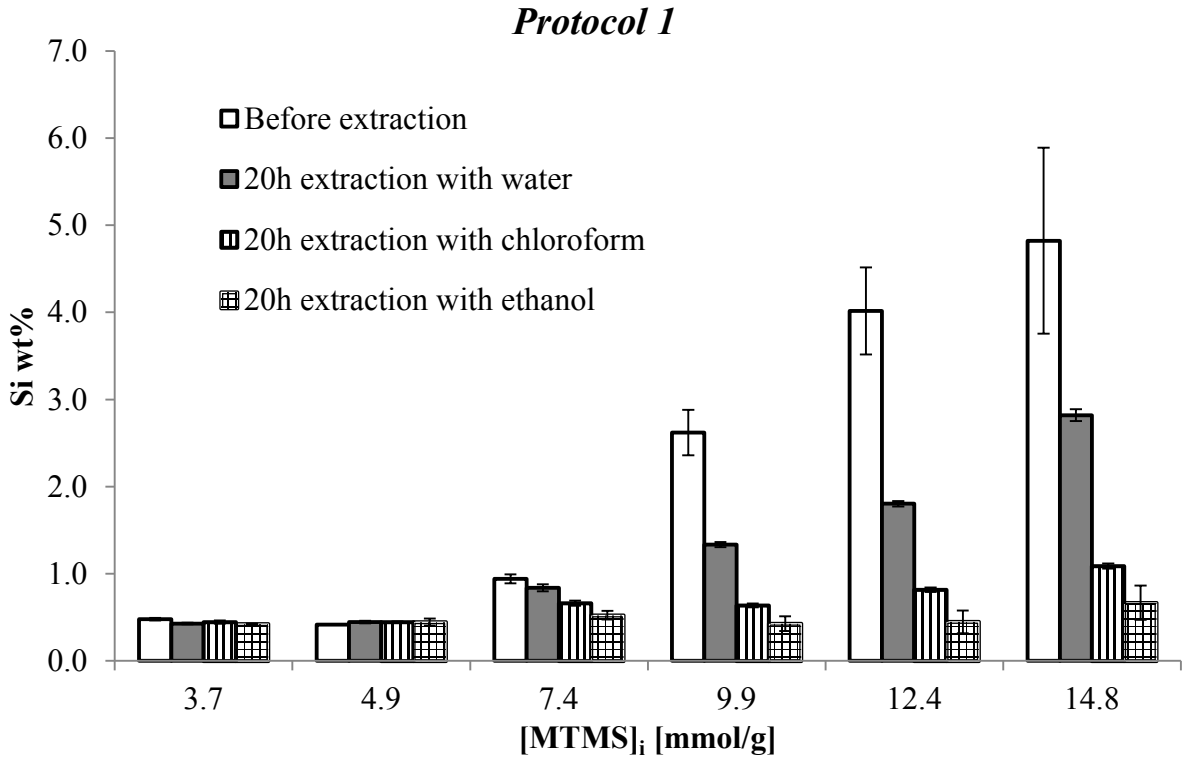

Figure 34: Evolution of the Si content in MTMS-treated NFC prepared at different $[MTMS]_i$ (*Protocol 1*), before and after extraction with water, chloroform and ethanol.

Most of the silane was removed after extraction with ethanol (and to a slightly lower extent) with chloroform, indicating that the polysiloxane was not covalent-bonded to the cellulosic substrate. The slight difference noted between the two solvents may be related to differences in the swelling capacity within the NFC network. It was also possible that some ethanolysis occurred with ethanol, liberating some condensed species from the NFC surface. With water, the extraction was only partial, probably because the high molecular weight polysiloxanes were not dissolved.

The sample with the highest Si content (4.8 Si wt%, *Protocol 1*) was further analysed by ^{29}Si CP-MAS NMR spectroscopy, before and after each extraction (Figure 35). Results revealed that the T_2/T_3 ratio of the polysiloxane remaining attached to the NFC surface was quasi the same as before extraction, regardless of the solvent. Hence, there was no specific extraction of T_2-rich or T_3-rich species by a particular solvent. For instance, water did not specifically extract species with a high T_2 content (expectedly more polar). In the same way, chloroform or ethanol did not specifically extract polymers with a high T_3 content (expectedly less polar). This means that all polysiloxane molecules (big or small) are *a priori* composed of both T_2 and T_3 structures in the same ratio.

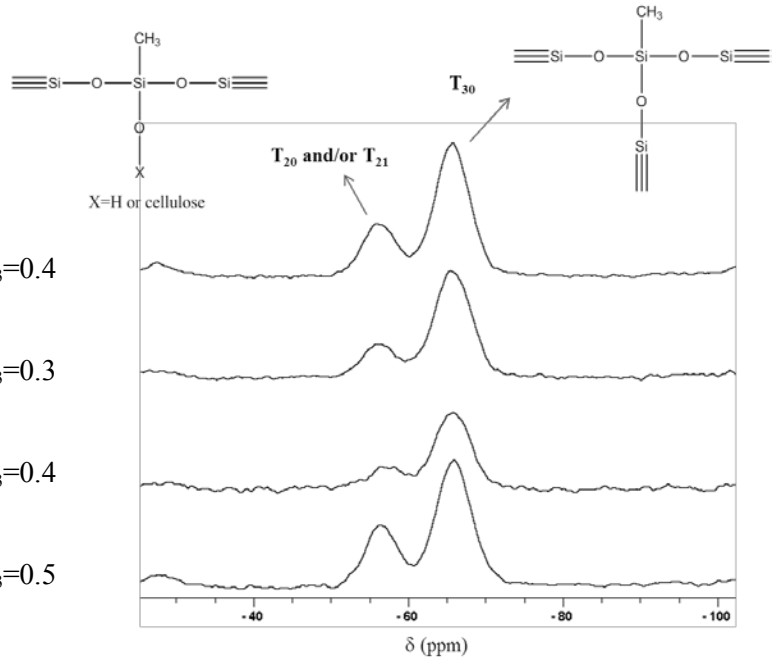

water	2.8 Si wt%	T_2/T_3=0.4
chloroform	1.1 Si wt%	T_2/T_3=0.3
ethanol	0.7 Si wt%	T_2/T_3=0.4
Before extraction	4.8 Si wt%	T_2/T_3=0.5

Figure 35: ^{29}Si CP-MAS NMR of NFC treated by 14.8 mmol MTMS/g_{NFC} (*Protocol 1*), before and after extraction with water, chloroform and ethanol.

In contrast, samples prepared with *Protocol 2* exhibited a high resistance to leaching by any of the solvents investigated (Figure 35). This result tends to confirm what was hypothesized in Chapter II.2.3, *i.e.* the condensation or hydrogen bonding between the cellulosic substrate and the polysiloxane was highly favoured in the case of *Protocol 2*.

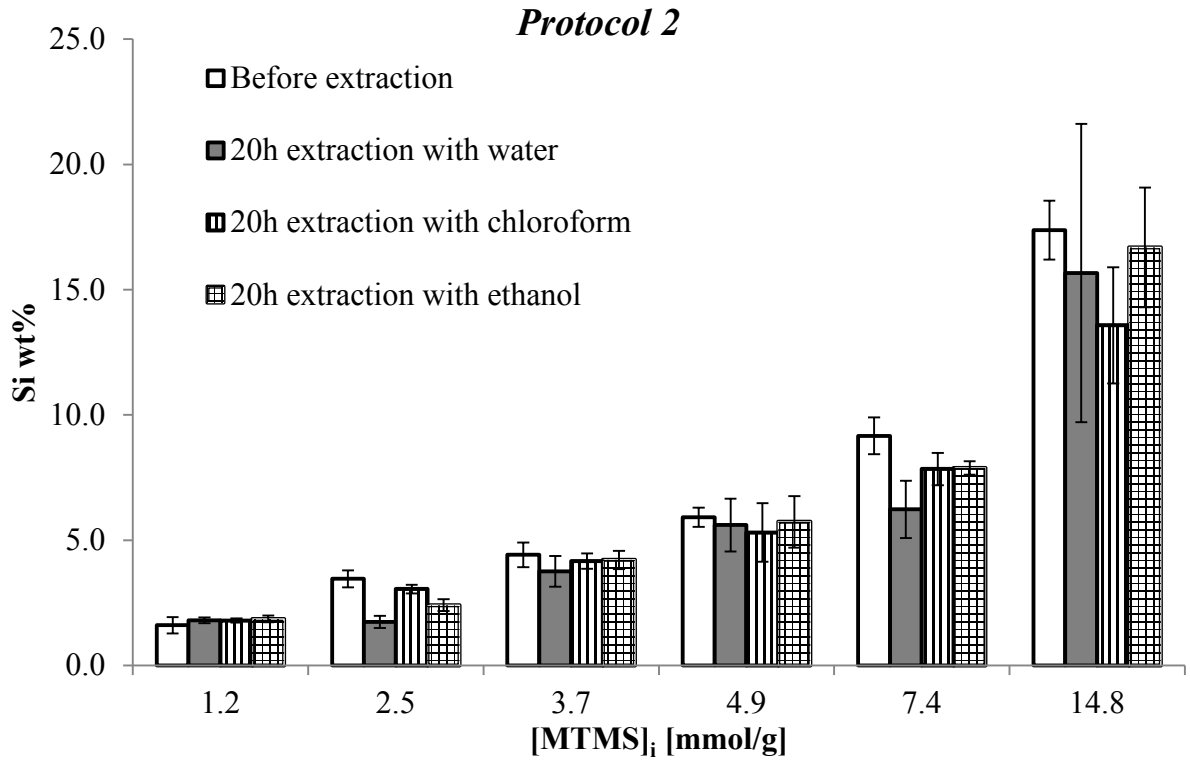

Figure 36: Evolution of the Si content in MTMS-treated NFC prepared at different $[MTMS]_i$ (*Protocol 2*), before and after extraction with water, chloroform and ethanol.

Generally, a heat treatment is required (110 °C - 120 °C), to ensure the covalent bonding between cellulose and alkoxysilanes, because the process is too slow at room temperature.[155, 156, 158] In view of our results with *Protocol 2*, it seems possible to ensure an appropriate covalent bonding between polysiloxane and NFC without heating.

II.3.2. Crystallinity

The impact of silylation on the NFC crystal structure was evaluated by X-ray diffraction (XRD) analysis. Since strong acidic conditions may have an impact on the cellulose crystallinity,[187, 188] the samples prepared at different pH were investigated. Reactions were performed at room temperature, for 2 h, using an initial MTMS concentration of 7.4 $mmol/g_{NFC}$. *Protocol 1* (pH = 0 - 1; cf. chapter II.2.2) and *Protocol 2* (pH = 4; cf chapter

II.2.3) were compared. The diffraction profiles obtained after XRD analysis are presented in Figure 37.

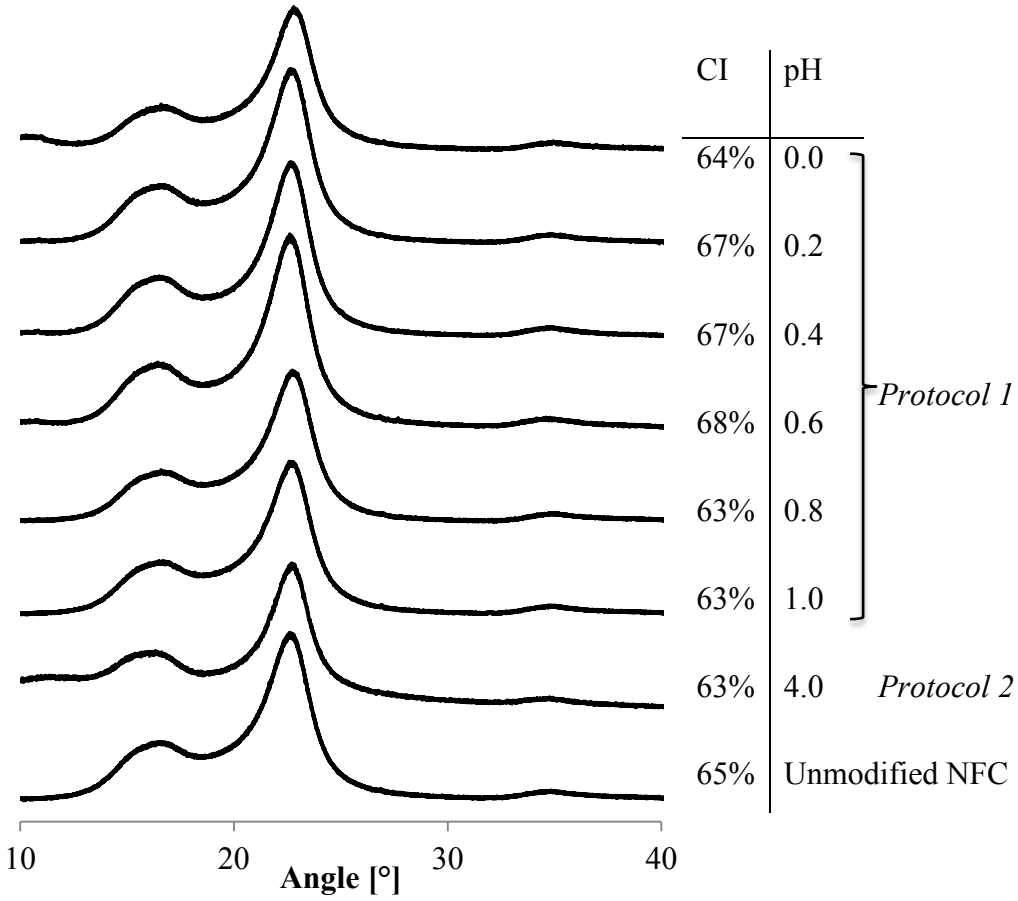

Figure 37: XRD profiles of unmodified NFC and NFC treated with MTMS at different pH with *Protocol 1* (pH = 0 - 1)or *Protocol 2* (pH = 4).

Unmodified NFC displayed the typical X-ray diffraction pattern of native cellulose (cellulose I), with characteristics diffraction peaks at 2Θ angles of 14.8, 16.6, 22.3 and 34.4° ($1\bar{1}0$, 110, 200 and 004 lattices, respectively).[189] After silylation, all samples still displayed the cellulose I pattern, indicating that the original cellulose structure was preserved, regardless of the pH. The crystallinity index (CI), which represents the percentage of crystalline material, did not vary much between the samples, confirming that the silylation treatment did not significantly affect the crystal structure of NFC. This is definitely an advantage of our method compared with reported methods such as carboxymethylation,[56] periodate-oxidation[57] and acetylation,[123] for which a decrease in crystallinity of NFC was noted, even at low modification rates.

II.3.3. Wettability and hygroscopicity

Only the samples prepared by varying the initial silane concentration were tested (*Protocol 1* and *Protocol 2* in paragraph II.2.4).

II.3.3.1. Wettability

The wettability at the NFC surface was evaluated by measuring the contact angle of a water droplet deposited on the freeze-dried silylated material.

All samples treated according to *Protocol 1* – even the sample with the highest Si content - were quite hydrophilic since in all cases, the water droplet was instantaneously absorbed by the substrate (no water contact angle (WCA) could be measured). With *Protocol 1*, polysiloxane particles are randomly dispersed within the NFC network, but the nanofibrils are not fully covered by the silane. Accordingly, a large amount of hydroxyl groups remained accessible to water at the NFC surface, resulting in hydrophilic properties.[155, 156, 158]

In contrast, all NFC treated according to *Protocol 2* were quite hydrophobic, since WCA above 100° were measured, even when the Si content was as low as 1.6 wt% (Figure 38). The WCA progressively increased with the amount of grafted polysiloxane, up to a maximum of 147° when the Si content was 9.2 wt%. The WCA reported here are higher than those generally reported when cellulosic fibers are modified by trialkoxysilanes (between 60° and 100°).[155, 190] This behaviour has been associated with a progressive covering of the nanofibres by the polysiloxane when the MTMS concentration was increased (cf II.2.4). Above 9.2 wt% Si ($[MTMS]_i$ = 7.4 mmol/g_{NFC}), a plateau was reached and no more modification of the WCA was observed, probably because the amount of MTMS introduced was sufficient to fully cover the NFC surface. Interestingly, the WCA values obtained here are similar to the values reported for NFC modified with chlorodimethylisopropylsilane,[140] a very hydrophobic silylating agent. But the MTMS-silylation in water is an easier and much more environmentally friendly route.

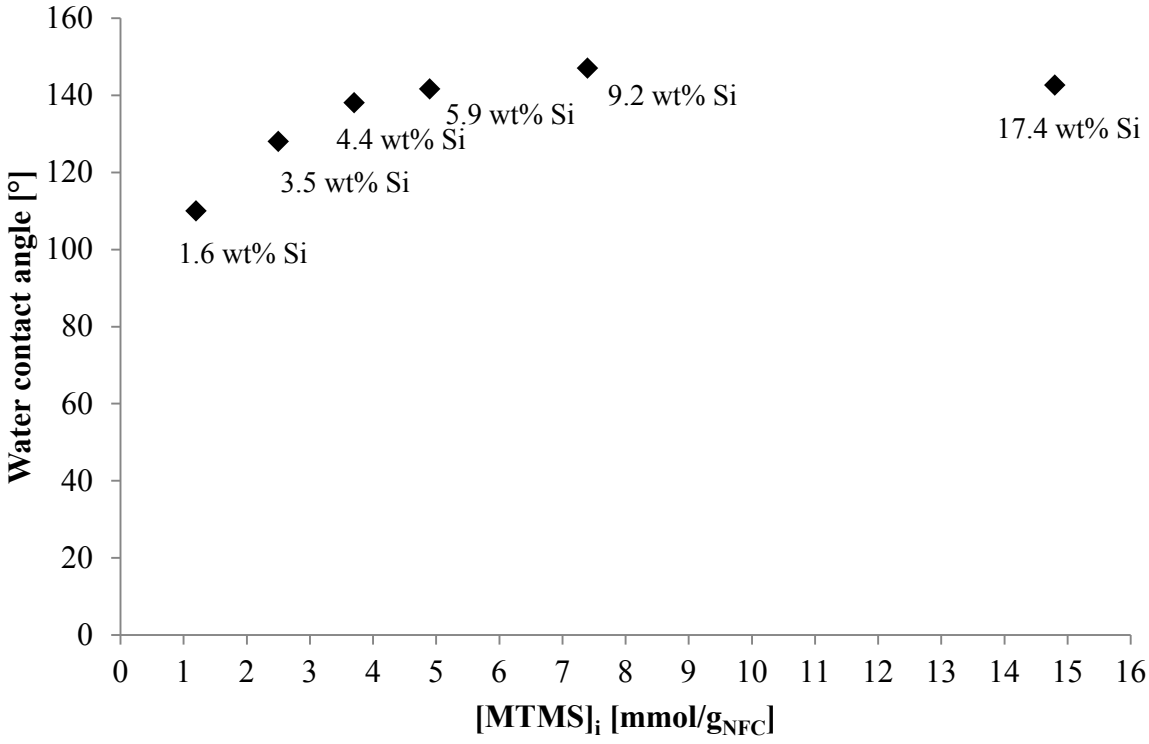

Figure 38: Water contact angle (WCA) values at the surface of NFC treated at different $[MTMS]_i$ with *Protocol 2*.

II.3.3.2. Hygroscopicity

The hygroscopic properties of silylated NFC were evaluated by Dynamic Vapour Sorption (DVS). The water sorption isotherms obtained are presented in Figure 39 and Figure 40 (*Protocol 1* and *Protocol 2*, respectively).

The moisture sorption isotherm pattern was similar in all samples, and was divided into three regions correlated with the three types of water generally co-existing in the material:[191] i) in the RH range 0-20 %, sorption of monomolecular water is involved; ii) in the RH range 20-80 %, sorption of multimolecular water occurs; iii) above 80 % RH, capillary water forms in the material. Whereas the mobility of the mono- and multimolecular water is limited, the capillary water can move easily inside the cellulosic materials.[191]

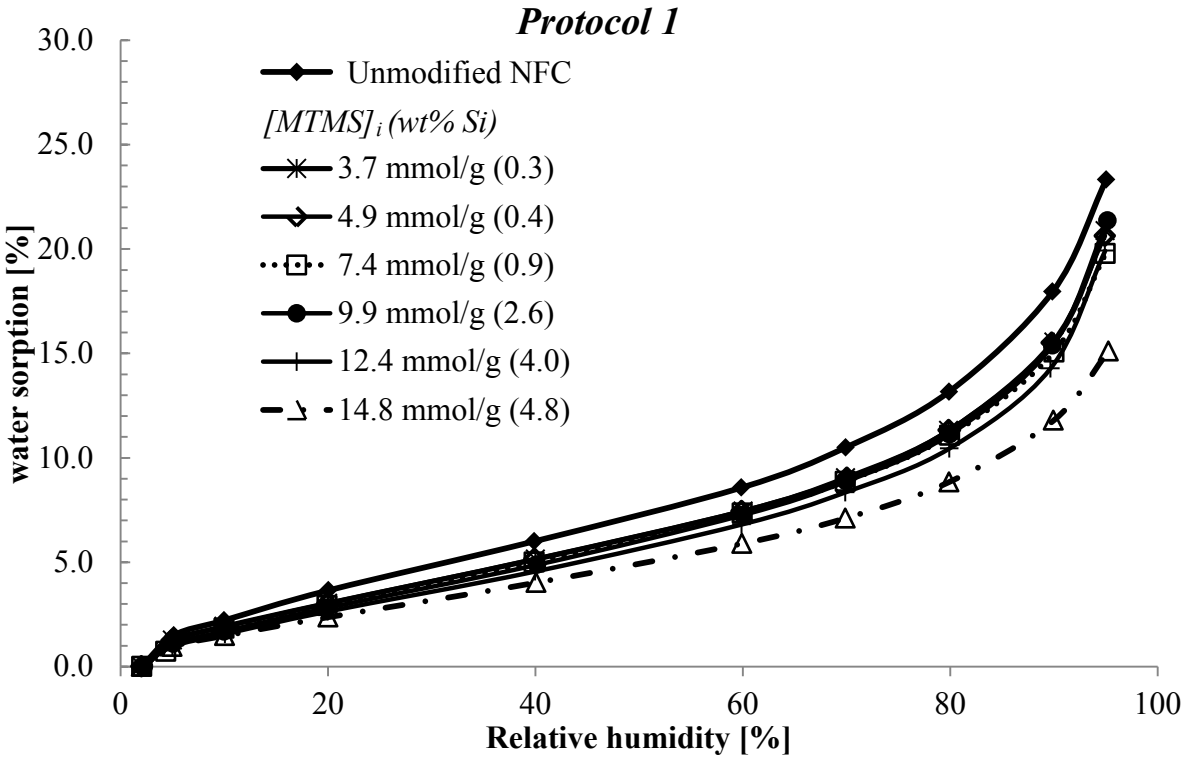

Figure 39: Water sorption isotherms of unmodified NFC and NFC treated at different $[MTMS]_i$ according to *Protocol 1* (T = 23 °C).

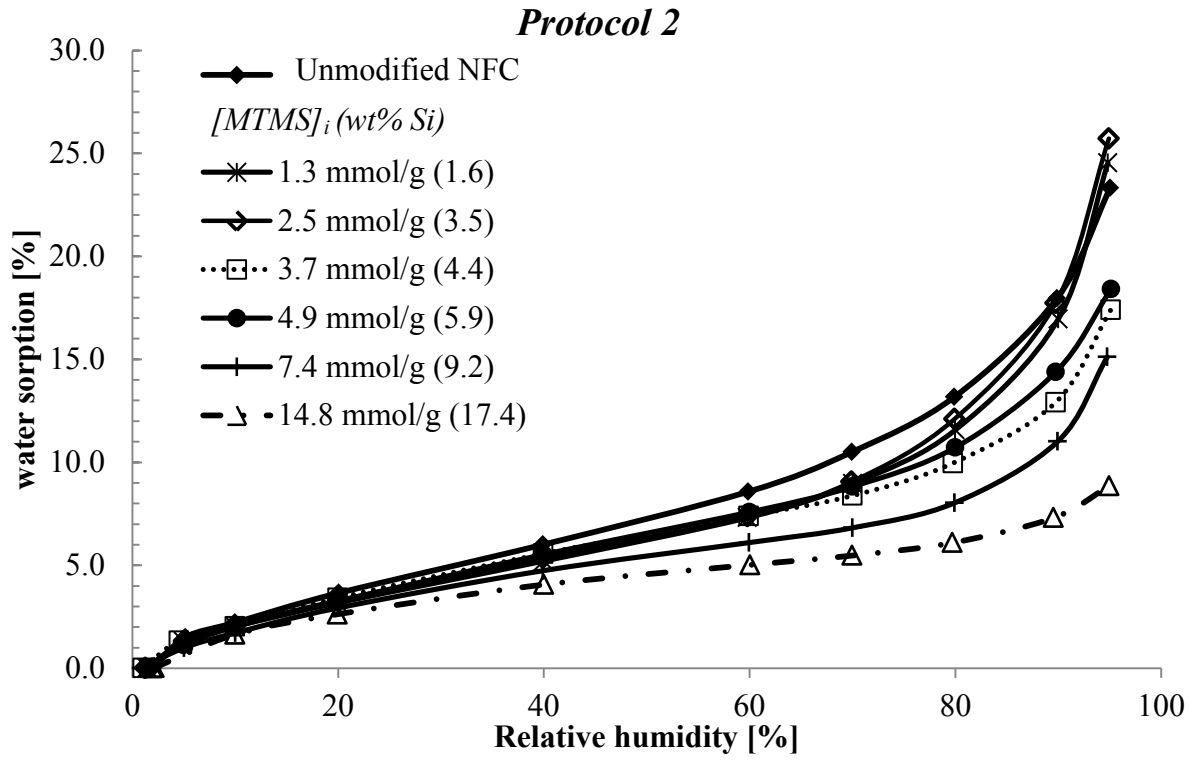

Figure 40: Water sorption isotherms of unmodified NFC and NFC treated at different $[MTMS]_i$ according to *Protocol 2* (T = 23 °C).

Regardless of $[MTMS]_i$, NFC treated according to *Protocol 1* or *Protocol 2* presented lower water sorption capacity compared with unmodified NFC, in particular at high silylation level. Some hydroxyl groups might become inaccessible to water after silylation, but this decrease might be simply due to the fact for a given weight, the silylated samples contained less cellulosic material (there is less cellulose in 1 g silylated NFC than in 1 g unmodified NFC).

Differences were noted between the two protocols at lower Si content. Samples treated according to *Protocol 2* were more hydrophilic above 90 % RH, when Si content was 3.5 wt % or lower. Since capillary water was involved in this range of RH,[191] some water condensation may have occurred in that case.

II.3.4. Thermal stability

The impact of silylation on the thermal stability of NFC was evaluated by thermogravimetric analysis (TGA), under inert atmosphere. Only the samples prepared by varying the initial silane concentration were analysed (cf. II.2.4). The thermograms of samples silylated according to *Protocol 1* and *Protocol 2* are presented in Figure 41 and Figure 42, respectively. The degradation data, *i.e.* temperatures associated with a 5 % weight loss ($T_{5\ \%}$), maximum degradation temperatures (T_d) and weight percentage residue at 900 °C, are reported in Table 6.

Table 6: Degradation data obtained from TGA analysis of unmodified NFC and NFC treated at different $[MTMS]_i$. $T_{5\,\%}$: temperature associated with a 5 % weight loss; T_d: maximum degradation temperature; $W_{900\,°C}$: weight percentage residue at 900 °C.

Samples	$[MTMS]_i$ [$mmol/g_{NFC}$]	Si wt %	$T_{5\%}$ (°C)	T_d (°C)	$W_{900\,°C}$ (%)
Unmodified	-	-	257	382	0.5
Silylation with *Protocol 1*	3.7	0.3	293	385	2.5
	4.9	0.4	299	393	3.1
	7.4	0.9	294	394	3.8
	9.9	2.6	169	390	4.2
	12.4	4.0	141	377	6.6
	14.8	4.8	142	374	10.3
Silylation with *Protocol 2*	1.2	1.6	278	393	8.3
	2.5	3.5	288	392	13.9
	3.7	4.4	278	381	17.3
	4.9	5.9	292	396	23.5
	7.4	9.2	306	400	29.7
	14.8	17.4	318	404	42.0

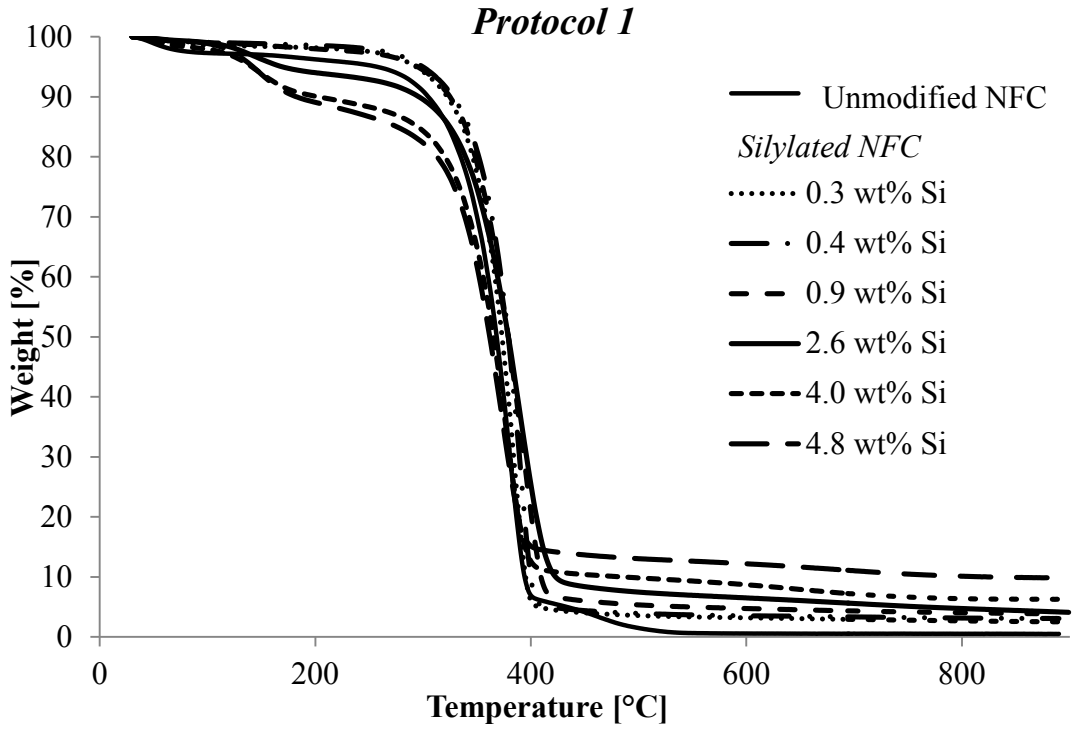

Figure 41: Thermograms of unmodified NFC and NFC treated at different $[MTMS]_i$ with *Protocol 1*.

All the samples displayed a weight loss between 50 and 100 °C, which was associated with the loss of residual moisture.[192] The most important mass loss occurred between 300 and 400 °C in all samples, which was correlated with the degradation of cellulose.[193, 194] The maximum degradation temperatures (T_d) of unmodified and silylated NFC were in the range between 374 and 394 °C. This is higher than the values generally reported for unmodified NFC (~350 °C),[153, 195] but any comparison is tricky since degradation depends on cellulose source, heating rate, gas environment, fibrillation process and drying process.[195]

With *Protocol 1*, a significant weight loss was noted between 120 °C and 300 °C, with samples contained 2.6 wt % Si or more. The $T_{5\ \%}$ was also lower in that case (Table 6), indicating that degradation occurred earlier. Since with *Protocol 1*, polysiloxane particles are not covalent-bonded to the NFC surface (cf. II.3.1), the weight loss measured in this temperature range was associated with the elimination of adsorbed low molecular weight polysiloxanes.

At low Si content (below 0.9 wt %), a slight improvement in thermal stability was noted as $T_{5\ \%}$ was higher than the one of unmodified NFC (Table 6).

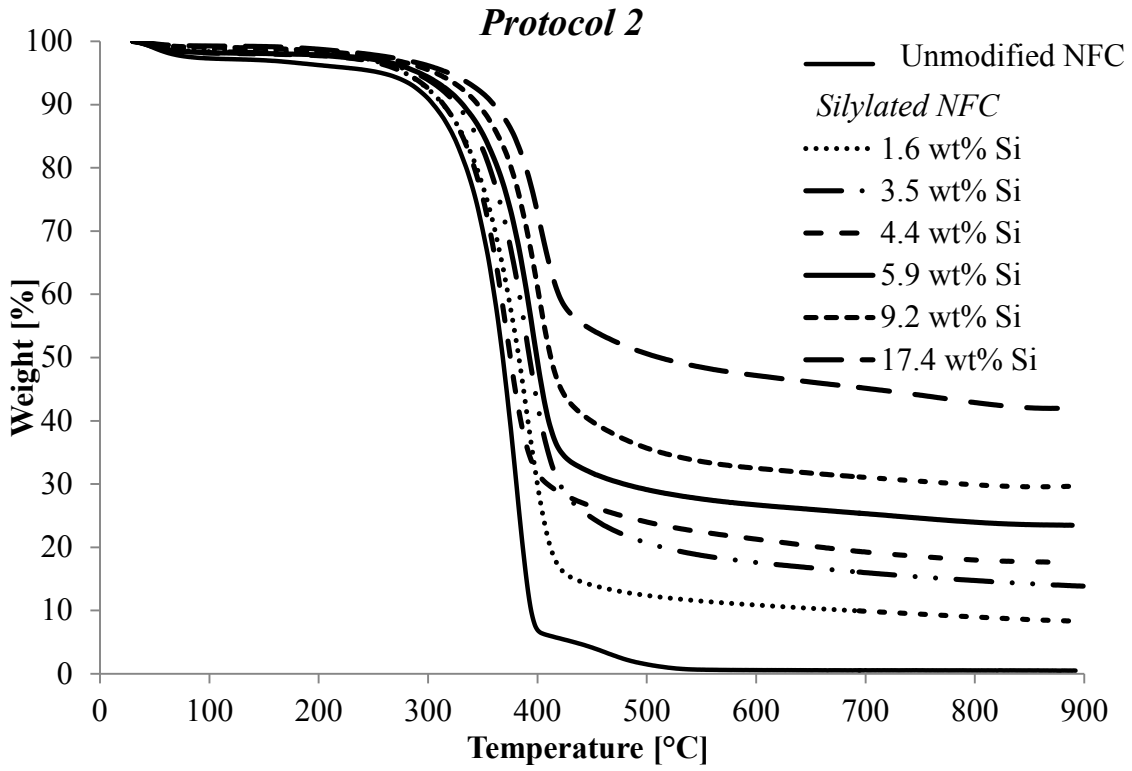

Figure 42: Thermograms of unmodified NFC and NFC treated at different $[MTMS]_i$ with *Protocol 2*.

However, the best improvements in thermal stability were obtained with *Protocol 2*. There was no weight loss between 120 °C and 300 °C, confirming that the polysiloxanes were strongly bonded to the substrate in that case. $T_{5\ \%}$ was found to increase with increasing Si content, indicating that silylation improved the thermal stability. This was further confirmed in the temperature range between 300 and 400 °C since a significant increase in T_d was also noted (except for sample with 4.4 wt % Si, probably because of inhomogeneities in the silane distribution within the treated sample). Silylation with alkoxysilanes has already been reported to have a positive influence on the thermal stability of cellulosic fibres.[150, 196] Our results indicate that the surface covering of NFC by a homogeneous silane layer is a prerequisite to obtain an efficient improvement.

After each experiment, the process left a residue, which percentage increased with increasing silylation level ($W_{900\ °C}$ in Table 6). This increase was assigned to the silica remaining after thermal degradation of high molecular weight polysiloxanes.[197-199]

II.4. Concluding remarks

The results presented in the present chapter have shown that NFC could be silylated with MTMS in aqueous medium. Two different types of silylated NFC were produced, without modification of the original crystalline structure. The first type consisted in a cellulose nanofibrils network, in which polysiloxane particles were dispersed (*Protocol 1*), while the second type consisted in nanofibrils covered by a homogeneous polysiloxane layer (*Protocol 2*). The size of the particles or the thickness of the polysiloxane layers could be controlled by monitoring the initial silane concentration.

Leaching experiments have shown that the polysiloxane particles produced with *Protocol 1* were not firmly anchored to the cellulosic substrate, whereas the polysiloxane layer covering the NFC treated according to *Protocol 2* was strongly bonded.

Differences were also noted in terms of wettability and thermal stability. While NFC treated with *Protocol 1* remained hydrophilic, very hydrophobic nanofibrils were produced with *Protocol 2*. The thermal stability was also significantly improved in that case, due to the efficient covering of the NFC surface by the silane polymer.

III. Silylated NFC as reinforcing agents in composites

III.1. Objectives and methodology

The fundamental work presented in Chapter II has highlighted the possibility to silylate NFC in water, in a controlled manner. Results have shown that the nanofibres surface could be tailored to some extent by varying the experimental protocol and adjusting the silylation level.

In the current chapter, the potential of silylated NFC as reinforcing agent in composites has been investigated. NFC's with different silylation level were produced by varying the initial silane concentration ($[MTMS]_i$), using *Protocol 1* and *Protocol 2*. The impact of silylation on the composites properties was subsequently studied. Two distinctive polymer matrices were selected for these experiments, namely polydimethylsiloxane (PDMS) and poly(lactic acid) (PLA). A solvent casting process in chloroform was used with both polymers (Scheme 20). The resulting composite materials were compared with regards to their mechanical, thermal and hygroscopic properties.

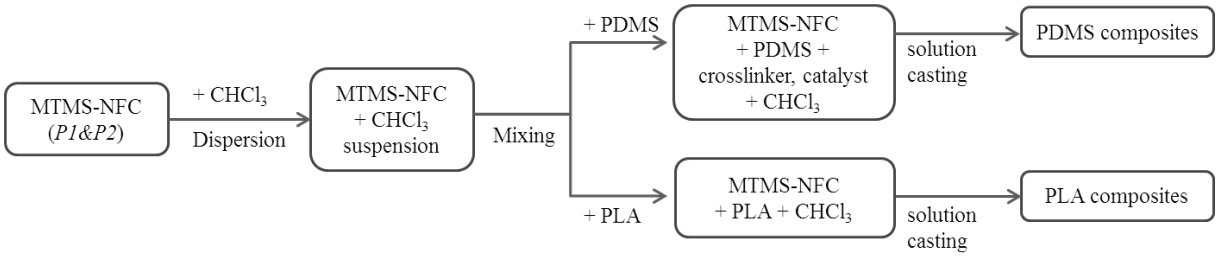

Scheme 20: Solvent casting process used for the preparation of NFC composites based on PDMS and PLA.

III.2. PDMS composites

All composites samples were prepared by solvent casting, using suspensions containing 1 wt % of unmodified or MTMS-treated NFC in chloroform. Higher concentrations were avoided, due to an excessive increase in the viscosity of the chloroform suspension. Composites were prepared based on a formulation already described in the literature, with tetrapropylorthosilicate as cross-linker and tin(II) 2-ethylhexanoate as catalyst.[200]

III.2.1. Viscoelastic properties

The viscoelastic properties (shear modulus *G'*) of the composites were evaluated using the torsion pendulum experiment, during which the deformation of the samples is measured at different temperatures and constant applied shear stress.[201, 202] Dynamic Mechanical Analysis in tension mode was attempted but led to unreliable results due to a lack of sensitivity of the equipment in the whole temperature range.

According to theory, the relation between shear modulus *G'* and modulus of elasticity *E'* is given by the equation:[203] $G' = \frac{E'}{2(1+\upsilon)}$ (1),

in which ν is the Poisson's ratio. For elastomer such as silicone, the Poisson's ratio is ~0.5.[204]

The evolution of shear modulus (G') and damping factor (tan δ) for PDMS composites reinforced with 1 % NFC treated at different $[MTMS]_i$ (*Protocol 1* and *Protocol 2*), are presented in Figure 43 and Figure 44. The evolution for neat PDMS is also reported.

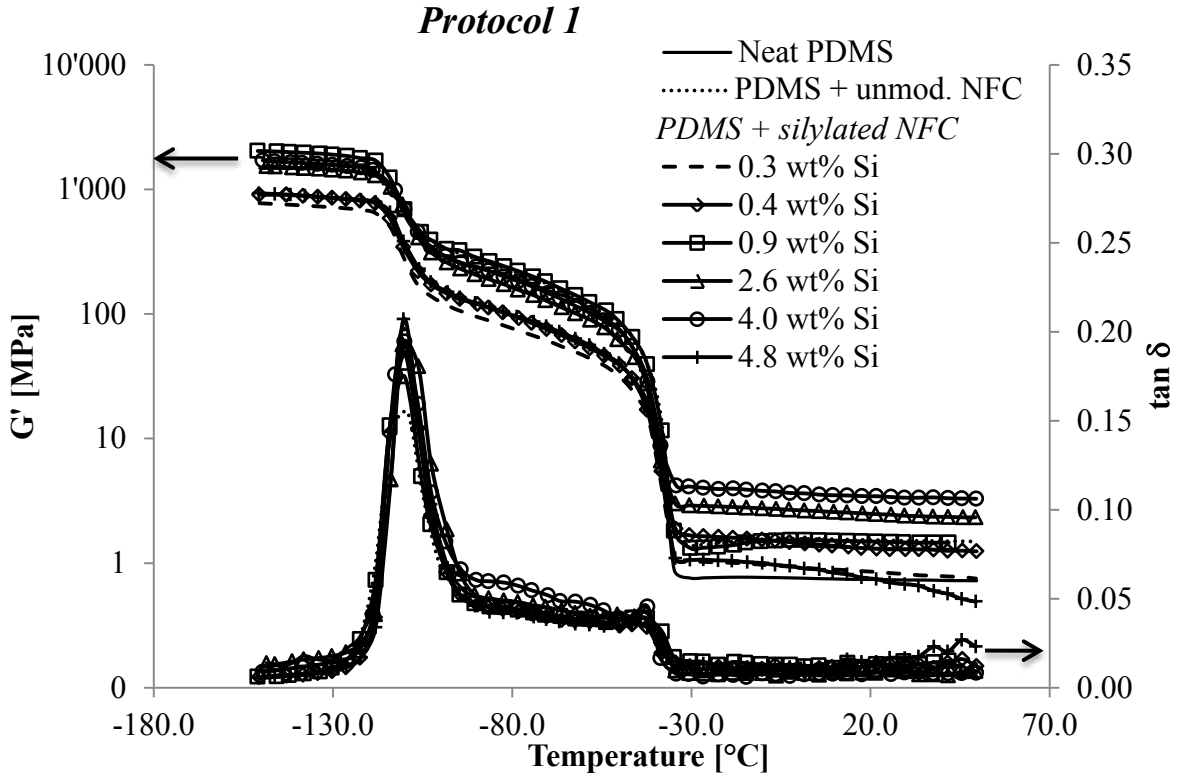

Figure 43: Temperature-dependant shear modulus and damping factor (tanδ) of composites containing 1 % NFC treated at different $[MTMS]_i$ (*Protocol 1*)

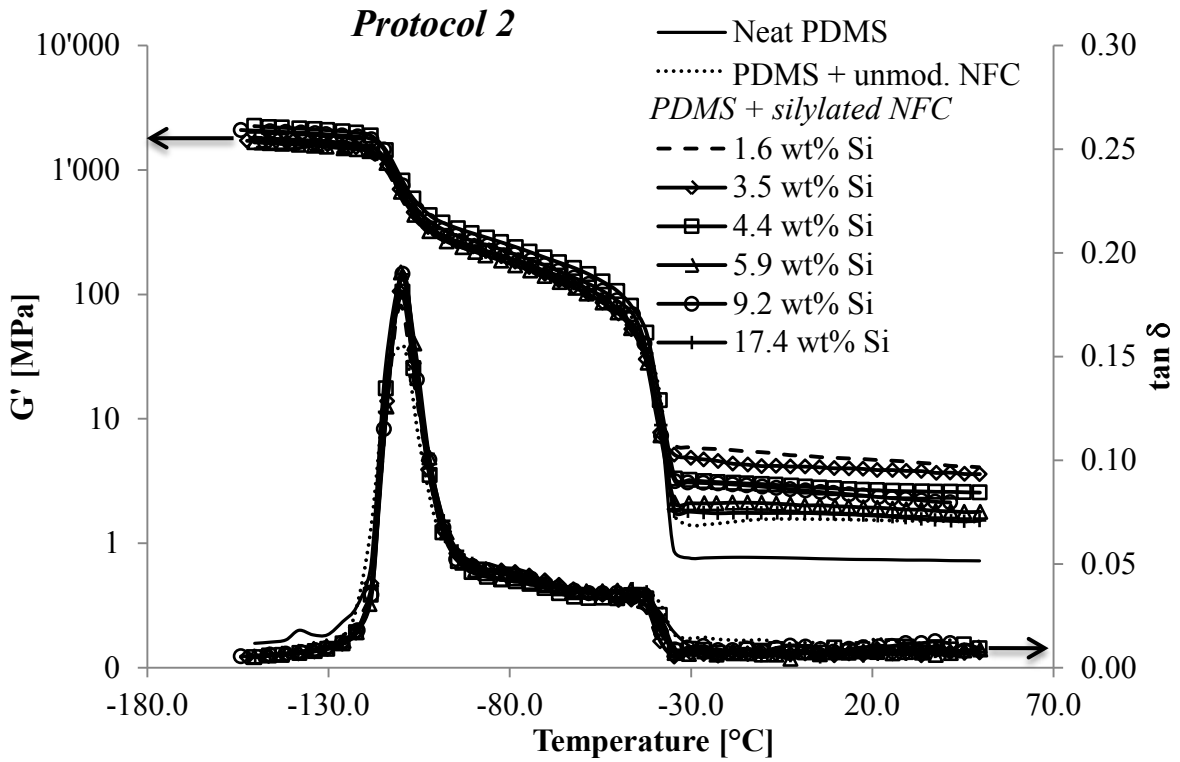

Figure 44: Temperature-dependant shear modulus and damping factor (tanδ) of PDMS composites containing 1 % NFC treated at different $[MTMS]_i$ (*Protocol 2*).

Spanning from low to high temperatures, three different regions could be identified for neat PDMS: the glassy state (below -110 °C), the rubbery state (approx. between -110 and -40ºC) and finally the melting plateau (above -40 °C). The neat PDMS exhibited a glass transition (T_g) of – 110 ºC and a melting temperature of – 42 °C according to the tan δ curve. These results are in agreement with the literature.[205]

The presence of unmodified or silylated NFC had quasi no influence on the viscoelastic response of the resulting nanocomposites, except in the higher temperature region, above -40 °C.

The G' values obtained at 40 °C for neat PDMS and its composites have been reported in Figure 45.

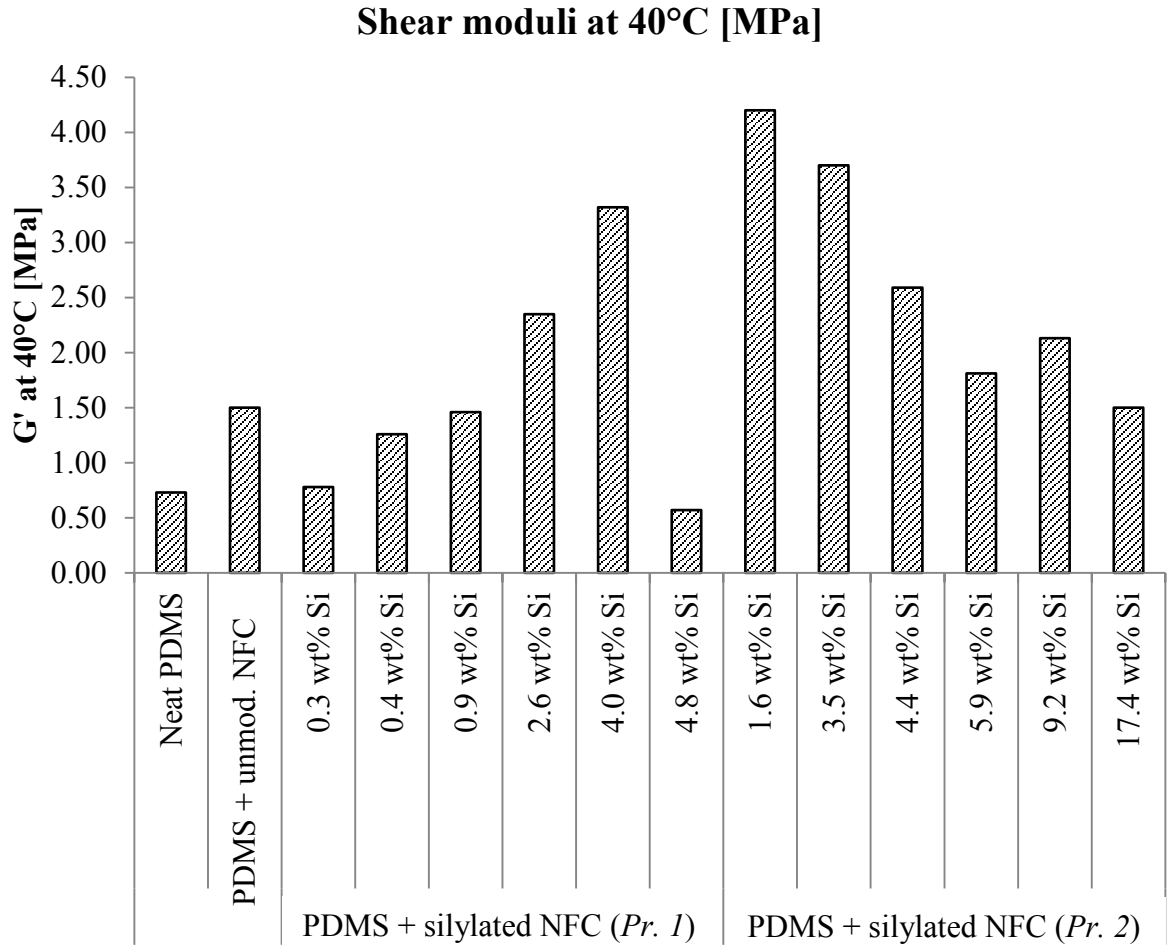

Figure 45: Shear moduli of the different PDMS composites at 40 °C.

The incorporation of 1 % unmodified NFC in the PDMS polymer led to an increase in G' by a factor of ~ 2. A further increase was noted after silylation, depending on the protocol used and the silylation level. The best results were obtained with *Protocol 2*, when the NFC surface was only slightly silylated (Si wt% = 1.6 %), of which the shear modulus was increased by a factor of ~ 6 in that case. This was attributed to an improved compatibility at the fibre-matrix interface, which was believed to be optimal at this level of modification. By increasing further the silane content, a progressive decrease in G' was observed, confirming the importance of controlling the silylation level at the NFC surface. Although the improvement was less when *Protocol 1* was used, an increase in G' by a factor of ~ 5 was still noted with NFC containing 4 % Si. Unlike in the case of *Protocol 2*, G' was lower at low Si content, but a different behaviour was expected since the coverage and distribution of polymerized MTMS at the NFC surface was significantly different (see Chapter II.2.4). A better interfacial adhesion was obviously obtained when the NFC surface was uniformly covered by the silane (*Protocol 2*),

rather than simply decorated with dispersed particles (*Protocol 1*). But an excessive coverage can also have a detrimental effect.

The very low G' obtained with NFC containing 4.8 % Si (Protocol 1) may be related to the presence of large polysiloxane particles in the NFC sample (see Figure 32 in Chapter II.2.4.3), which might impact negatively the interfacial properties.

No clear modification of tan δ intensity could be detected in the composite materials compared with neat PDMS. Probably the NFC content (1 %) wass not sufficient to significantly alter the mobility of the PDMS chains.

III.2.2. Tensile properties

The tensile properties of PDMS composites were evaluated by performing tensile tests experiments. The elastic modulus (E), tensile strength (σ) and strain at break (ε) of the composites are presented in Figure 46.

Different parameters can influence the mechanical properties of fiber-reinforced composites, such as fiber/matrix interfacial adhesion, fiber aspect ratio, fiber orientation etc.[206]

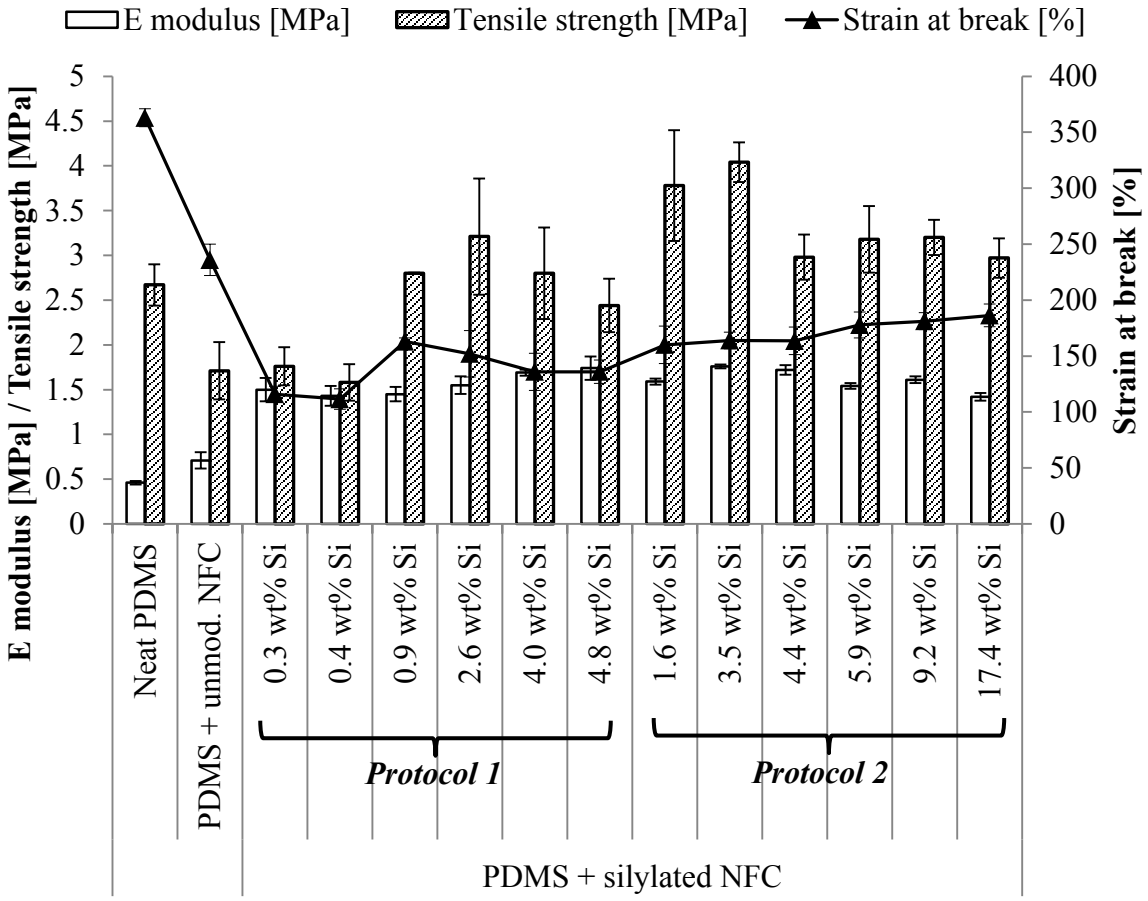

Figure 46: Elastic modulus (E), tensile strength (σ) and strain of break (ε) of PDMS composites containing 1 % NFC treated at different $[MTMS]_i$ according to *Protocol 1* or *Protocol 2*.

A slight increase in E modulus was noted after 1% of unmodified NFC was incorporated into the PDMS polymer, but after silylation, the increase was more significant. The E modulus increased by a factor of ~ 3 after NFC was treated with MTMS, regardless of the protocol and or the silylation level, indicating that the compatibility between the silylated NFC and the PDMS matrix was improved to some extent.

For tensile strength, significant improvement was obtained only when NFC was silylated according to *Protocol 2*, and when the Si content was not excessively high (1.6 and 3.5 %), which is in consistency with viscoelastic results (see Figure 45). All other silylated samples displayed σ values in the same order of magnitude than PDMS or lower when the Si content was low. A 30 % decrease in σ was noted with unmodified NFC, or when the Si content was below 0.4 %, confirming the poor compatibility between the hydrophobic PDMS and the hydrophilic NFC.

The strain at break was significantly decreased after the addition of 1 wt % unmodified NFC into the PDMS matrix, indicating that the material became more brittle. To our knowledge, no other studies on PDMS composites containing NFC have been reported. But this result is not surprising, since the introduction of NFC in other polymers often leads to a reduction in ε, as mentioned in I.4.1.2. ε decreased further after silylation, but no significant difference was noted between the composites prepared with the different types of silylated materials.

III.2.3. Thermal stability

The thermal stability of neat PDMS and its composites was evaluated by thermogravimetric analysis (TGA), under inert atmosphere. The thermograms are presented in Figure 47a and 47b (*Protocol 1 & 2*, respectively). The degradation data, *i.e.* temperatures associated with a 5 % weight loss ($T_{5\ \%}$), maximum degradation temperatures (T_d) and weight percentage residue at 900 °C ($W_{900\ °C}$), are reported in Table 7.

Table 7: Degradation data obtained from TGA analysis of PDMS composites containing 1 % unmodified or MTMS-treated NFC. $T_{5\ \%}$: temperature associated with a 5 % weight loss; T_d: maximum degradation temperature; $W_{900\ °C}$: weight percentage residue at 900 °C.

Filler	Si wt %	$T_{5\ \%}$ [°C]	T_d [°C]	$W_{900\ °C}$ [%]
No	-	392	426	1.1
1 wt % unmodified NFC	0	396	435	1.9
1 wt % MTMS-treated NFC (*Protocol 1*)	0.3	374	444	1.6
	0.4	389	451	2.0
	0.9	407	467	1.8
	2.6	374	433	2.2
	4.0	377	432	2.1
	4.8	397	449	2.1
1 wt % MTMS-treated NFC (*Protocol 2*)	1.6	377	432	2.5
	3.5	376	428	3.0
	4.4	403	462	2.0
	5.9	387	428	2.3
	9.2	398	452	2.3
	17.4	373	432	2.2

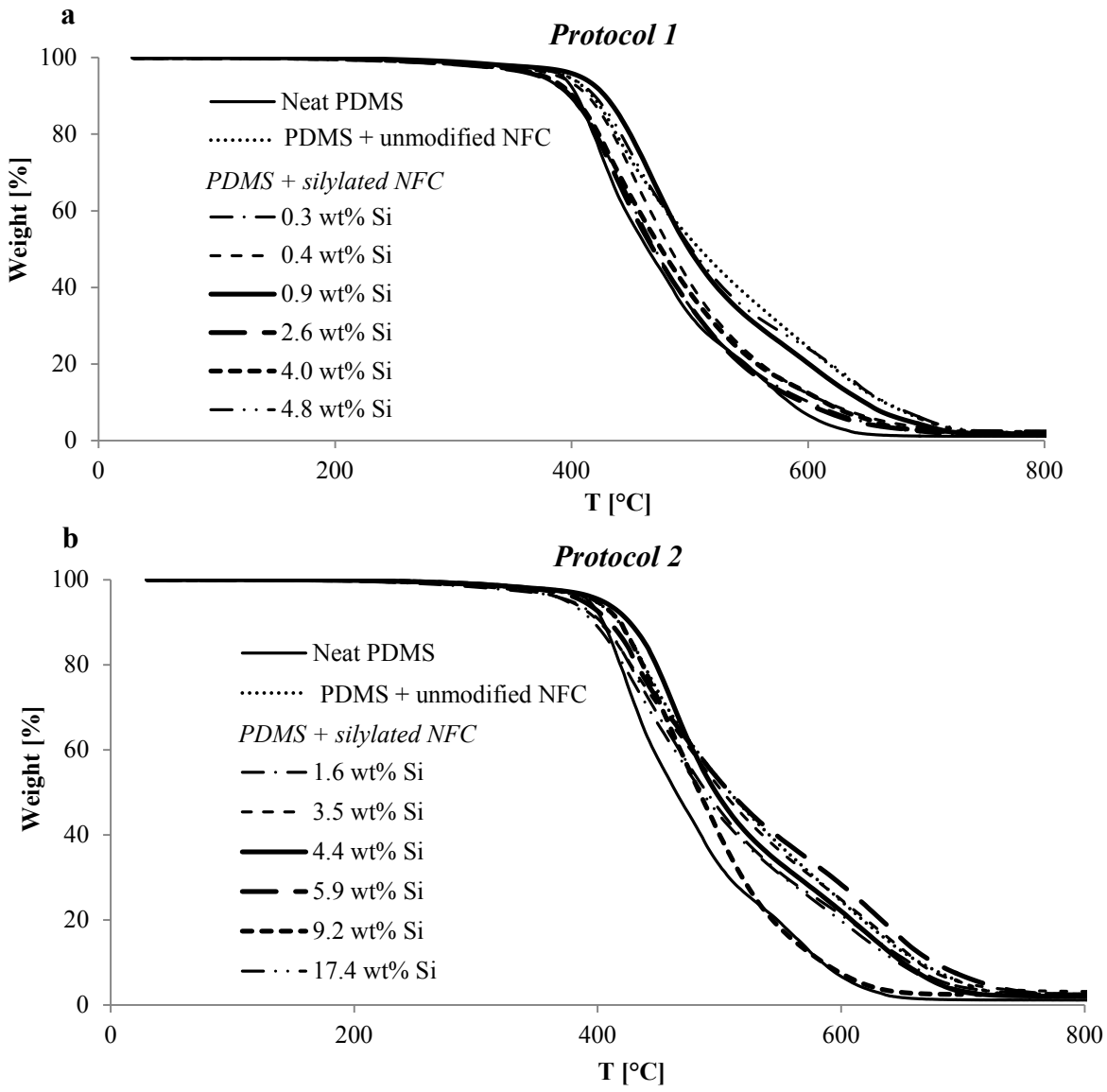

Figure 47: Thermograms of PDMS composites containing 1 wt % unmodified or MTMS-treated NFC (a: *Protocol 1* and b: *Protocol 2*).

All samples were thermally stable up to 300 °C, followed by a major weight loss in the temperature range between 300 °C and 750 °C, assigned to the decomposition of PDMS. Its maximum degradation temperature (Td) was recorded at 426 °C, in agreement with literature data.[200] The incorporation of unmodified NFC improved the thermal stability of the composites, as illustrated by the higher $T_{5\,\%}$ and T_d values measured in that case (Table 7). After silylation, further improvement was noted in some cases (increase in $T_{5\,\%}$ and T_d), degradations in others (decrease in $T_{5\,\%}$), but no clear trend could be neither established nor correlated with the viscoelastic and mechanical properties measured in previous chapter.

The introduction of unmodified or silylated NFC increased the weight percentage residue obtained at 900 °C ($W_{900\ °C}$), but once again, no clear trend could be established when comparing the samples.

III.2.4. Hygroscopicity

PDMS is a highly hydrophobic polymer,[207, 208] while cellulose is hydrophilic. It was thus important to investigate the impact of NFC on the hygroscopic properties of PDMS composites.

These properties were evaluated using Dynamic Vapour Sorption (DVS) experiments. The water sorption isotherms of the composites are presented in Figure 48a and 48b (*Protocols 1 & 2*, respectively).

In all cases, a continuous increase in water sorption was measured, when RH was increased from 5 to 95 %. With neat PDMS, the maximum moisture uptake was low (0.1 %), confirming the hydrophobic character of this material. The incorporation of NFC in the PDMS matrix slightly increased the hygroscopicity of the material, but the maximum moisture uptake remained low in all cases (below 0.3 %). Water uptake tended to be more limited when NFC was highly silylated.

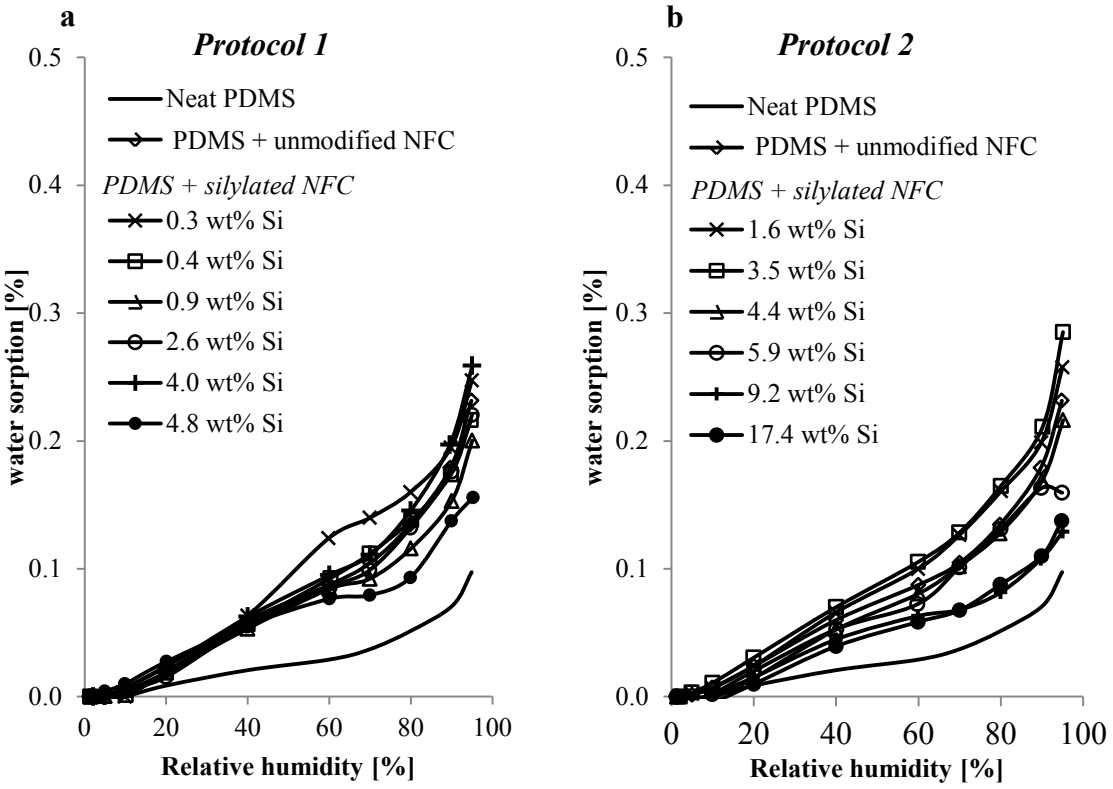

Figure 48: Water sorption isotherms of PDMS composites containing 1 wt % unmodified or MTMS-treated NFC (a: *Protocol 1* and b: *Protocol 2*).

III.3. PLA composites

All composites samples were prepared by solvent casting, using suspensions containing 10 wt % of unmodified or MTMS-treated NFC in chloroform. Composites were prepared based on a formulation already described in the literature.[72]

III.3.1. Crystallinity of PLA in composites

The mechanical properties of PLA and its composites are highly impacted by the crystallinity of the polymer.[74, 209] The crystallinity (X_c) of the neat PLA and its composites was accordingly evaluated from the melting enthalpies (ΔH_m) measured by DSC (Table 8).

All PLA composites presented a higher crystallinity compared with neat PLA (X_c = 34 %), which can be assigned to the nucleation effect of NFC.[149, 210] A crystallinity of about 40 % was measured in all cases, regardless of the protocol used and the silylation level.

The glass transition temperature (T_g) of PLA measured by DSC, did not show any significant modification after incorporation of unmodified or silylated NFC ($T_g \approx 60$ °C in all cases).

Hence, the chains mobility in PLA was not significantly impacted by the nanofibres dispered within the material.[149]

Table 8: DSC and DMA data obtained after analysis of PLA composites containing 10% of unmodified or MTMS-treated NFC.

Filler	Si wt % (of NFC)	DSC			DMA		
		T_g [b] [°C]	ΔH_m [c] [J/g]	X_c [%]	E' at 33 °C [GPa]	E' at 100 °C [GPa]	T_g [a] [°C]
no	0	60	31.6	34.0	2.9 ± 0.39	0.15 ± 0.02	64
10 wt % unmodified NFC	0	59	33.7	40.2	3.0 ± 0.10	0.34 ± 0.02	62
10 wt % MTMS-treated NFC (*Protocol 1*)	0.3	60	33.1	39.6	2.8 ± 0.08	0.32 ± 0.01	61
	0.4	60	33.3	39.8	2.4 ± 0.11	0.28 ± 0.02	61
	0.9	60	32.4	38.7	3.2 ± 0.14	0.34 ± 0.02	61
	2.6	59	33.6	40.1	2.8 ± 0.15	0.33 ± 0.02	59
	4.0	59	35.3	42.2	3.0 ± 0.10	0.33 ± 0.02	60
	4.8	59	32.3	38.6	2.9 ± 0.14	0.27 ± 0.01	62
10 wt % MTMS-treated NFC (*Protocol 2*)	1.6	60	32.2	38.5	2.4 ± 0.32	0.24 ± 0.06	62
	3.5	59	34.0	40.6	2.7 ± 0.13	0.31 ± 0.01	61
	4.4	60	33.0	39.4	2.3 ± 0.07	0.26 ± 0.01	64
	5.9	61	31.2	37.3	2.6 ± 0.11	0.26 ± 0.01	63
	9.2	59	31.4	37.5	2.2 ± 0.18	0.23 ± 0.01	62
	17.4	61	32.4	38.7	2.0 ± 0.05	0.14 ± 0.01	64

[a] T_g evaluated by DMA (tanδ); [b] T_g evaluated by DSC during the second heating run; [c] ΔH_m determined by DSC during the first heating run.

III.3.2. Viscoelastic properties

The viscoelastic properties of the PLA composites were evaluated by Dynamic Mechanical Analysis (DMA) in tension mode. The evolution of storage modulus (E') and damping factor (tan δ) of neat PLA and PLA reinforced with NFC treated at different $[MTMS]_i$ (*Protocol 1* or *Protocol 2*), are presented in Figure 49 and Figure 50. The E' values measured at 33 °C and 100 °C are reported in Table 8, along with the T_g extracted from the tan δ curves.

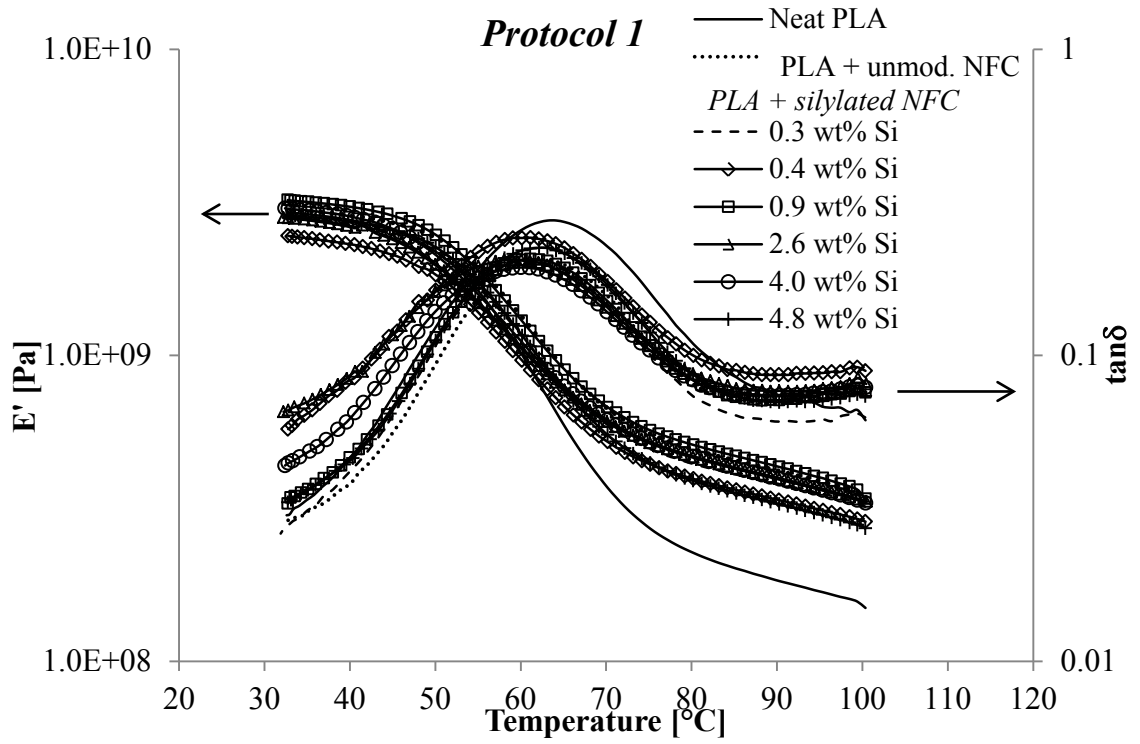

Figure 49: Storage moduli (E', left-side Y-axis) and damping factor (tanδ, right-side Y-axis) of PLA composites containing 10 % NFC treated at different $[MTMS]_i$ (*Protocol 1*)

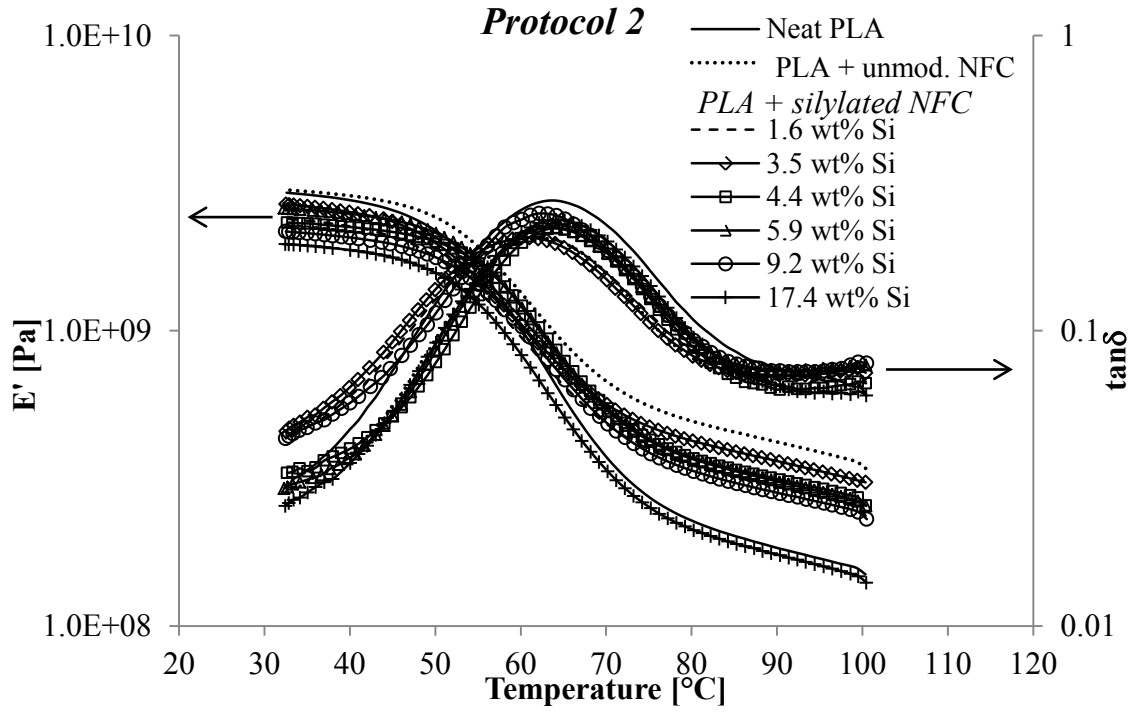

Figure 50: Storage moduli (E', left-side Y-axis) and damping factor (tanδ, right-side Y-axis) of PLA composites containing 10 % NFC treated at different $[MTMS]_i$ (*Protocol 2*)

The reproducibility of the response was very good, as demonstrated by the low standard deviations measured (Table 8).

Spanning from low to high temperatures, three different regions could be identified: the glassy state (below 45ºC), the glass transition (approx. between 45 and 80ºC) and the rubbery plateau (approx. between 80 and 100ºC). The neat PLA exhibited a T_g of 64 ºC, in agreement with the literature data.[72]

The presence of unmodified or silylated NFC had quasi no influence on the viscoelastic response in the glassy region. In the glass transition region, the damping intensity (tan δ) was not significantly modified, in the presence of fillers, regardless of the type of NFC used. This confirms that the mobility of PLA chains was not significantly impacted by the nanofibres.

In the rubbery region, a significant reinforcing effect was generally observed in presence of unmodified NFC, but silylation did not improve further the performances of the composites. With *Protocol 1*, performances were often similar to the ones obtained without the treatment, but with *Protocol 2*, the reinforcement effect was systematically lower. With this method, the NFC surface was increasingly covered by the polysiloxane when $[MTMS]_i$ was increased (see Figure 32g-l). This increasingly prevents the formation of hydrogen bonds between nanofibrils. As a consequence, it is more difficult for silylated NFC to create a percolation network within the PLA matrix, which is known to participate to the reinforcing effect in composites.[73, 74, 135, 209, 211] With *Protocol 1*, NFC was simply decorated by polysiloxane particles (see Figure 32b-f) and hydroxyl groups are still available for hydrogen bonding. This may explain why the properties were less degraded in that case.

As a comparison, significant improvement were noted when 10 wt% acetylated NFC were dispersed in PLA.[72, 122, 123]

III.3.3. Tensile properties

The tensile properties of the PLA composites were evaluated by performing tensile test experiments. The elastic modulus (E), tensile strength (σ) and strain at break (ε) are presented in Figure 51.

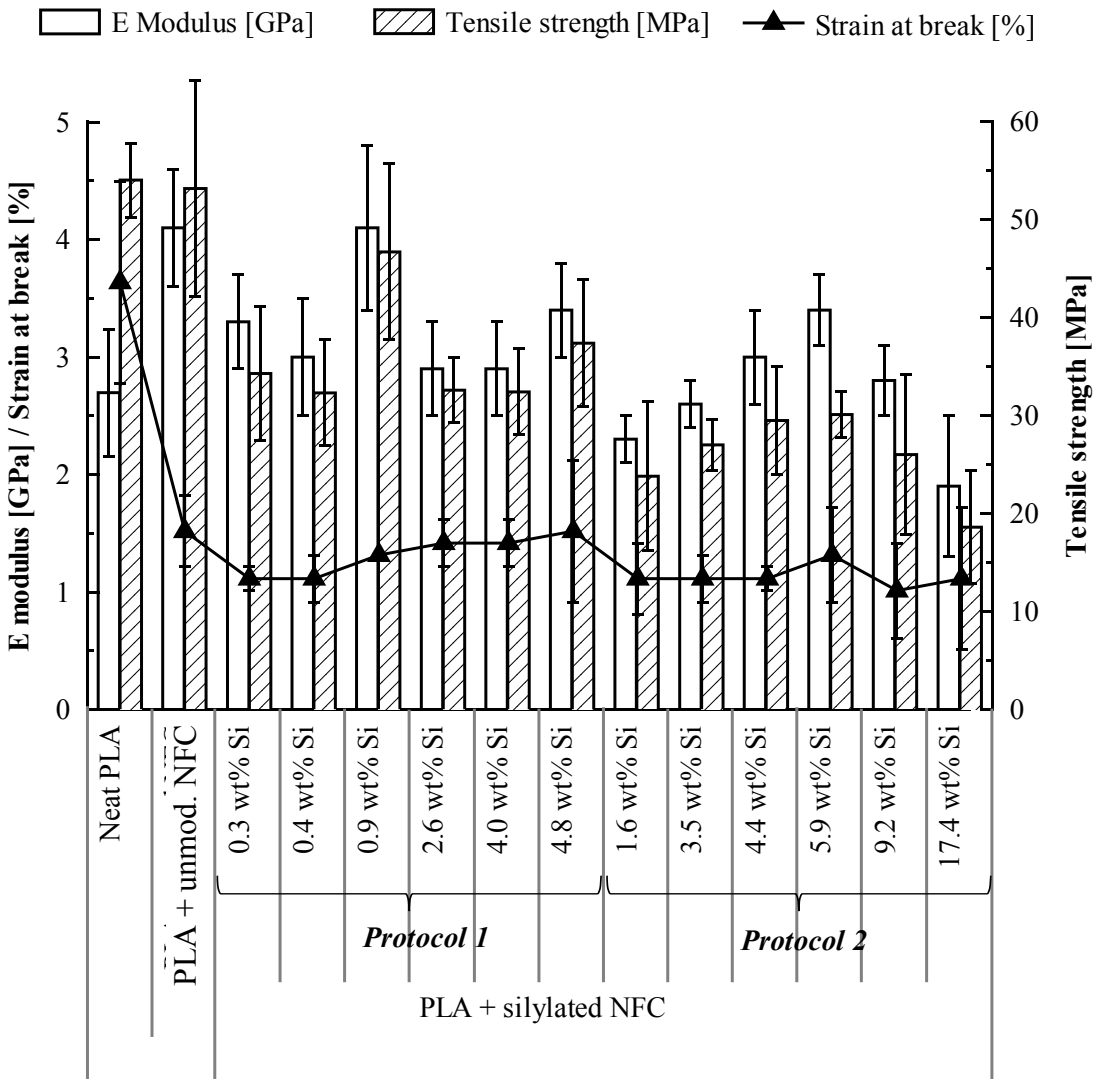

Figure 51: Elastic modulus (E), tensile strength (σ) and strain of break (ε) of PLA composites containing 10 % NFC treated at different $[MTMS]_i$ according to *Protocol 1* or *Protocol 2*.

Neat PLA displayed E modulus and tensile strength values of 2.7 ± 0.5 GPa and 54 ± 3.8 MPa, respectively, in good agreement with literature data.[212, 213]

The presence of 10 % unmodified NFC increased the E modulus by a factor of ~ 1.5, but tensile strength was not modified and strain at break decreased. The increase in E was correlated with the nucleating effect of NFC, which significantly increased the crystallinity of PLA (see chapter II.3.2). No improvement or rather a degradation of the composites performances was noted after silylation, in consistency with DMA results. Obviously, the compatibility between PLA and NFC was not improved by the MTMS treatment and/or the

possibility for hydrogen bonding was decreased (especially with *Protocol 2*). In addition, the silylated NFC could be badly dispersed within the PLA matrix and agglomerates might have formed.

III.3.4. Thermal stability

The thermal stability of neat PLA and its composites was evaluated by TGA under inert atmosphere. The thermograms are presented in Figure 52a and 52b (*Protocol 1 & 2*, respectively). The degradation data, *i.e.* $T_{5\,\%}$, T_d and $W_{600°C}$ are reported in Table 9.

Table 9: Degradation data obtained from TGA analysis of neat PLA and PLA composites containing 10 wt% unmodified NFC or MTMS-treated NFC. $T_{5\,\%}$: temperature associated with a 5 % weight loss; Td: maximum decomposition temperature; $W_{600\,°C}$: weight percentage residue at 600 °C.

Filler	Si wt%	$T_{5\,\%}$ [°C]	T_d [°C]	$W_{600\,°C}$ [%]
no	0	353	396	0.7
10 wt % unmodified NFC	0	316	391	1.1
10 wt % MTMS-treated NFC (*Protocol 1*)	0.3	336	394	1.7
	0.4	336	393	1.6
	0.9	336	395	1.6
	2.6	276	389	1.7
	4.0	234	392	1.8
	4.8	334	397	2.1
10 wt % MTMS-treated NFC (*Protocol 2*)	1.6	313	389	2.0
	3.5	315	384	2.6
	4.4	331	394	3.4
	5.9	335	394	3.8
	9.2	339	397	4.3
	17.4	339	397	4.3

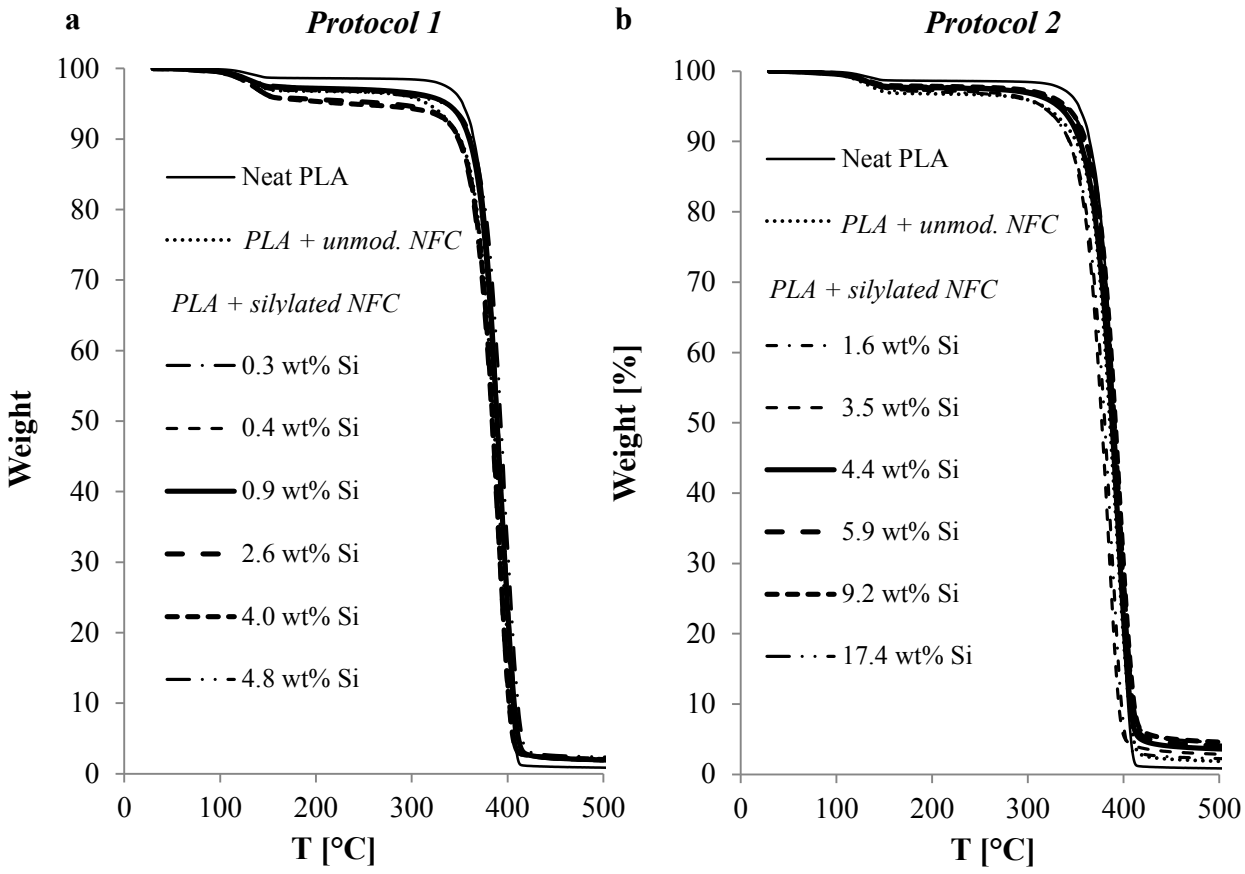

Figure 52: Thermograms of PLA composites containing 10 wt % unmodified or MTMS-treated NFC (a: *Protocol 1* and b: *Protocol 2*).

All the samples displayed a weight loss of 2 - 5 % at about 150 °C, which was associated with the loss of residual moisture and/or solvent (chloroform) present in the composites. The main degradation temperature of neat PLA was recorded at 396 °C, which agrees with literature data.[214]

The incorporation of unmodified NFC significantly decreased the thermal stability of the composites, as illustrated by the lower $T_{5\ \%}$ and T_d values measured in that case (Table 9). After silylation, some improvement in $T_{5\ \%}$ was often noted, but degradation still started earlier than in the case of neat PLA. The better results were obtained with NFC treated at high Si content with *Protocol 2*, but no clear trend could be established nor correlated with the viscoelastic and mechanical properties measured in previous chapter.

As expected, the weight percentage residue at 600 °C ($W_{600\ °C}$) increased steadily with increasing Si content.

III.3.5. Hygroscopicity

Despite its hydrophobic character, PLA is sensitive to moisture, which can in certain conditions result in polymer hydrolysis, self-catalysed by the carboxylic acid end groups of PLA chains.[215] In this context, the hygroscopic properties of PLA composites towards water vapour were evaluated by DVS. The water sorption isotherms of the composites are presented in Figure 53a and 53b (*Protocol 1 & 2*, respectively).

In all cases, a continuous increase in water sorption was measured, when RH was increased from 5 to 95 %. With neat PLA, the maximum moisture uptake remained low (0.8 %), confirming the hydrophobic character of this material. The incorporation of 10 % unmodified or silylated NFC in the PLA matrix increased significantly the hygroscopicity of the film, although the water uptake tended to be more limited when NFC was silylated.

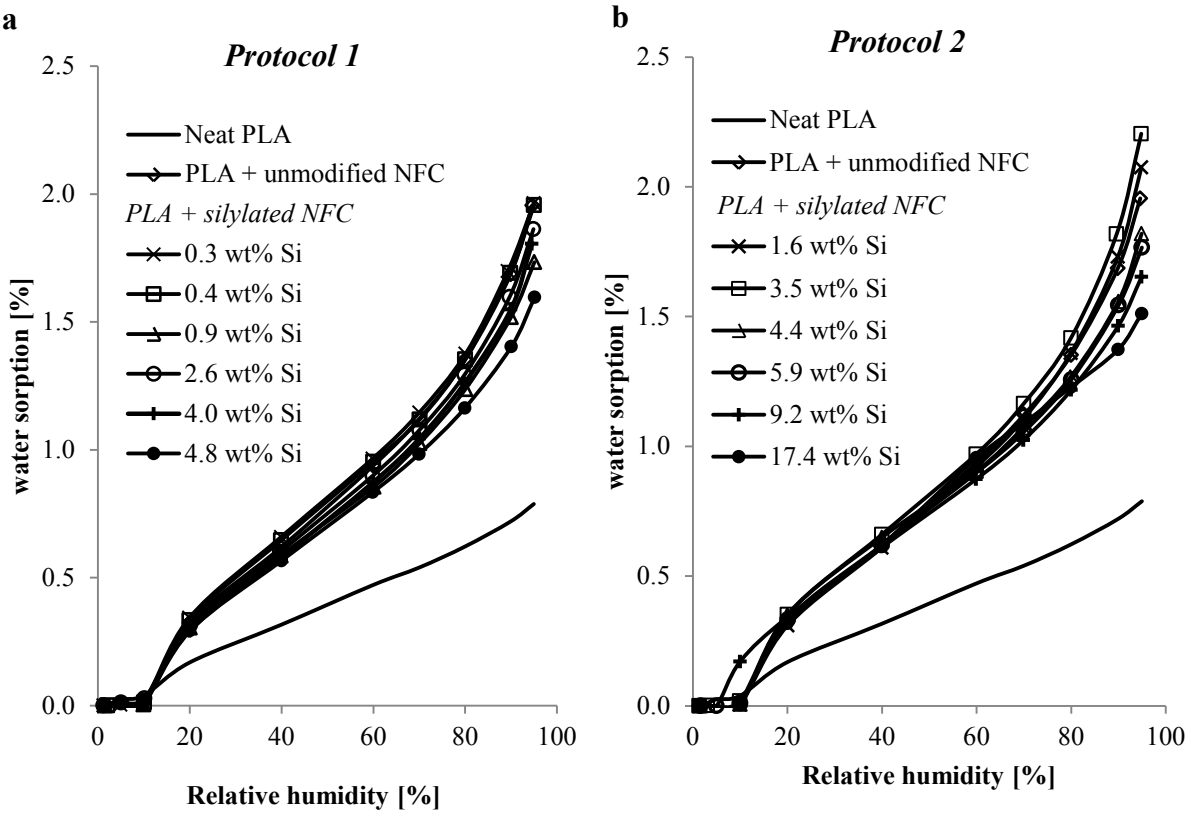

Figure 53: Water sorption isotherms of PLA composites containing 10 wt % unmodified or MTMS-treated NFC (a: *Protocol 1* and b: *Protocol 2*).

III.4. Concluding remarks

The results presented in the present chapter have shown that silylation had a different impact on the properties of NFC composites, depending on the matrix used.

With PDMS composites (1 wt% NFC), the shear modulus (G'), E modulus and tensile strength could be all improved after silylation with *Protocol 2*, as long as the experimental conditions were correctly controlled. But the strain at break systematically decreased after silylation, regardless of the method and silane content. The incorporation of NFC in the PDMS matrix slightly increased the hygroscopicity of the material, but the maximum moisture uptake remained low in all cases.

With PLA composites (10 wt% NFC), no significant improvement of the mechanical performances was noted after silylation, in the conditions investigated. The water uptake tended to be more limited at higher silylation level, but all NFC composites were more hydrophilic than neat PLA.

The thermal stability of both types of composites was improved in some cases, deteriorated in others, but no clear trend could be established or correlated with the silylation level or protocol used.

IV. Utilisation of silylated NFC for the elaboration of foams

IV.1. Objectives and methodology

As stated in Chapter I, cellulose nanofibres are increasingly being considered as building blocks for the elaboration of aerogels and foams, in replacement of already existing materials prepared from inorganic or non-renewable resources. Since aqueous NFC suspensions are characterized by the presence of long and interconnected hydrophilic cellulose nanofibrils, the subsequent replacement of water with air results in an aerogel or foam with long entangled cellulose nanofibres. Using the freeze-drying process, different morphologies can be obtained depending on the speed with which the freezing step is performed, from porous structures composted of nanofilaments to cellular structures (cf. Chapter I.4.2.3).

Despite the promising potential of cellulosic foams from NFC, several challenges must be addressed for these materials to compete with already existing technologies. While recent studies have shown that the stiffness and morphological structure of NFC foams can be adjusted with the concentration of the nanofibres in the gel (*i.e.*, increase in foam density), the shape recovery properties of the material are generally limited. Moreover, the hydrophilicity of cellulosic foams is detrimental to some applications, such as thermal insulation or oil-water separation.

In this chapter, silylated NFC foams have been investigated, with the aim to produce porous cellulosic materials with improved properties. Since *Protocol 2* was the only method allowing the grafting of a homogeneous polysiloxane layer at the NFC surface, it was selected as the silylation treatment, with slight modification of the freezing method. Instead of freezing quickly the NFC suspension to obtain thin films, a significant volume of the suspension was frozen slowly to favour the formation of cell wall sheet structures during freeze-drying (Cf. Scheme 23 in Chapter VI.4.3). This protocol, labelled as *Protocol 2*' in following paragraphs, allowed preparing silylated specimen that could be tested with regards to some basic properties, such as porosity, compressive properties, wettability, hygroscopicity, oleophilicity and thermal conductivity.

IV.2. Silylation of NFC foams

IV.2.1. Evolution of Si content

NFC foams with different silylation level were produced by varying the initial silane concentration (Table 10), using *Protocol 2'* (cf. Chapter VI.3.3). The evolution of Si content was again estimated from the calibration chart of Figure 15 (II.1.2.2). A linear increase in Si content was again noted with increasing $[MTMS]_i$, as was observed when NFC was silylated according to *Protocol 2* (cf. Chapter II.2.4.1).

Table 10: Si content in modified NFC foams prepared at different $[MTMS]_i$ according to *Protocol 2'*

$[MTMS]_i$ [mmol/g_{NFC}]	0	1.2	2.5	3.7	4.9	7.4	14.8	30.9
Si wt %	-	2.1	3.5	4.4	6.8	9.1	18.9	38.1

Reaction at room temperature, for 2 h and at pH 4

IV.2.2. Solid-state NMR characterization

The silylated NFC foams were characterized by ^{13}C and ^{29}Si CP-MAS NMR spectroscopy but since no significant difference was noted compared with former experiments with *Protocol 2* (cf. Chapter II.2.4.2), results were not included in the thesis.

The modification of the freezing method in Protocol 2' did not significantly impact the molecular structure of the polysiloxane species bonded to the cellulosic substrate. The presence of silane at the NFC surface was again confirmed by ^{13}C CP-MAS NMR, the intensity of the MTMS methyl moiety increasing gradually with increasing $[MTMS]_i$. In the ^{29}Si CP-MAS NMR spectra, the two signals corresponding to the di-condensed (T_{20} and/or T_{21}) and tri-condensed (T_{30}) structures were again detected at -56 and -65 ppm, respectively ($T_2/T_3 \sim 1$).

IV.2.3. Microscopy

The silylated NFC foams were analyzed by SEM microscopy. In general, differences are expected between the surface and the core of the foam when the freezing step is slow as in *Protocol 2'* (Figure 12 in I.4.2.3): the bottom layer, which freezes quickly, is generally composed of nanofilaments, while the core layer, which freezes slowly, is composed of cell wall sheet structures.

Accordingly, micrographs were taken at the top, bottom and core of each sample, when analyzing the foams by SEM (Scheme 21).

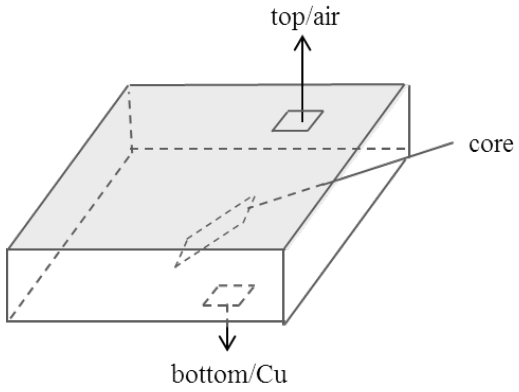

Scheme 21: Sketch of a foam prepared according to *Protocol 2'*. "Top" refers to the surface in contact with air during freezing; "bottom" refers to the surface which was in contact with the copper mold.

Three samples with low, medium and high Si content were analysed by SEM (Figure 54).

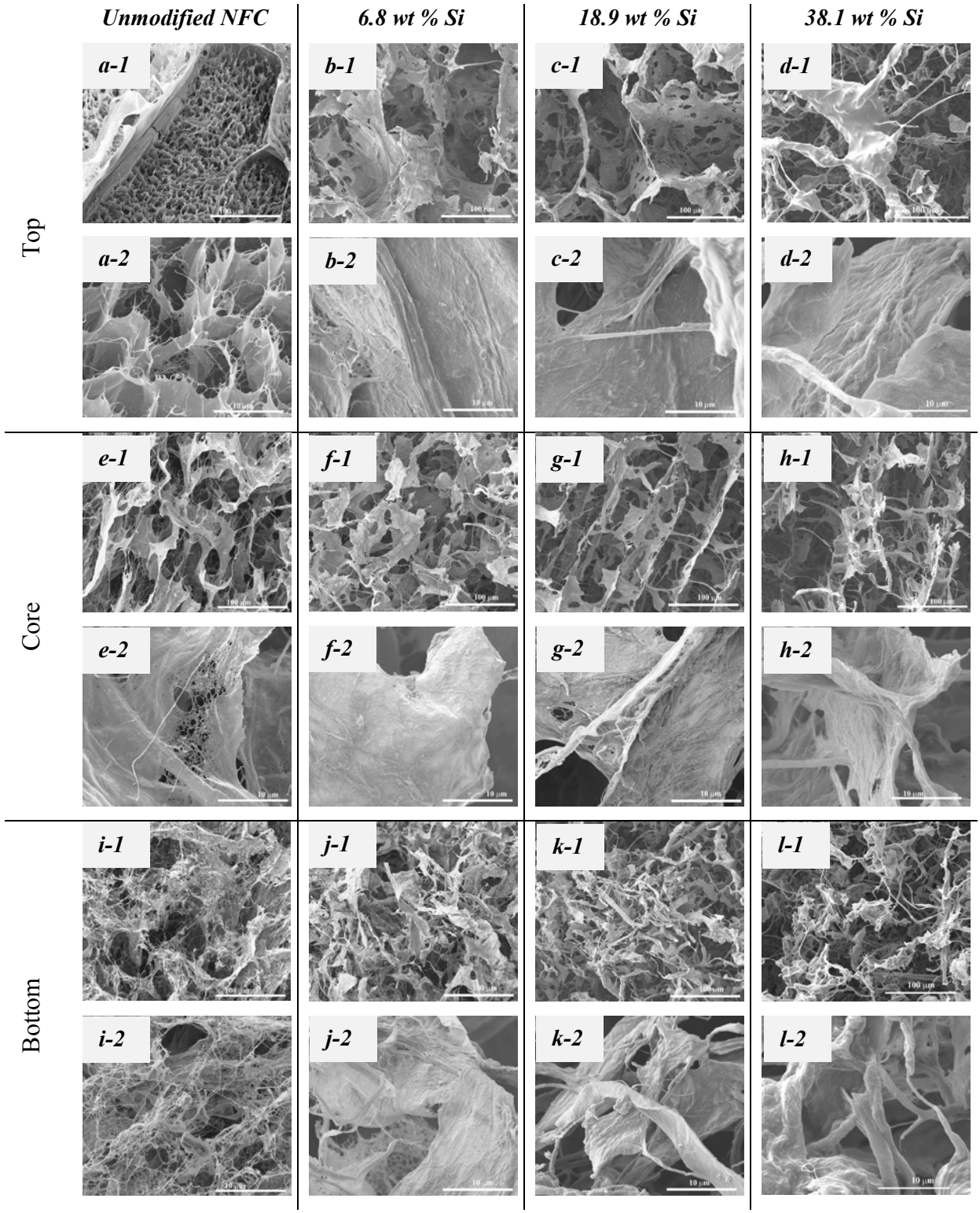

Figure 54: SEM micrographs of NFC foams containing 0, 6.8, 18.9 and 38.1 wt % Si. Three different locations within each sample were investigated: the top surface (a-d), the core (e-f) and the bottom (i-l). Two magnifications of each sample are shown: scale bar of 100 μm (1) and 10 μm (2).

The **top surface** of unmodified NFC foam (Figure 54a) displayed a regular arrangement of cells composed of thin sheet structures interconnected with nanofibrils of cellulose. After

silylation (Figure 54b-d), a less organized surface was obtained with thicker sheets structures and nanofibrils, while the pore size increased. Pores diameter was about 10 μm in the picture of unmodified NFC foams, while diameters ranged between 50 and 200 μm in the images of silylated samples. Probably the presence of silane in the water suspension promoted the formation of larger ice crystals during freezing, leading to bigger pores.

The structure of silylated foams was similar in the **core part** (Figure 54e-h), except that the nanofibrils and sheet structures tended to form "tubular" arrangements at high Si content (Figure 54g-h), which means that the ice crystals tended to grow in a regular manner during freezing. The unmodified NFC foams lost their regular arrangement in the core of the sample (Figure 54e).

As expected, the **bottom part (**which froze quickly) was composed mainly of nanofilaments, as in the case of samples prepared using the fast freezing process (Scheme 22). Similarly to samples prepared according to *Protocol 2*, the nanofibrils diameter tended to increase with increasing Si content. Sheet structures, which might correspond to hornified NFC covered with silane or to polysiloxane films, were also detected after silylation (Figure 54j-l).

The WDX Si mapping of the samples compressed to flat films is presented in Figure 55. An increase in overall image brightness was noted with increasing Si content, indicating that the NFC surface was increasingly modified. Similarly to the samples prepared according to *Protocol 2*, the NFC was fully and homogenously covered by the polysiloxane.

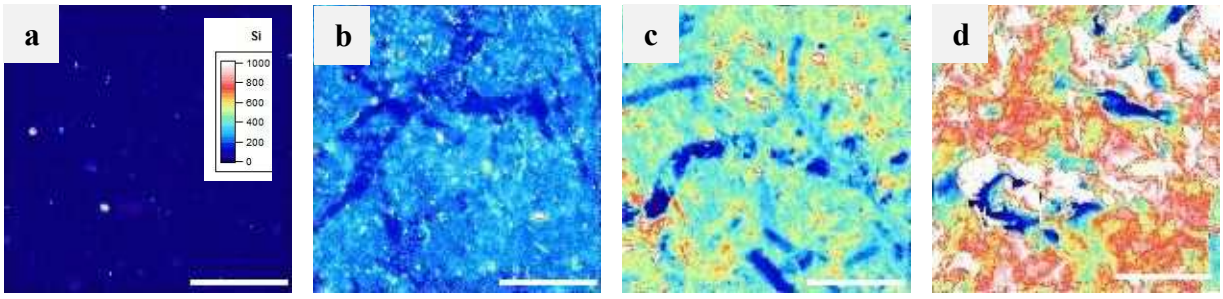

Unmodified NFC ***2.1 wt% Si*** ***6.8 wt% Si*** ***18.9 wt% Si***

Figure 55: WDX Si mapping of unmodified NFC foam (a) and silylated NFC foams prepared at different $[MTMS]_i$ according to *Protocol 2'*. (Scale bar is 100 μm)

IV.3. Properties of silylated NFC foams

IV.3.1. Density, porosity and specific surface area

The density, porosity and specific surface area of the various NFC foams were measured using experimental procedures widely described in the literature (Chapter VI.5.3).

The density of the foam (ρ_{foam}) and density of the cellulosic skeleton (ρ_s) were first evaluated, then the relative density of the material was calculated ($\phi = \rho_{foam}/\rho_s$). The porosity was estimated from ϕ, and the specific surface area was measured by the BET method. Results are summarized in Table 11.

Table 11: Physical and compressive proporties of unmodified and silylated foams. ρ_{foam}: bulk density of the foam; ρ_s: density of cellulose or MTMS-treated cellulose; ϕ: relative density; E: elastic modulus; $\sigma_{50\,\%}$: compressive stress at 50% strain.

Si wt %	Density			Porosity [%]	BET surface area [m^2/g]	E [kPa]	$\sigma_{50\,\%}$ [kPa]
	ρ_{foam} [kg/m^3]	ρ_s [kg/m^3]	ϕ				
0	6.70	1500	0.004	99.6	24.0	27.7	6.2
2.1	5.07	1510	0.003	99.7	25.0	1.3	0.8
3.5	5.56	1530	0.004	99.6	24.7	1.4	1.6
4.4	6.08	1560	0.004	99.6	23.3	1.9	1.3
6.8	8.60	1620	0.005	99.5	18.0	3.2	3.4
9.1	9.20	1650	0.006	99.4	12.3	3.2	2.8
18.9	11.0	1680	0.007	99.3	10.6	6.4	4.1
38.1	17.3	1750	0.010	99.0	3.1	12.7	6.1

Regardless of the silylation level, NFC foams were ultra-light weight and highly porous. The porosities and densities measured were consistent with the values mentioned in the literature, for foams prepared in similar conditions.[106, 131] A gradual increase in ρ_{foam} was noted with increasing Si content, which can be explained by the higher density of polymerized MTMS (ρ = 1900 kg/m^3)[216] compared with cellulose (ρ = 1500 kg/m^3).[111] Conversely, the BET surface area tended to decrease, indicating that the cellulose nanofibrils were increasingly aggregated during the freeze-drying process. This is in agreement with SEM images, where thicker sheets structures and microfibrils could be spotted at higher Si content (Figure 54e-h). Nevertheless, the highly silylated material remained very porous and light.

IV.3.2. Compressive properties

During our experiments, we noted that unmodified NFC foams were very fragile, while silylated NFC foams could be manipulated without breaking and showed high flexibility. Accordingly, the mechanical and shape recovery properties of the foams were evaluated by compression tests.

IV.3.2.1. Compressive stress-strain curves

Compressive stress-strain curves of NFC foams, with various Si content, compressed to 50 % of their original thickness, are presented in Figure 56.

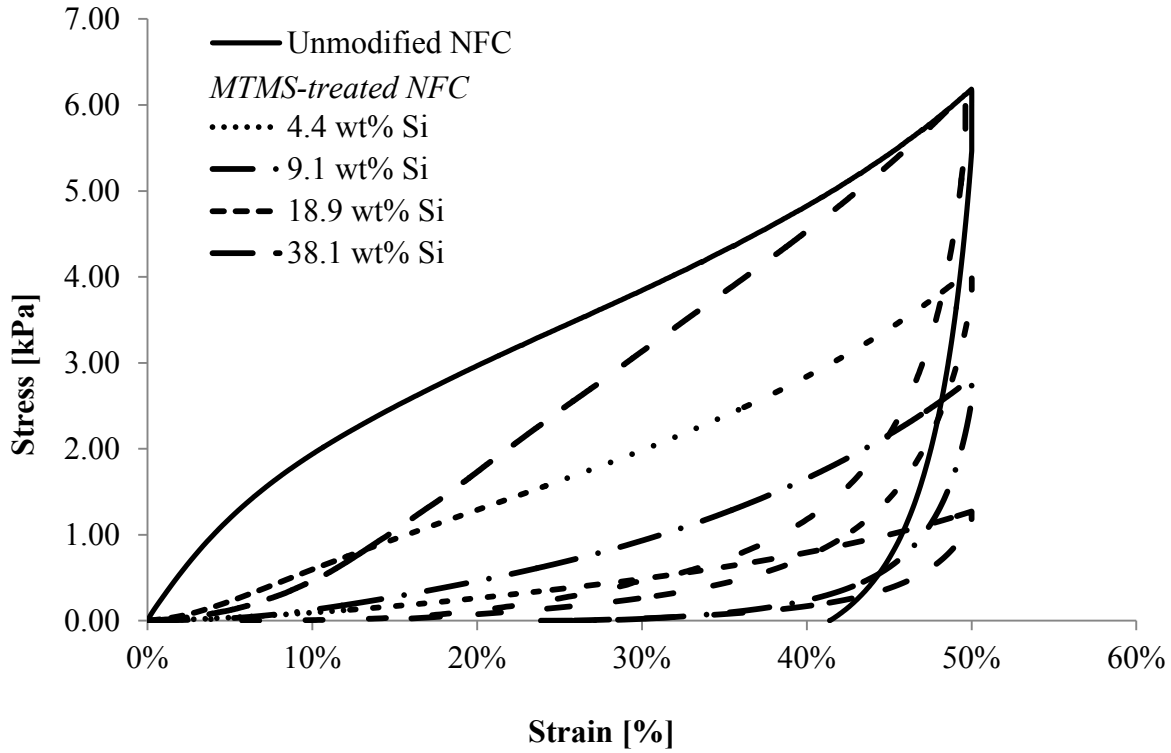

Figure 56: Compressive stress-strain curves of unmodified NFC foam and silylated NFC foams, prepared at different $[MTMS]_i$ according to *Protocol 2'*.

With unmodified NFC foam, a linear stress-strain behaviour was observed below 3 % initial strain, which was associated with elastic cell wall bending.[106] The Young's modulus (E) (27.7 kPa), extracted from this part of the curve, was lower than that already reported for NFC foams of similar density (*i.e.* 56 kPa).[106] But comparison is tricky since E depends on many factors, such as strain-rate, temperature, anisotropy and multiaxial loading.[67] In the range between 3 and 50 % strain, the transition from linear to non-linear behaviour was gradual, in a region where cell collapse takes place.[105, 106, 109] The substantial plastic deformation noted on

unloading the sample was assigned to irreversible collapsing of the cells and eventual hydrogen bonds formed during compression.

After silylation, the Young's modulus and stress at 50 % deformation ($\sigma_{50\,\%}$) were generally lower than for unmodified NFC foams, indicating that different deformation mechanisms occurred under compression. This is consistent with SEM results, which showed that the original cellular structure was significantly modified by the presence of MTMS during freeze-drying (Cf. Chapter IV.2.3). Both E modulus and $\sigma_{50\,\%}$ were quite low at low silylation level, but their value increased significantly with increasing Si content. Notably, the $\sigma_{50\,\%}$ value of the foam with the highest Si content (38.1 wt % Si) was in the same range for the unmodified material.

IV.3.2.2. Shape recovery experiments

The shape recovery properties of the foams were evaluated by unloading the specimens at 50 % strain and recording the residual strain (ε_{final}). The thickness recovery S, expressed in percentage of original thickness, was calculated according to Equation 6 (Chapter VI.5.3.4). The results obtained are plotted in Figure 57.

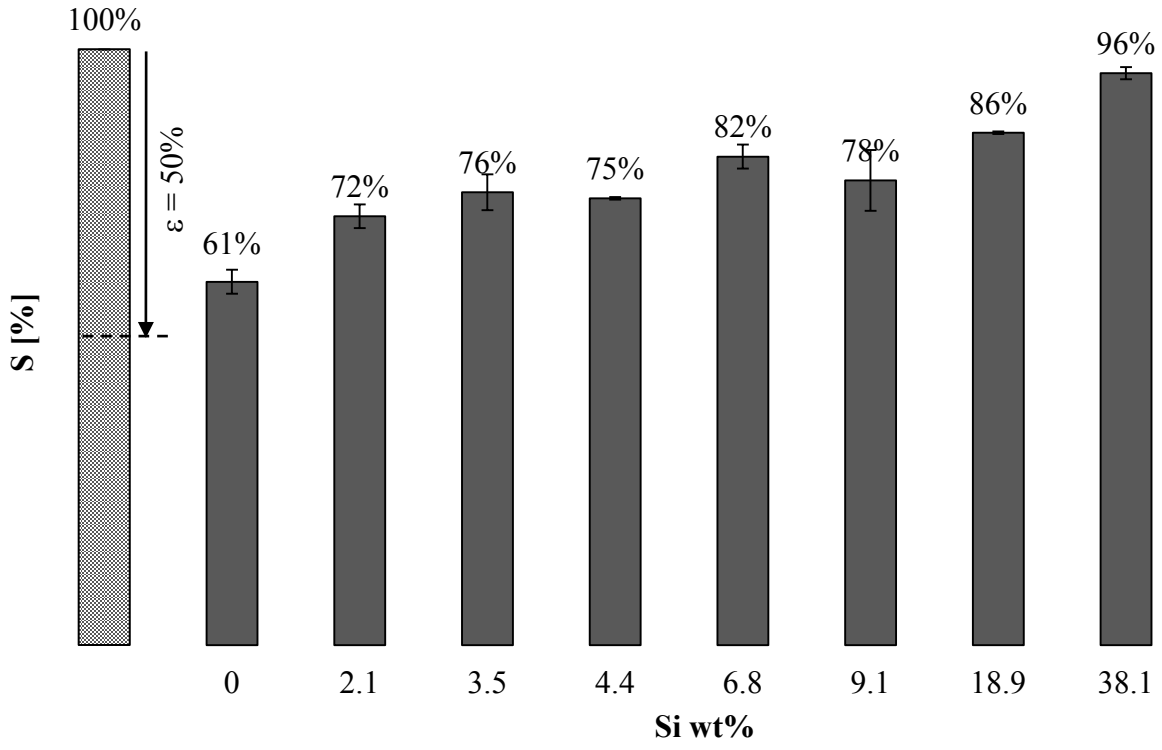

Figure 57: Thickness recovery (S) of unmodified and silylated NFC foams upon unloading at 50 % strain.

While unmodified NFC foam could recover only 59 % of its original thickness, S values between 70 and 96 % were obtained with the silylated material. Shape recovery was particularly important at high Si content, since 96 % of the original thickness could be recovered when the sample contained 38.1 wt % Si. To our knowledge, this is the first time that such flexibility is obtained with NFC-based foams, but flexible silica aerogels based on MTMS have been reported.[216, 217] These materials displayed a thickness recovery of 100 % on unloading the specimens at 60 % compression strain, which was explained by the repulsive interactions existing between methyl groups and the decrease in crosslinking density within the material. Accordingly, similar mechanisms could be considered for silylated NFC foams, since NFC was covered by a polysiloxane layer, and the interactions between neighbouring hydroxyl groups were limited.

IV.3.3. Wettability and hygroscopicity

IV.3.3.1. Wettability

The wettability of the foam surfaces was evaluated by measuring the contact angle of a water droplet deposited directly on the silylated materials. Top and bottom surfaces were evaluated since different morphological structures were observed by SEM (see Figure 54). The water contact angle (WCA) values obtained are presented in Figure 58.

As expected, the unmodified NFC foam displayed a strong hydrophilic character, as the water droplet was instantaneously absorbed by the substrate (no WCA could be recorded in that case on both surfaces).

The silylated NFC foams, on the other hand, were quite hydrophobic, since WCA values above 105° were always measured.

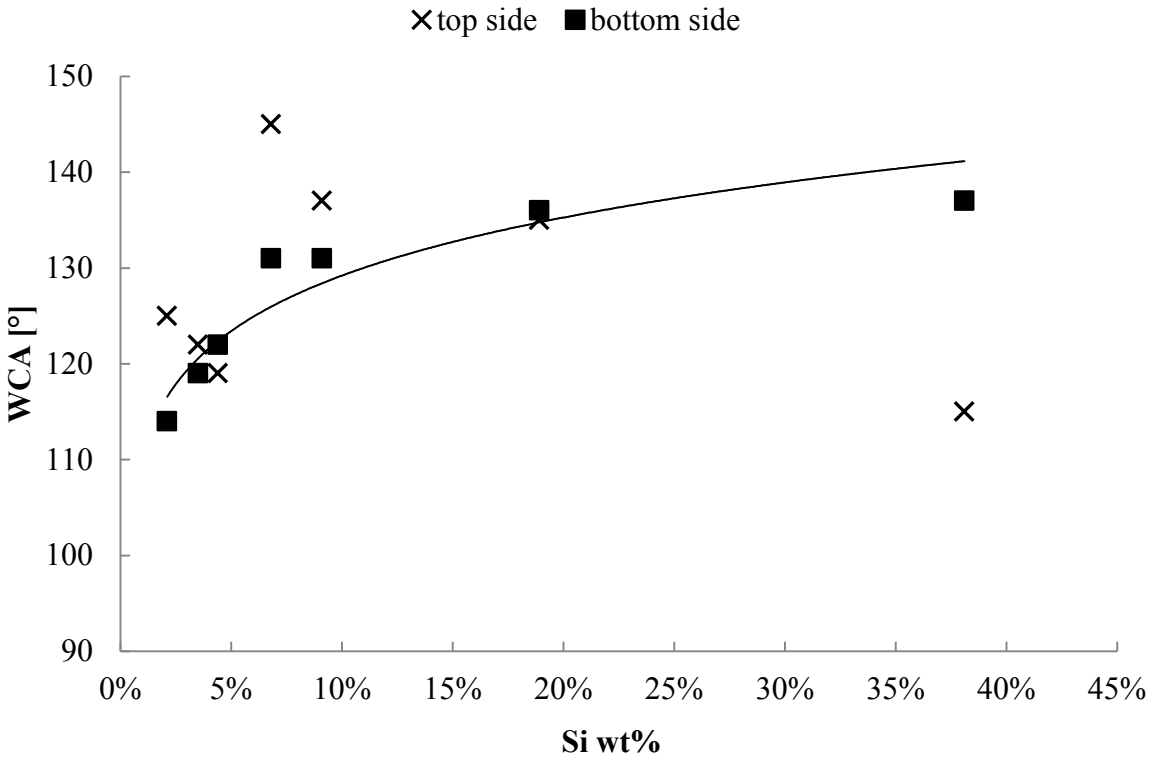

Figure 58: Water contact angle values (WCA) measured at the surface of NFC foams treated at different $[MTMS]_i$ according to *Protocol 2'*.

Nevertheless, differences were noted between the top and the bottom surfaces. The WCA on the bottom surface increased with the extent of silylation up to a maximum of 136° when the Si content was 18.9 wt %. These results correlated well with the wettability's measured at the surface of NFC modified according to *Protocol 2* in Chapter II.3.3.1 (Figure 38). This was expected since both of these surfaces underwent the same fast-freezing step, which led to nanofilaments of similar structure and morphology. The WCA values obtained at high silylation level were close to those already reported for NFC foams modified with chlorosilanes[131, 142, 143] or TiO_2 nanoparticles.[114, 144]

The WCA at the top surface did not show any specific trend with Si content, indicating that the surface morphology was more heterogeneous. It is well established that wettability is not only influenced by surface chemistry, but also by surface morphology and structure.[218] Unlike the bottom surface, the top surface underwent a slow-freezing step, which led to a porous structure composed of cell wall sheets interconnected with nanofibrils (see Chapter IV.2.3). The size of the pores and the structure of the NFC network at the surface were shown to vary depending on the silylation level (see Chapter IV.2.3).

IV.3.3.2. Hygroscopicity

The hygroscopicity of the foams was evaluated by Dynamic Vapour Sorption (DVS). The water sorption isotherms obtained are presented in Figure 59.

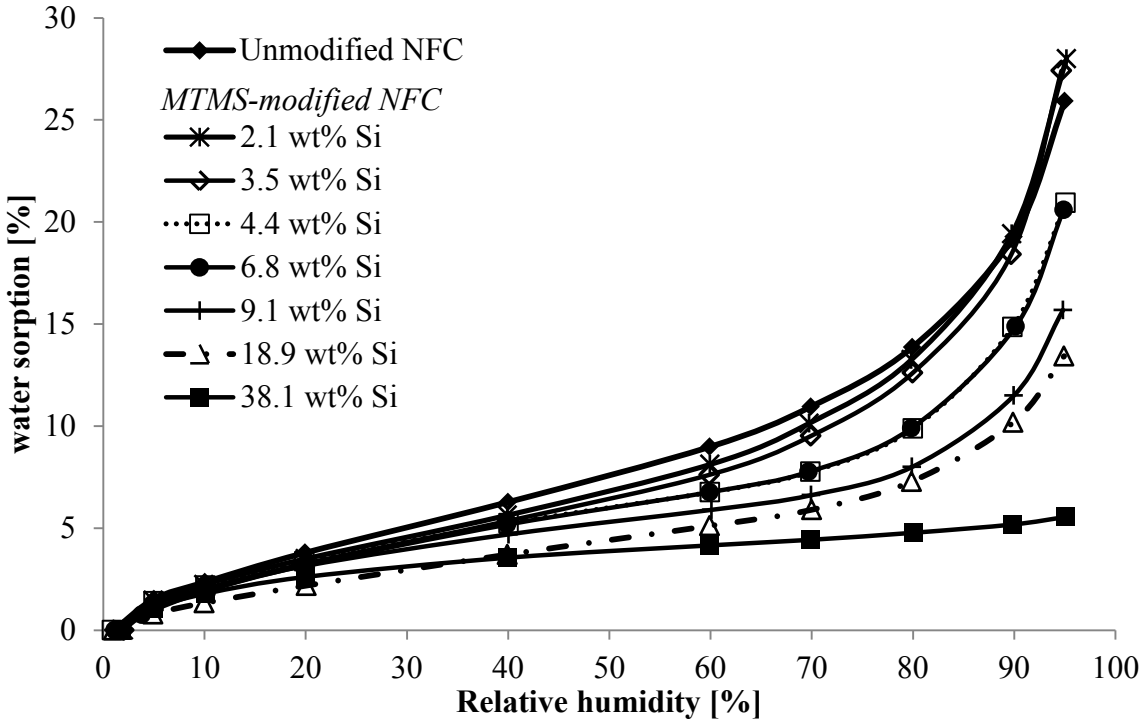

Figure 59: Water sorption isotherm of unmodified NFC foam and NFC foams prepared at different [MTMS]i according to *Protocol 2'* (T = 23 °C).

The silylated NFC foams presented water sorption values, which tended to decrease with increasing Si content. The accessibility to water of NFC hydroxyl groups most probably decreased after decoration of the surface by polysiloxane molecules, but the analysed silylated samples contained also less cellulosic material compared with the unmodified control. In any case, the hygroscopicity of NFC foam containing 38.1 wt % Si was particularly low.

IV.3.4. Oleophilic properties

The silylated foams were further characterized with regards to their oleophilic properties, to verify their potential as absorbent for oil removal.

For these experiments, the silylated foam sample containing 18.9 wt % Si was used and compared with an unmodified sample having the same density and porosity (Table 12).

Table 12: Physical and compressive properties of unmodified and silylated foams prepared at different NFC concentration (C_{NFC}). ρ_s: density of cellulosic skeleton; ϕ: relative density; BET: BET surface area; E: elastic modulus; $\sigma_{50\,\%}$: compressive stress at 50 % strain.

Si wt %	C_{NFC} wt %	ρ_{foam} [kg/m^3]	ρ_s [kg/m^3]	ϕ	Porosity [%]	BET [m^2/g]	E [kPa]	$\sigma_{50\,\%}$ [kPa]
0	1.0	10.6	1500[67]	0.007	99.3	14.6	79.6	21.6
18.9	0.5	11.0	1680	0.007	99.3	10.6	6.4	4.1

Dodecane was used as model oil and was coloured in red using the *Sudan III* dye. Water was coloured in blue using the *Neolan Blau* dye.

IV.3.4.1. Absorption test

Drops of water and dodecane were deposited at the surface of unmodified and silylated foams (Figure 60). As expected, dodecane was instantaneously absorbed by the silylated sample, while the water drop remained at the surface, confirming the combined hydrophobicity/oleophilicity properties of the material. The unmodified sample, on the other hand, absorbed both dodecane and water, demonstrating its amphiphilic character in line with literature data.[219-221]

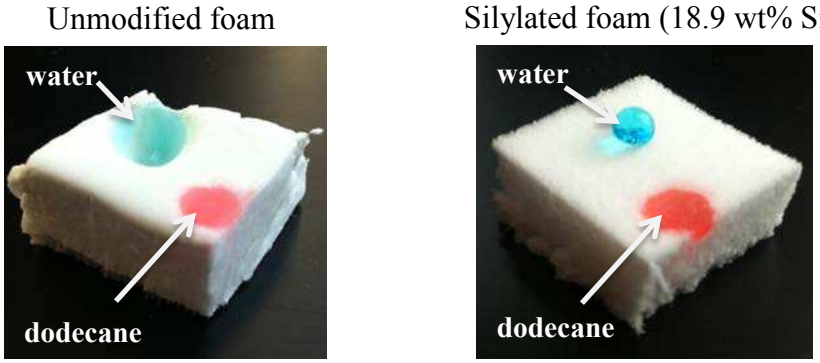

Figure 60: Demonstration of the combined hydrophobic/oleophilic properties of MTMS-treated NFC foam, compared with unmodified foam.

The oil absorption capacity (C_m), expressed as the weight gain ratio of absorbed dodecane compared with the initial to dry foam (Equation 10 in Chapter VI.5.3.8), was calculated for both unmodified and silylated foam and compared with literature data (Table 13).

Table 13: Oil absorption capacity (C_m) of unmodified and silylated NFC foams. Some literature data are also reported for comparison.

Sample	ρ_{foam} [kg/m^3]	oil	ρ_{oil} [g/ml]	C_m (initial)	C_m (recycled)
unmodified NFC	11	dodecane	0.75	44	16
MTMS-NFC	11	dodecane	0.75	53	52
TiO_2-NFC[144]	20-30	paraffin oil	0.87	30	30
		dodecane	0.75	24	-
Carbon nanotube sponges[222]	5-10	hexane	0.66	89	-
		diesel oil	0.84	142	-
		vegetable oil	0.90	109	-
		chloroform	1.48	~ 180	-
PDMS sponge[223]	180-750	transformer oil	0.89	4-5	4-5

The unmodified NFC foam absorbed a significant amount of dodecane, but the silylated material gave better results. Both foams displayed better C_m values compared with TiO_2-NFC foams and PDMS sponges, but lower ones compared with carbon nanotube sponges. This was assigned to differences in the materials density, as C_m is obviously correlated with the density of the foams or sponges. In addition, higher C_m values are expected when the density of the oil increases.[144, 222]

IV.3.4.2. Oil removal properties

The combined hydrophobic/oleophilic properties displayed by the silylated foam allowed envisaging its utilisation as selective absorbent for the removal of oil or other organic molecules from polluted water. This was demonstrated by realising an experiment in which 0.2 g of dodecane was spilled at the surface of 15 mL water in a beaker, and subsequently removed by the silylated foam (Figure 61b). For comparison purpose, the unmodified foam was also tested (Figure 61a).

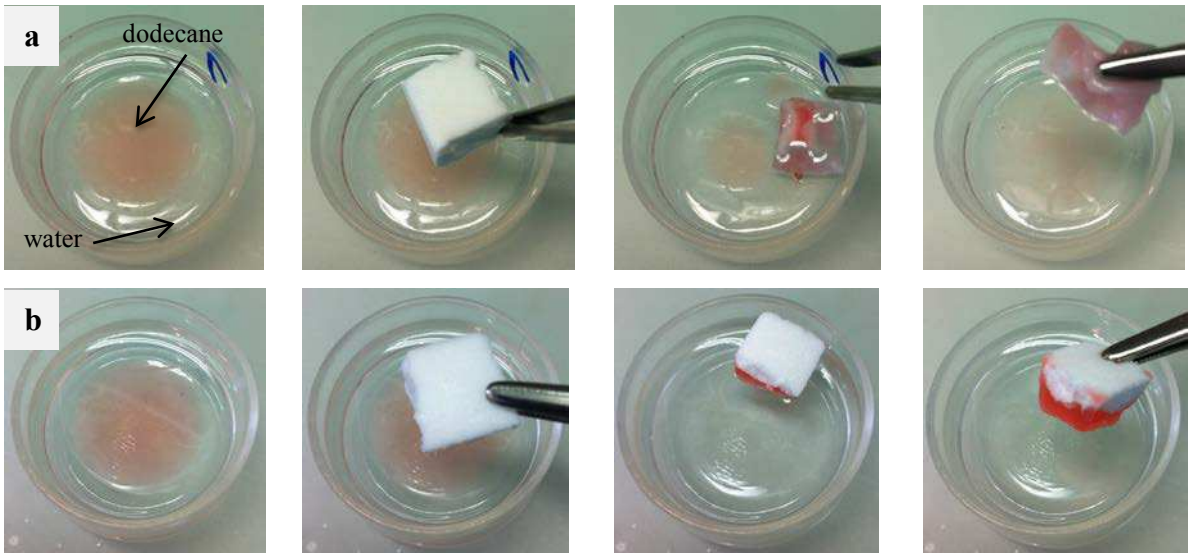

Figure 61: Removal of dodecane (in red) from water surface by unmodified (a) or silylated (b) NFC foam.

When 0.02 g of unmodified NFC foams was brought in contact with dodecane, both water and dodecane were absorbed, and the saturated material sunk at the bottom of the beaker (Figure 61a). Moreover, a significant amount of dodecane remained at the surface after removing the foam.

When the same weight of silylated material was used, only dodecane was absorbed, and the organic compound was completely removed from the water surface. The silylated foam kept floating on the water surface during the experiment, and its mechanical integrity was not altered. Moreover, the silylated foam was not saturated and could remove an additional amount of dodecane.

IV.3.4.3. Recyclability

The recyclability of the foams was evaluated by rinsing the unmodified and silylated foams with toluene, and then drying the material at 65 °C under vacuum. The absence of dodecane after rinsing was inferred by observing the vanishing of the red colour and the recovering of the initial weight of the foams (Figure 62).

Figure 62: Aspect of unmodified and silylated NFC foams after rinsing with toluene and drying (1 cycle).

With the silylated foam, the oil absorption capacity remained at around 50 after 10 cycles (Figure 63), while C_m of unmodified NFC decreased significantly after only one cycle (Table 13). Moreover, the shape of the silylated foam was not significantly altered, while unmodified foam was highly distorted upon drying, because of the hornification phenomenon (Figure 62).

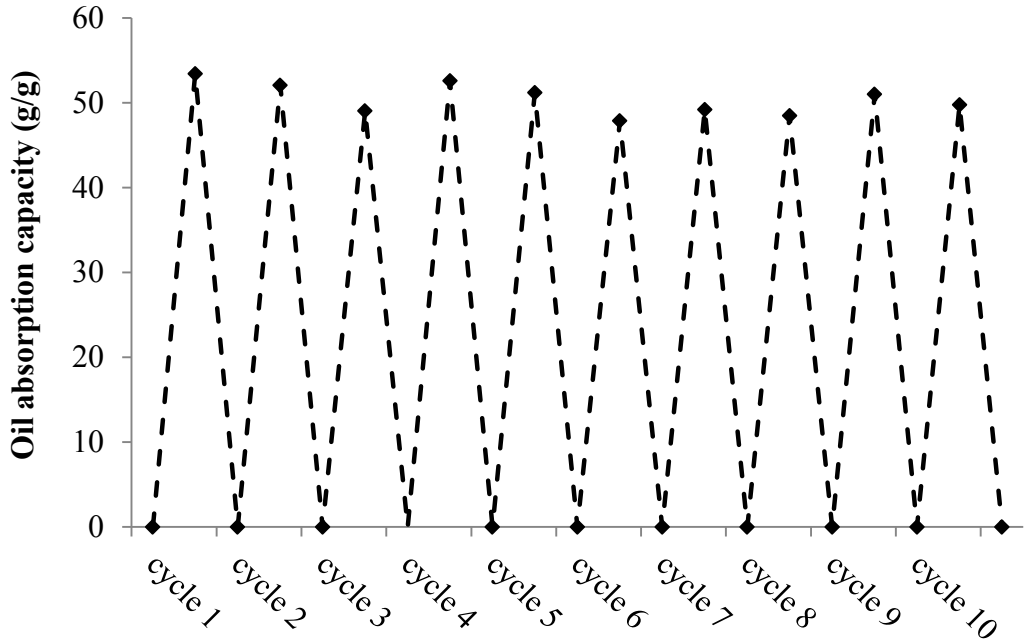

Figure 63: Recyclability of silylated NFC foam for oil removal

IV.3.5. Thermal conductivity

The thermal conductivity (λ) of unmodified and silylated NFC foams was evaluated using a home-made experimental device especially designed for the analysis of small size aerogel and

foam samples (see Figure 68 in Chapter VI.5.3.5). λ was reported as a function of silylation level in Figure 64.

The thermal conductivity of the NFC foams decreased after silylation, regardless of the silylation level and the relative density (ϕ) of the material. Moreover, λ tended to decrease with increasing Si content.

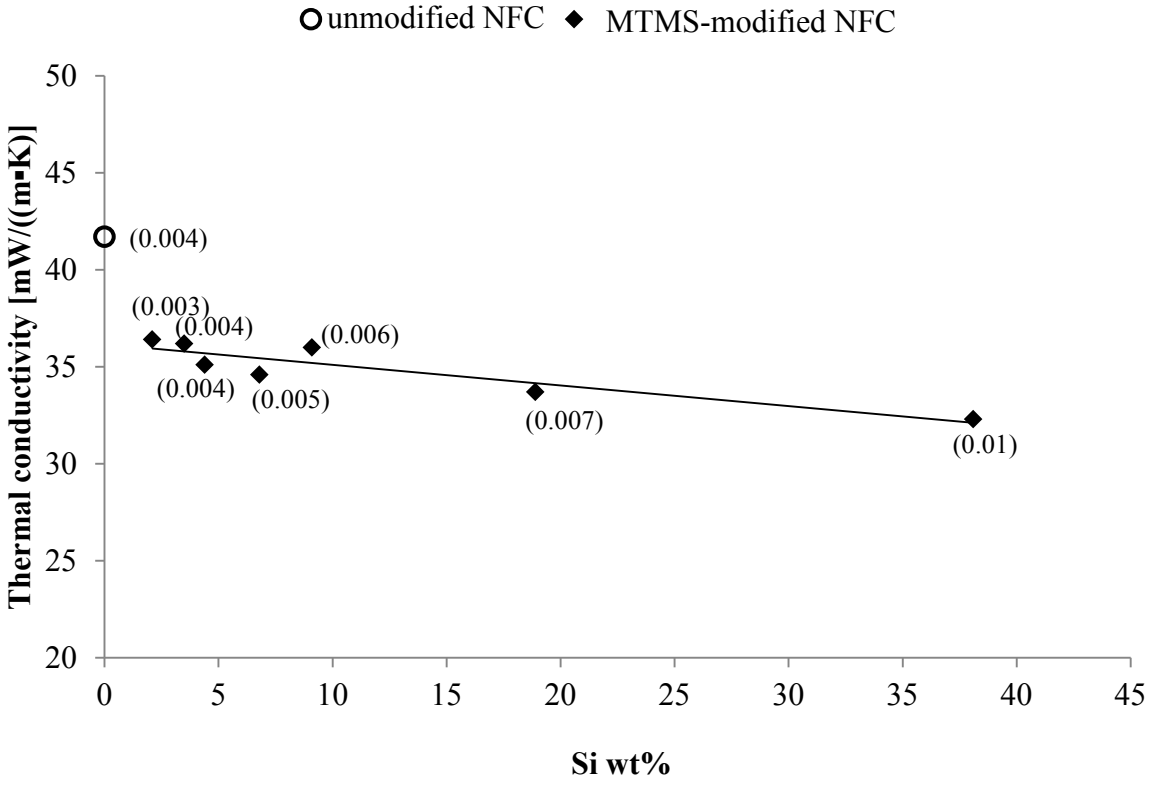

Figure 64: Evolution of the thermal conductivity (λ) with the Si content in NFC foams. The relative density of the foam is given in bracket.

IV.4 Concluding remarks

The experiments relevant to this chapter have shown that our silylation process could have a positive impact on the properties of NFC foams.

Ultra-light weight and porous silylated NFC foams composed of sheet structures interconnected with nanofibrils were produced base on *Protocol 2'*, using a controlled freeze-drying process.

Under compression, the Young's modulus and stress at 50 % deformation of the samples was found to increase with increasing silylation level. Notably, the shape recovery of the NFC foams was significantly improved after silylation and was as high as 96 % at high silylation level. To our knowledge, this is the first time that such flexibility was obtained with NFC-based foams.

Silylated NFC foams were highly hydrophobic in contact with liquid water, and their oil absorption capacity was significantly improved compared with the unmodified material. These combined hydrophobic/oleophilic properties benefited to the foam, which proved to be very efficient in selectively removing dodecane spills from water surface. In addition, the silylated material could be recycled more than 10 times without modification of its oil absorption capacity, and without alteration of its mechanical integrity.

The thermal conductivity of the NFC foams also decreased after silylation, which could have applications in the area of insulation materials.

V. General conclusion

The objectives of this research project were i) to develop an environmentally friendly method based on alkoxysilanes, allowing the chemical functionalization of nanofibrillated cellulose (NFC) in water and ii) to investigate the impact of silylation on the properties of composites and foams.

In this context, the surface of NFC produced from oat straw was modified in water by methyltrimethoxysilane (MTMS) - chosen as a model trialkoxysilane - using different reaction parameters and experimental protocols (*Protocols 1 & 2*). Two different types of silylated NFC were produced, without modification of the original crystalline structure. The first type consisted in a cellulose nanofibrils network, in which polysiloxane particles were dispersed (*Protocol 1*), while the second type consisted in a nanofibrils covered by a homogeneous polysiloxane layer (*Protocol 2*). The size of the particles or the thickness of the polysiloxane layers could be controlled by monitoring the initial silane concentration.

Leaching experiments have shown that the polysiloxane particles produced with *Protocol 1* were not firmly anchored to the cellulosic substrate, whereas the polysiloxane layer covering the NFC modified according to *Protocol 2* was strongly bonded.

Differences were also noted in terms of wettability and thermal stability. While NFC modified with *Protocol 1* remained hydrophilic, very hydrophobic nanofibrils were produced with *Protocol 2*. The thermal stability was also significantly improved in the latter case, due to the efficient covering of the NFC surface by the silane polymer.

Following this comprehensive study, we investigated the impact of the silylation treatment on the properties of composites prepared by solvent casting, using polydimethylsiloxane (PDMS) and poly(lactic acid) (PLA) as matrices. Different results were obtained, depending on the matrix employed.

With PDMS composites (1 wt% NFC), the shear modulus (G'), E modulus and tensile strength could be all improved after silylation with Protocol 2, as long as the experimental conditions were correctly controlled. But the strain at break systematically decreased after silylation, regardless of the method and silane content. The incorporation of NFC in the PDMS matrix slightly increased the hygroscopicity of the material, but the maximum moisture uptake remained low in all cases.

With PLA composites (10 wt% NFC), no significant improvement of the mechanical performances was noted after silylation, in the conditions investigated. The water uptake tended to be more limited, but all NFC composites were more hydrophilic than neat PLA.

The thermal stability of both types of composites was improved in some cases, deteriorated in others, but no clear trend could be established or correlated with the silylation level or protocol used.

Cellulose nanofibrils are increasingly considered for the elaboration of foams, hence, we also envisaged studying the impact of silylation on the properties of NFC foams prepared using a controlled freeze-drying process. Ultra-light weight and porous silylated NFC foams composed of sheet structures interconnected with nanofibrils were accordingly produced, based on *Protocol 2'*.

Under compression, the Young's modulus and stress at 50 % deformation of the samples was found to increase with increasing silylation level. Notably, the shape recovery of the NFC foams was significantly improved after silylation and was as high as 96 % at high silylation level. To our knowledge, this is the first time that such flexibility is obtained with NFC-based foams.

Silylated NFC foams were highly hydrophobic in contact with liquid water, and their oil absorption capacity was significantly improved compared with the unmodified material. These combined oleophilic/hydrophobic properties benefited to the foam, which proved to be very efficient in selectively removing dodecane spills from water surface, the cellulosic material being able of absorbing 50 times its own weight in dodecane. In addition, the silylated material could be recycled more than 10 times without modification of its oil absorption capacity, and without alteration of its mechanical integrity.

The thermal conductivity of the NFC foams also decreased after silylation, which could have applications in the area of insulation materials.

This research work has highlighted the potential of alkoxysilanes to serve as functionalization agents for the control of NFC surface in water. Experiments performed with methyltrimethoxysilane have shown that different types of value-added composites or foams could be produced, provided that the reaction conditions and process are properly tailored. The results presented here are definitely encouraging, but further research is still required to

realize the full potential of the method. In particular, the fine-tuning of the NFC surface by alkoxysilanes with various functional groups should be investigated to optimize further the properties of the composites and foams, and also to widen the spectrum of application. Other polymer matrices could be also tested when examining the reinforcing effect of silylated NFC. Finally, additional characterisations could be performed, to explore further the potential of the silylated material in other application fields (acoustic, electrical insulating material, etc.).

VI. Materials and Methods

VI.1. Materials

VI.1.1. Chemicals

Cellulose pulp powder from oat straw (Jelucel OF300) was provided by Jelu (Rosenberg, Germany). Its chemical composition was determined by sugar analysis (Table 14).

Table 14: Sugar analysis of Jelucel OF 300 and NFC after isolation

	Glucose	Xylose	Rhamnose	Mannose	Arabinose	Galaktose	Others
pulp	73.9%	25.06%	0.08%	0.19%	0.51%	0.07%	0.2%
NFC	75.3%	23.57%	0.08%	0.19%	0.46%	0.10%	0.3%

Methyltrimethoxysilane (Dynasylan® MTMS) and poly(dimethylsiloxane) (PDMS) (M_n=80000 g/mol) were purchased from Evonik Industries (Rheinfelden, Germany) and kindly sponsored by Falcone Chemical Specialities Ltd. (Siebnen, Switzerland). Polydimethylsiloxane (PDMS) hydroxyl terminated (M_n = 550 g/mol), tin(II) 2-ethylhexanoate (~ 95 %), tetrapropyl orthosilicate (TPOS) (≥ 98 %) and dodecane (≥ 99 %, ρ = 0.75 g/ml) were purchased from Sigma Aldrich (Switzerland). Trichloromethane (≥ 99 %) and sodium hydroxide (NaOH, ≥ 99 %) were purchased from ROTH (Switzerland). Hydrochloric acid (HCl) fuming (EMPROVE® exp, 37 %) was purchased from Merck (Germany). Sudan III (Standard Fluka) was purchased from Fluka AG (Switzerland). Neolan Blau (E-A 235 %) was purchased from CIBA GEIGY (Switzerland). Diluted HCl (10 wt%) was prepared with HCl fuming (37 %) by adding deionized water. Poly(lactic acid), Ingeo PLA 2002D (T_m = 145-160 °C, T_g = 55 - 60 °C, ρ = 1240 kg/m^3, M_w ~ 120900 g/mol, melting flow rate of 5-7 g/mol (210 °C/2.16 kg), NatureWorks, USA) was supplied by Polykemi (Sweden). All chemicals and solvents were used as received without further purification.

VI.1.2. Laboratory equipment

- Mechanical stirrer, Eurostar power control visc, IKA®-Werke, Staufen, Germany
- Magnetic stirrer, MR 3001K, Heidolph Instruments Switzerland, Solothurn, Switzerland
- Homogenizer, inline Ultra-Turrax system, Megatron MT 3000, Kinematica AG, Lucern, Switzerland

- Higher-shear homogenizer, Microfluidizer, type M-110Y, Microfluidics Corporation, USA
- Homogenizer, Ultra-Turrax system, T25 basic, IKA-Werke, Staufen, Germany
- Centrifuge, Rotina 380, Hettich Laborapparate, Bäch, Switzerland
- Freeze dryer, LYO GT2, SRK System Technik GmbH, Germany

VI.2. Production of nanofibrillated cellulose

8 L of 1.5 wt % aqueous suspension of cellulose pulp in deionized water was prepared in a reactor and allowed to swell for one week at 10 °C, under mechanical stirring. Subsequently, the suspension was homogenized with an inline Ultra-Turrax (UT) system at 20000 rpm for 2h. The fibrillation was performed with a high-shear homogenizer, by first pumping the suspension through two consecutive chambers of 400 and 200 µm (*i.e.*, $H230Z_{400\mu m}$ and $H30Z_{200\mu m}$, respectively) for 12 passes, and second through two consecutive chambers of 200 and 75 µm (*i.e.*, $H30Z_{200\mu m}$ and $F20Y_{75\mu m}$ chambers, respectively) for 16 passes. Pressure up to 100 MPa was applied to generate high stress on the cellulose fibres. After the mechanical disintegration, the NFC gel-like suspension was concentrated by centrifugation (5000 rpm, 25 °C, three times for 15 min.) to obtain a paste-like material with a solid content of about 8 wt %. The process is presented in Figure 65.

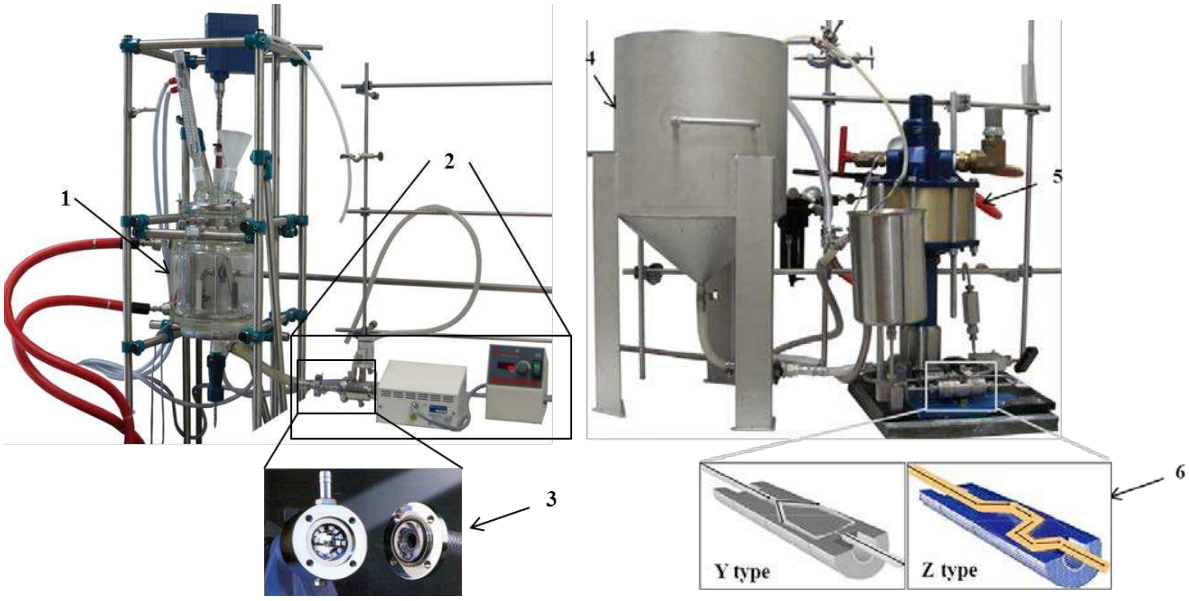

Figure 65: Demonstration of NFC production process: 1. Swelling of cellulose suspension in 10L reactor. 2. Pretreatment with homogenizer (inline Ultra-Turrax system). 3. Inside Ultra-Turrax system. 4. After pretreatment, cellulose suspension was

transferred in the container. The process is a closed loop. 5. High pressure pump. 6. Interaction chambers Y- and Z-type.

As can be seen in Figure 66, the starting material contained fibres with diameter in μm-range, while the product NFC presented a network of fibrils with diameter in nanometer range.

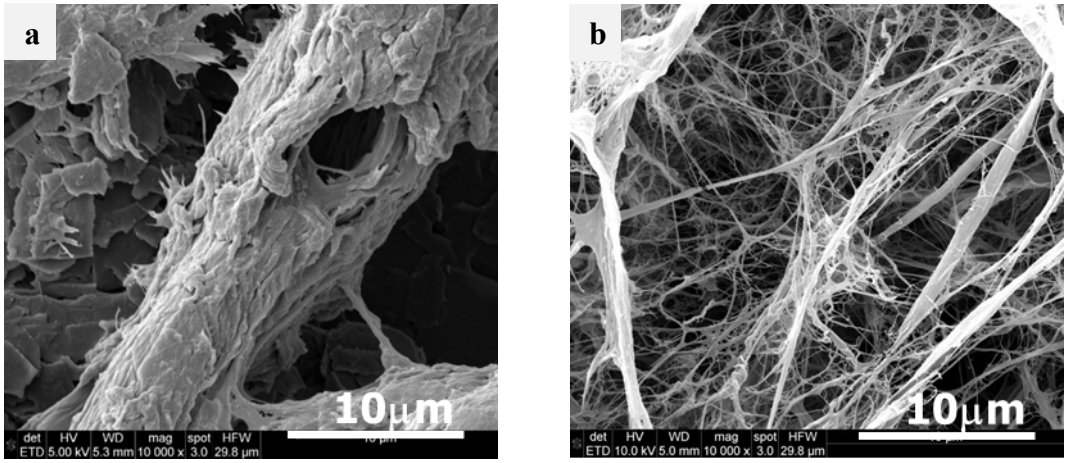

Figure 66: Micrographs of oat straw cellulose pulp powder (a) and NFC (b).

VI.3. Silylation of NFC's

During this thesis, three different protocols were investigated.

VI.3.1. Protocol 1

VI.3.1.1. Reaction

The NFC paste (8 wt %) was diluted with deionised water to obtain a 1 wt % NFC suspension and homogenized with an Ultra-Turrax system at 11000 rpm for 30 s. The NFC suspension was adjusted to different pHs with HCl (37 wt % or 10 wt %) or NaOH (10 wt %) solutions.

In each experiment, the water-based silane solution was prepared separately. The required mass of deionised water was first introduced in a beaker and the solution was adjusted to the same pH as in the NFC suspension. Different amounts of silane were added into the solution and stirred for 5 min at 500 rpm with magnetic stirrer. This solution was then added drop wise to the NFC suspension in order to reach a final NFC concentration of 0.5 wt %. The final suspension was stirred at room temperature for different reaction times (between 30 min and 72 h).

VI.3.1.2. Washing

The modified material was subsequently washed three times with deionised water in order to remove all non-bonded water-soluble chemicals, and any excess of acid or base. Each washing step included one homogenization (UT, 11000 rpm, 30 s)/centrifugation step (4000 rpm, 8 min) step.

VI.3.1.3. Freeze-drying

To obtain dried silylated NFC, the wet cake after washing was diluted with deionised water to an NFC-concentration of 0.5 wt % and freeze-dried using a "fast freezing process" (FFP) adapted from the method of Jin et al.[108] (Scheme 22).

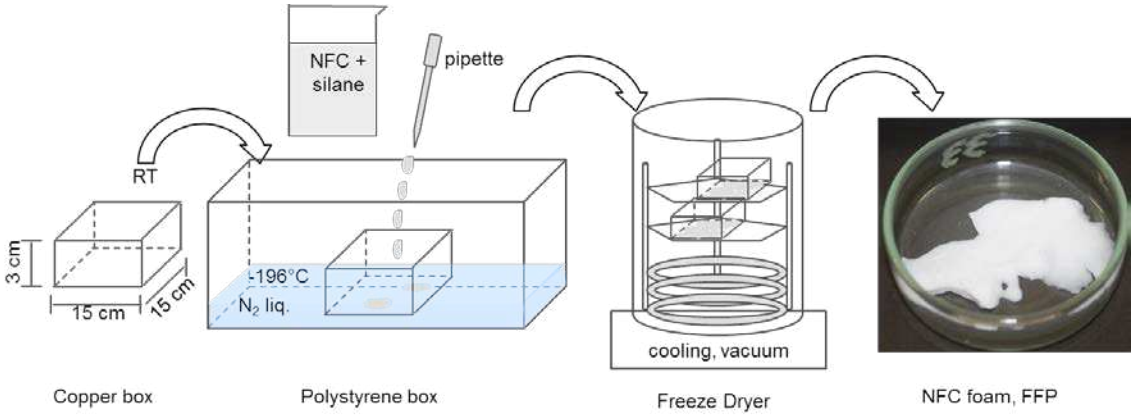

Scheme 22: Freeze-drying of NFC using the fast freezing process (FFP)

A 15 x 15 cm copper box was placed in a polystyrene box filled with liquid nitrogen. After the temperature of the copper box reached equilibrium, the suspension was introduced dropwise into of the copper box. Subsequently, the copper box was transferred into a freeze dryer. The drying was complete after 48 h as observed by the non-fluctuation of the pressure inside the freeze-dryer (final pressure inside the freeze dryer was approximately 3.5 x 10^{-2} mbar).

With this method, the NFC suspension formed a very thin layer in the mould and the freezing was very fast. As a consequence, a porous structure composed mostly of nanofilaments was obtained (cf. Figure 12a).

VI.3.2. Protocol 2

Silylation and freeze-drying were performed as in *Protocol 1*, except that the NFC suspension and silane solution were adjusted to a single pH of 4 (with a 10 wt % HCl solution), and no

washing step was performed after silylation. With this method, all the silane contained in the suspension (bonded or not) remained in the dry material after freeze-drying.

The materials prepared with *Protocol 1* & *2* were used for preparation of polymer composites.

VI.3.3. Protocol 2'

Silylation was performed as in *Protocol 2*, but a different freeze-drying method was employed in that case: the final suspension containing both NFC and silane was freeze-dried using a "slow freezing process" (SFP) (Scheme 23).

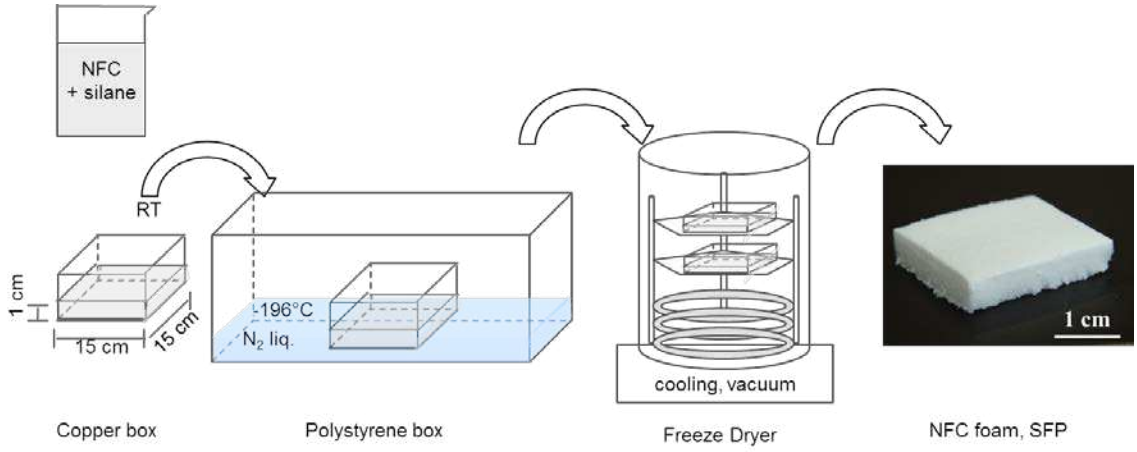

Scheme 23: Freeze-drying of NFC using the slow freezing process (SFP)

225 cm^3 of the NFC/silane mixture was transferred at room temperature into a 15 x 15 cm copper box, which was subsequently placed into a polystyrene box filled with liquid nitrogen. After the complete freezing of the suspension, the copper box was transferred into the freeze-dryer. The drying was complete after 48 h with constant pressure of approximate 3.5 x 10^{-2} mbar.

Here again, all the silane contained in the suspension (bonded or not) remained in the dry material after freeze-drying. But with this protocol, the layer of NFC gel in the copper box was thick enough for the freezing to be slow, and the formation of cell wall structures resulting from the agglomeration of cellulose nanofibres was favoured during freezing. (cf. Figure 12b).

VI.4. Elaboration of composite films and silylated foams

Two different polymer matrices were investigated in this chapter: polydimethylsiloxane (PDMS) and polylactic acid (PLA).

VI.4.1. Elaboration of PDMS-composites

14 g PDMS (Mn~80000 g/mol) and 6 g PDMS (M_n ~ 550 g/mol) were introduced in a 150 mL PE cup and mixed with a mechanical stirrer for 5 min at room temperature. Concurrently, 0.2 g of unmodified or silylated NFC (prepared according to *Protocol 1 & 2*), and 75 g of chloroform were introduced in a beaker and the suspension was homogenized with an UT at 11000 rpm for 5 min. This suspension was incorporated into the PDMS mixture and stirred for 20 min with a mechanical stirrer. 1.75 g tetrapropylorthosilicate (TPOS) and 0.13 g tin(II) 2-ethylhexanoate were then added under stirring and the suspension was cooled down to 2 °C. After the final mixture was stirred for 2 min, composite films were obtained by casting 20 g of the suspension in a Polypropylene (PP) mould. Four films were obtained and dried at room temperature in a fumed hood for 24 h. In order to remove any traces of solvent, the films were finally heated at 60 °C for 20 h and subsequently stored in a desiccator containing silica gel until being analysed. The thickness of the composite films ranged between 500 μm and 800 μm.

VI.4.2. Elaboration of PLA-composites

3 g of PLA pellets and 127g chloroform were added into a round flask, and the mixture was stirred with a magnetic stirrer, at 500 rpm for 14 h. Concurrently, 0.33 g of unmodified or silylated NFC (prepared according to *Protocol 1* or *2*) were dispersed in 69.1 g chloroform using a blender (Ultra-Turrax) at 11000 rpm for 5 min. This suspension was incorporated into the PLA solution and the resulting mixture was homogenized with an UT at 11000 rpm for 2 min, followed by three degasing cycles (*i.e.*, vacuum/atmospheric pressure cycles) to degas the suspension. The composites films were obtained by casting the NFC/PLA mixture in a Teflon mould. After drying at room temperature for 7 days in a fumed hood, the films were removed from the mould and heated at 100 °C for 10 min. to remove the residual solvent. The thickness of the composite films ranged between 120 μm and 170 μm.

VI.4.3. Elaboration of unmodified and silylated NFC foams

NFC foams were prepared according to *Protocol 2'*, using both unmodified and silylated NFC.

VI.5. Characterization methods

VI.5.1. Characterization of NFC

VI.5.1.1. Elemental analysis

The Si content in silylated NFC samples was evaluated by elemental analysis. Samples were calcinated at 800 °C followed by mineralization at 1050 °C in the presence of lithium tetraborate. The Si content was then determined by Plasma Emission Spectrometry.

This analysis was subcontracted to SGS MULTILIAB.

VI.5.1.2. Infrared spectroscopy (FTIR-ATR)

Infrared spectra of the dried modified and unmodified NFC were recorded using a Tensor 27 FT-IR spectrometer (Bruker, Switzerland). For each sample, the diamond crystal of an Attenuated Total Reflectance (ATR) accessory was brought into contact with the area to be analyzed. The contact area was a circle of about 1.5 mm in diameter. All spectra were recorded between 4000 and 600 cm^{-1} with a resolution of 4 cm^{-1} and 32 scans per sample. For comparison purpose, spectra were adjusted to the same baseline and were normalized to the C-H in-plane bending of cellulose at about 1317 cm^{-1},[182] which is not affected by the modification with MTMS. The peak heights ratio of 1272 cm^{-1} to 1317 cm^{-1}, vibrations ($I_{Si\text{-}C}/I_{C\text{-}H}$), in each spectrum was calculated using a baseline constructed between 1518 cm^{-1} and 1217 cm^{-1}.

VI.5.1.3. ^{13}C and ^{29}Si CP-MAS NMR Spectroscopy

Solid state ^{13}C and ^{29}Si CP-MAS (Cross Polarization - Magic Angle Spinning) NMR spectra of dried unmodified and silylated NFC were performed at room temperature on a Bruker Avance 400 NMR spectrometer (Bruker BioSpin AG, Fällanden, Switzerland). 200 mg of dried unmodified or silylated NFC were cryo-ground to a fine powder and packed in a 7 mm CP/MAS probe using zirconia.

The ^{13}C and ^{29}Si CP-MAS NMR spectra were recorded at 100.61 MHz and 79.49 MHz, respectively, using the following parameters: 7.5 μs π/4 excitation pulse on ^{1}H channel; 3 ms contact time with a ramp from 100 to 50 % of power level; 3000 Hz spinning speed; 4 s relaxation delays and an appropriate number of scans to yield reasonable signal to noise ratios.

During acquisition, 33 kHz TPPM15 proton decoupling was applied and the raw data were processed using an exponential function of 50 Hz.

The alkoxysilanes used in the silylation treatments were analysed by solution state NMR spectroscopy. Spectra were recorded on the spectrometer presented above, using an inverse probe equipped with z-gradient. The 1D ^{1}H and ^{13}C NMR spectra and the ^{1}H, ^{29}Si 2D correlation experiments were recorded with the Bruker standard pulse programs and parameter sets. The $^{1}H/^{13}C$ chemical shifts were referenced internally using the resonance signals of chloroform at 7.26 and 77.0 ppm for ^{1}H and ^{13}C experiments, respectively. The ^{29}Si chemical shifts were referenced externally to tetramethylsilane.

The software used for treatment of NMR spectra was TopSpin 3.0 (Bruker). All ^{13}C spectra were normalized to the peak of C_1 of cellulose at 105 ppm.

VI.5.1.4. Scanning electron microscopy (SEM)

SEM analysis was performed using a Jeol 6300F scanning electron microscope (Jeol Ltd. Tokyo Japan) with an acceleration voltage of 5 kV, a working distance of 16 mm and a probe current of $6x10^{-11}$ A.

The starting NFC suspension was analysed as followed: one drop of a 0.1 wt % NFC suspension was deposited on the mica plate surface of the sample holder and vacuumed (< 10^{-2} mbar) for 15 min to remove water. Subsequently, the sample was coated with 7.5 nm platinum.

The dried unmodified or silylated NFC samples were analysed by sticking the sample on the holder with a carbon pad, and then coated with 7.5 nm platinum.

VI.5.1.5. Wavelength dispersive X-ray spectroscopy (WDX)

The WDX measurements were carried out with a scanning electron microscope (JEOL, JXA-8800RL), equipped with a wave-dispersive X-ray detector. The dried unmodified or silylated NFC samples were pressed for 30 sec. under a pressure of 12 bars (with a Perkin-Elmer hydraulic press), to produce samples with flat and smooth surfaces. The films with sizes of ~0.5 cm^2, were stuck on a holder using a carbon pad, and were coated with carbon. The detection of silicon was obtained at an accelerating voltage of 15 kV and illuminating current of $2x10^{-8}$ A. The mapping of Si was performed on a surface area 300 x 300 μm, with steps of 2 μm.

VI.5.1.6. X-ray diffraction (XRD)

X-ray diffraction patterns were obtained using a PANalytical X´Pert PRO θ-2θ scan system equipped with a Johansson monochromator (Cu-Kα1 radiation, 1.5406 Å) and an X'Celerator linear detector. The diffraction patterns were recorded between 10° and 60° (2θ). ~50 mg unmodified or silylated NFC materials were pressed to form pellets with diameter of 1cm and the surface was analysed.

The crystallinity index of unmodified and silylated NFC's was calculated by using the XRD peak height method (Equation 2):[224]

$$CI = \frac{I_{200} - I_{AM}}{I_{200}} \times 100\% \qquad (2)$$

where I_{200} is the peak intensity of the highest peak (200) and I_{AM} is the peak intensity of the minimum position between the 200 and 110 peaks.

VI.5.1.7. Thermogravimetric analysis (TGA)

Thermogravimetric analyses of freeze-dried unmodified and silylated NFC (sample weight ~2mg) were performed with a TGA7 apparatus (Perkin-Elmer, USA), under helium atmosphere, within the temperature range between 30 °C and 900 °C and at a heating rate of 20 °C/min.

VI.5.1.8. Water sorption tests

The sorption of water by unmodified and silylated NFC was evaluated using a vapour sorption analyser (VTI-SA$^+$, TA Instruments). Prior to measurement, the freeze-dried NFC sample (~15 mg) was further dried at 105 °C for 60 min. The weight of the sample was then measured as a function of relative humidity, which was increased from 0 % to 95 %, with increments of 5 %. The sample weight was recorded at equilibrium, *i.e.* when a weight change lower than 0.01 % was noted within 5 min. The maximum measurement time for each RH was 5 h.

VI.5.1.9. Contact angle measurements

The wettability of freeze-dried unmodified and silylated NFC was evaluated by contact angle measurement, using a Contact Angle System OCA (Dataphysics), combined with a high

speed camera. The volume of the water droplet was 5 µL and the tip used was a precision stainless steel tip (Gauge 32, EFD, USA).

VI.5.1.10. Resistance tests towards solvents

Silylated NFC samples after freeze drying were washed by Soxhlet extraction for 20 h. Three solvents, water, ethanol and chloroform, were tested separately. After the extraction, the samples were dried firstly 8 h at 60 °C and then 14 h at 105 °C.

VI.5.2. Characterizations of composites

VI.5.2.1. Thermogravimetric analysis (TGA)

Thermogravimetric analysis of NFC composites was performed using the same protocol used for NFC characterization, which was detailed in previous paragraph (c.f. VI.5.1.7). The sample weight was ~ 2 mg.

VI.5.2.2. Differential scanning calorimetry (DSC)

The DSC measurement of NFC/PLA composite films was performed with a DSC 8000 (Perkin-Elmer, USA). 5 mg of each sample was heated from 30 °C to 200 °C, at a heating rate of 20 °C/min, under dry nitrogen gas. The glass transition temperature (T_g) was measured at half-height of the specific heat increment at the glass-rubber transition, while the melting point (T_m) was taken as the peak temperature of the melting endotherm. Each sample was analysed twice.

The degree of crystallinity (X_c) was calculated as followed (Equation 3):

$$X_c = \frac{\Delta H_m}{w \times \Delta H_{m_o}} \times 100\% \quad (3),$$

where ΔH_m is the melting enthalpy of PLA composites; ΔH_{m_o} is the melting enthalpy of 100 % crystalline PLA (taken as 93 J/g), and w is the weight fraction of PLA in the composites.[72] The cristallinity values were determined during the second heating run, as the T_g determined by the first run could be influence by several factors such as residue of solvent, impurity or inhomogenity in the samples.[225]

VI.5.2.3. Water sorption tests

The sorption of water by NFC composites was evaluated using the same protocol used for NFC characterization, which is detailed in previous chapter (c.f. VI.5.1.8). The specimens were composites films of about 0.3 cm^2 with a dry weight of 15-30 mg.

VI.5.2.4. Tensile tests

PLA and PDMS composite films were cut into dog-bone-shaped specimens with an overall length of 50 mm, a width of 8.5 mm at the clamping zone and a width of 4 mm at the stretching zone. Prior to the measurement, the specimens were conditioned for at least 1 week at 50 % RH and 23 °C. The modulus of elasticity (MOE), nominal tensile strength (σ_{max}) and strain at break (ε), were recorded with a Universal Testing System Z010 (Zwick, Germany), in a conditioned room (50 % RH and 23 °C). For each sample, at least 5 specimens were tested.

The characterization of the PLA composite films was conducted using the following parameters: 100 N loading cell, preforce 0.1 N, testing speed 5 mm/min. The strain at break was detected by a Multisense system combined with the testing machine.

The characterization of the PDMS composite films was conducted using the following parameters: 20 N loading cell, perforce 0.1 N, testing speed 100 mm/min. The strain was detected by crosshead travel.

VI.5.2.5. Dynamic mechanical analysis (DMA)

The PLA composite films were cut into rectangular specimens having the following dimensions: 6mm in width and 45 mm in length. The viscoelastic properties of the composite films were studied using a RS III Rheometrics System Analyzer (TA Instruments) in tension mode. The sample was first heated from 30 °C to 100 °C, at 10 °C/min, 1 Hz of frequency, and 0.01 % of strain, to remove any trace of solvent. The temperature was maintained at 100 °C for 10 min and the sample was measured with dynamic cooling scans from 100 °C to 30 °C, at 2 °C/min, 1 Hz of frequency and 0.1 % of strain. During the DMA experiment, the static load was kept at 15 % of the dynamic load. For each sample, three replicates were tested.

VI.5.2.6. Torsion pendulum analysis

The PDMS composite films were cut into rectangular specimens having 10 mm width and 60 mm length. The viscoelastic properties of the composites were measured with the torsion pendulum test (ATM 3, Myrenne, Germany), following the norm DIN EN ISO 6721-2. Measurements were performed in the temperature range between -150 °C and 50 °C, and the data were recorded every 4 °C. The vibration frequency was 1 Hz.

VI.5.3. Characterizations of NFC foams

VI.5.3.1. Determination of the density

The bulk density of dried unmodified and silylated NFC foams was calculated using the following formula: $\rho_{foam} = \frac{m}{V}$ (4),

where m and V are for the weight and the volume of the foams, respectively.

VI.5.3.2. Determination of the porosity

To calculate the porosity of unmodified and silylated foams, the following equation was used:

$$porosity[\%] = (1 - \frac{\rho_{foam}}{\rho_s}) \times 100\% \quad (5),^{67}$$

where ρ_{foam} and ρ_s are for the density of the foam and density of cellulosic skeleton respectively.

The relative density (ϕ) is one of the characteristics of foam materials, and is calculated as followed:[67]

$$\phi = \frac{\rho_{foam}}{\rho_s} \quad (6).$$

MTMS-modified NFC foams were regarded as composites of two solids: cellulose and polymerized MTMS (*i.e.* polymethylsiloxane). Therefore, the density of MTMS-modified cellulose was calculated by using equation 7:[226]

$$\rho_s = \frac{1}{\frac{w_{cellulose}}{\rho_{cellulose}} + \frac{w_{poly(MTMS)}}{\rho_{poly(MTMS)}}} = \frac{1}{\frac{1 - w_{poly(MTMS)}}{\rho_{cellulose}} + \frac{w_{poly(MTMS)}}{\rho_{poly(MTMS)}}} \quad (7),$$

where $w_{cellulose}$ and $w_{poly(MTMS)}$ are the weight fractions of cellulose and polymerized MTMS within the foams, respectively. A density of 1500 kg/m^3 was used for the cellulose[111] and a density of 1900 kg/m^3 was used for polymethylsiloxane.[216] $w_{poly(MTMS)}$ was estimated based on the weight gain measured after silylation of NFC accoding to *Protocol 2'*:

$$w_{poly(MTMS)} = \frac{m_{foam} - m_{NFC}}{m_{foam}} \times 100\% \quad (8),$$

where w_{NFC} and w_{foam} are the mass of the freeze-dried cellulosic material, before and after silylation.

VI.5.3.3. Evaluation of Brunauer-Emmett-Teller (BET) specific surface area

The surface area of unmodified and silylated NFC foams was determined by nitrogen adsorption, using a surface area and pore size analyser SA 3100 (Beckmann Coulter, USA). About 30 mg of cellulosic material was dried under synthetic gas flow at 105 °C for 18 h. The nitrogen adsorption was measured in a range of relative vapour pressure of 0.05-0.2, at -196 °C. BET specific surface area was evaluated from the obtained adsorption isotherm.

VI.5.3.4. Compression tests

Unmodified and silylated NFC foams were cut into rectangular specimens with dimensions of 30 mm in length, 30 mm in width and ~ 10 mm in height. Prior to measurement, the specimens were conditioned at least 24 h in the testing room (50 % RH, 23 °C). The compression tests were performed by using a Universal Testing System Z010 (Zwick, Germany) equipped with a loading cell of 200 N. Each sample, placed between two round testing plates with diameter of 40 mm (Figure 67, step 1), was compressed to 50 % of its original thickness and this position was kept for 10 sec (Figure 67, step 2). Afterward, the testing plates moved in the inversed direction, until the detected force turned to zero (Figure 67, step 3). The testing speed was 1 mm/min. Three replicates were measured for each sample.

Figure 67: Experimental set-up used for compression tests. The testing plates movement is symbolized by arrows.

After unloading the specimens at 50 % strain, the thickness recovery was calculated according to the following formula:

$S\ [\%] = 100\ \% - \varepsilon_{final}$ (9),

where the ε_{final} is strain at the final position when the force detected reached 0 N.

VI.5.3.5. Thermal conductivity measurement

Unmodified and silylated NFC foams were cut into specimens with dimensions of 50 mm in length, 50 mm in width and ~10 mm in height. The thermal conductivity of the foams was measured by a home-made (EMPA, Switzerland) special hot plate device designed for the analysis of small low conductivity materials.[227] The instrument is presented in Figure 68. The upper part consists of heating elements (light red) surrounded by a guarding zone (red), which ensures that the heat flow from heating elements to cold side is nearly vertical, controlled by Peltier's element (black). The bottom side of the foam is in touch with the cold side. The temperatures of both warm and cold sides are recorded and the thermal conductivity is accordingly calculated as a function of temperature difference and sample size.

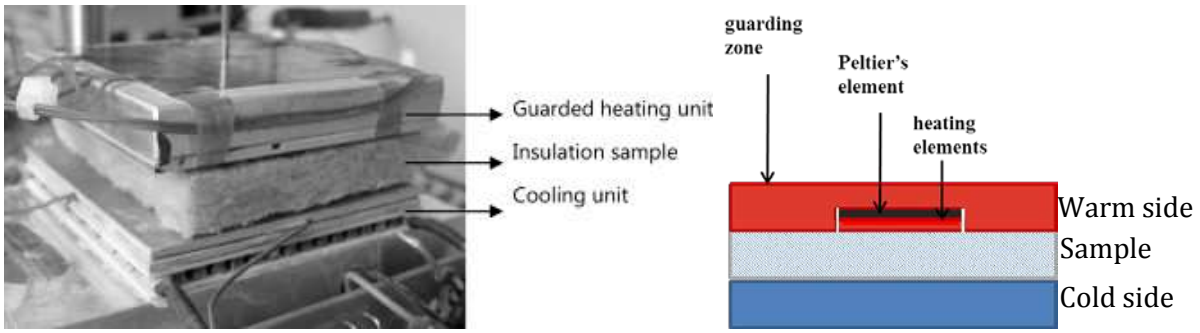

Figure 68: Home-made (EMPA) experimental device used for the evaluation of thermal conductivity of foams.[227]

VI.5.3.6. Water sorption tests

The sorption of water by NFC foams was evaluated using the same protocol used for NFC characterization, which is detailed in previous chapter (c.f. VI.5.1.8). The sample weight was of 15-30 mg.

VI.5.3.7. Contact angle measurements

The sorption of water by NFC foams was evaluated using the same protocol used for NFC characterization, which is detailed in previous chapter (c.f. VI.5.1.9). Measurements were performed on both sides of the foams, *i.e.* on bottom side, in contact with the copper box during freezing and on top side in contact with the air.

VI.5.3.8. Oil-water separation experiments

Silylated or unmodified NFC foams were immersed into dodecane. For visual demonstration, water was colourless or coloured to blue with Neolan Blau and dodecane was labelled red with Sudan III. For recycling of the foams after absorption of dodecane, the foams were immersed in toluene. After 10 min, toluene was removed and clean toluene was added. After this procedure was repeated for three times, toluene was removed and the foam was dried in vacuum oven for 8 h at 65 °C. The weight of the foams, before and after soaking oil, as well as after regeneration was determined. The mass absorption capacity (C_m) (w/w) was calculated as followed:

$$C_m(w/w) = \frac{m_1 - m_0}{m_0} \quad (10),$$

where m_0 is the original mass of the foam and m_1 is the mass of the foam after soaking oil.

References

1. Thomas, S.; Paul, S. A.; Pothan, L. A.; Deepa, B., Natrual Fibres: Structure, Properties and Applications. In *Cellulose Fibers: Bio- and Nano-Polymer Composites*, Kalia, S.; Kaith, B. S.; Kur, I., Eds. Springer-Verlag: 2011.
2. Klemm, D.; Heublein, B.; Fink, H.-P.; Bohn, A., Cellulose: Fascinating Biopolymer and Sustainable Raw Material. *Angewandte Chemie International Edition* **2005,** 44, (22), 3358-3393.
3. Bledzki, A. K.; Gassan, J., Composites reinforced with cellulose based fibres. *Prog. Polym. Sci.* **1999,** 24, (2), 221-274.
4. Samir, M.; Alloin, F.; Dufresne, A., Review of recent research into cellulosic whiskers, their properties and their application in nanocomposite field. *Biomacromolecules* **2005,** 6, (2), 612-626.
5. Eichhorn, S. J., Useful insights into cellulose nanocomposites using Raman spectroscopy. In *Acs Sym Ser*, Amer Chemical Soc: Washington, 2006; Vol. 938, pp 63-77.
6. Pandey, J. K.; Kumar, A. P.; Misra, M.; Mohanty, A. K.; Drzal, L. T.; Singh, R. P., Recent advances in biodegradable nanocomposites. *J. Nanosci. Nanotechno.* **2005,** 5, (4), 497-526.
7. Siro, I.; Plackett, D., Microfibrillated cellulose and new nanocomposite materials: a review. *Cellulose* **2010,** 17, (3), 459-494.
8. Azizi Samir, M. A. S.; Alloin, F.; Dufresne, A., Review of recent research into cellulosic whiskers, their properties and their application in nanocomposite field. *Biomacromolecules* **2005,** 6, (2), 612-626.
9. Bledzki, A. K.; Gassan, J., Composites reinforced with cellulose based fibres. *Progress in Polymer Science (Oxford)* **1999,** 24, (2), 221-274.
10. Tingaut, P.; Zimmermann, T.; Sebe, G., Cellulose nanocrystals and microfibrillated cellulose as building blocks for the design of hierarchical functional materials. *Journal of Materials Chemistry* **2012,** 22, (38), 20105-20111.
11. Lavoine, N.; Desloges, I.; Dufresne, A.; Bras, J., Microfibrillated cellulose - Its barrier properties and applications in cellulosic materials: A review. *Carbohydrate Polymers* **2012,** 90, (2), 735-764.
12. Tingaut, P.; Eyholzer, C.; Zimmermann, T., Functional Polymer Nanocomposite Materials from Microfibrillated Cellulose. In *Advances in Nanocomposite Technology*, Hashim, A., Ed. InTech: 2011; pp 319-334.
13. Hubbe, M. A.; Rojas, O. J.; Lucia, L. A.; Sain, M., Cellulosic Nanocomposites: A Review. *BioRes.* **2008,** 3, (3), 929-980.
14. Eichhorn, S. J.; Dufresne, A.; Aranguren, M.; Marcovich, N. E.; Capadona, J. R.; Rowan, S. J.; Weder, C.; Thielemans, W.; Roman, M.; Renneckar, S.; Gindl, W.; Veigel, S.; Keckes, J.; Yano, H.; Abe, K.; Nogi, M.; Nakagaito, A. N.; Mangalam, A.; Simonsen, J.; Benight, A. S.; Bismarck, A.; Berglund, L. A.; Peijs, T., Review: current international research into cellulose nanofibres and nanocomposites. *J. Mater. Sci.* **2010,** 45, (1), 1-33.
15. Satgé, C.; Granet, R.; Verneuil, B.; Branland, P.; Krausz, P., Synthesis and properties of biodegradable plastic films obtained by microwave-assisted cellulose acylation in homogeneous phase. *Comptes Rendus Chimie* **2004,** 7, (2), 135-142.
16. Matahwa, H.; Ramiah, V.; Jarrett, W. L.; McLeary, J. B.; Sanderson, R. D., Microwave assisted graft copolymerization of N-isopropyl acrylamide and methyl

acrylate on cellulose: Solid state NMR analysis and CaCO 3 crystallization. *Macromolecular Symposia* **2007,** 255, 50-56.
17. Kalia S., K. B. S., Kur I., *Cellulose Fibers: Bio- and Nano-Polymer Composites*. Springer-Verlag: 2011.
18. Rong, M. Z.; Zhang, M. Q.; Liu, Y.; Yang, G. C.; Zeng, H. M., The effect of fiber treatment on the mechanical properties of unidirectional sisal-reinforced epoxy composites. *Composites Science and Technology* **2001,** 61, (10), 1437-1447.
19. Wertz J-L., B. O., Mercier J.P.. *Cellulose science and technology*. EPFL Press: 2010.
20. Gandini, A., The irruption of polymers from renewable resources on the scene of macromolecular science and technology. *Green Chemistry* **2011,** 13, (5), 1061-1083.
21. Hon, D. N. S., *Chemical modification of lignocellulosic materials*. Marcel Dekker: New York, 1996.
22. Nishiyama, Y.; Johnson, G. P.; French, A. D.; Forsyth, V. T.; Langan, P., Neutron crystallography, molecular dynamics, and quantum mechanics studies of the nature of hydrogen bonding in cellulose Iβ. *Biomacromolecules* **2008,** 9, (11), 3133-3140.
23. Nishiyama, Y.; Langan, P.; Chanzy, H., Crystal structure and hydrogen-bonding system in cellulose Iβ from synchrotron X-ray and neutron fiber diffraction. *Journal of the American Chemical Society* **2002,** 124, (31), 9074-9082.
24. Nishiyama, Y.; Sugiyama, J.; Chanzy, H.; Langan, P., Crystal Structure and Hydrogen Bonding System in Cellulose Iα from Synchrotron X-ray and Neutron Fiber Diffraction. *Journal of the American Chemical Society* **2003,** 125, (47), 14300-14306.
25. Nevell T.P., Z. S. H., *Cellulose Chemistry and its applications*. Ellis Horwood Ltd, Chichester: 1985.
26. O'Sullivan, A. C., Cellulose: The structure slowly unravels. *Cellulose* **1997,** 4, (3), 173-207.
27. Atalla, R. H.; VanderHart, D. L., Native cellulose: A composite of two distinct crystalline forms. *Science* **1984,** 223, (4633), 283-285.
28. VanderHart, D. L.; Atalla, R. H., Studies of microstructure in native celluloses using solid-state 13C NMR. *Macromolecules* **1984,** 17, (8), 1465-1472.
29. Adler, E., Lignin Chemistry-Past, Present and Future. *Wood Sci. Technol.* **1977,** 11, 169-218.
30. Fengel, D.; Wegener, G., *Wood - Chemistry, Ultrastructure, Reactions*. Walter de Gruyter: Berlin, New York, 1989; p 613.
31. Mussatto, S. I.; Teixeira, J. A., Lignocellulose as raw material in fermentation processes. In *Current Research, Technology and Education Topics in Applied Microbiology and Microbial Biotechnology*, Méndes-Vilas, A., Ed. Formatex Research Center: 2010.
32. Xu, F., Structure, Ultrastructure, and Chemical Composition. In *Cereal straw as a resource for sustainable biomaterials and biofuels : chemistry, extractives, lignins, hemicelluloses and cellulose*, Sun, R. C., Ed. Elsevier B.V.: Amsterdam, 2010.
33. Jones, L. H. P., Mineral components of plant cell walls. *American Journal of Clinical Nutrition* **1978,** 31, (10 ,SUPPL.), S94-S98.
34. Sun, R. C.; Tomkinson, T., Essential guides for isolation/purification of polysaccharides. In *Encyclopedia of Separation Science*, Wilson, I. D.; Adlard, T. R.; Poole, C. F.; Cook, M., Eds. Academic Press: Lond, 2000.
35. Theander, O., Review of straw carbohydrate research. In *New Approaches to Research on Cereal Carbohydrates*, Hill, R. D.; Munck, L., Eds. Elsevier Science Publishers B. V.: Amsterdam, 1985.
36. Adapa, P.; Schonenau, L.; Canam, T.; Dumonceaux, T., Quantitative Analysis of Lignocellulosic Components of Non-Treated and Steam Exploded Barley, Canola, Oat

and Wheat Straw using Fourier Transform Infrared Spectroscopy. *Journal of Agricultural Science and Technology* **2011,** 1, 177-188.
37. Alberts B., J. A., Lewis J., Raff M., Roberts K. and Walter P., *Molecular Biology of the Cell*. 4th Edition ed.; Garland Publishing: New York, 2002.
38. Barnett, J. R.; Bonham, V. A., Cellulose microfibril angle in the cell wall of wood fibres. *Biological Reviews of the Cambridge Philosophical Society* **2004,** 79, (2), 461-472.
39. Moon, R. J.; Martini, A.; Nairn, J.; Simonsen, J.; Youngblood, J., Cellulose nanomaterials review: Structure, properties and nanocomposites. *Chemical Society Reviews* **2011,** 40, (7), 3941-3994.
40. Elazzouzi-Hafraoui, S.; Nishiyama, Y.; Putaux, J. L.; Heux, L.; Dubreuil, F.; Rochas, C., The shape and size distribution of crystalline nanoparticles prepared by acid hydrolysis of native cellulose. *Biomacromolecules* **2008,** 9, (1), 57-65.
41. Dong, X. M.; Revol, J. F.; Gray, D. G., Effect of microcrystallite preparation conditions on the formation of colloid crystals of cellulose. *Cellulose* **1998,** 5, (1), 19-32.
42. Zimmermann T.; Bordeanu N.; Strub E., Properties of nanofibrillated cellulose from different raw materials and its reinforcement potential. *Carbohydrate Polymers* **2010,** 79.
43. Dufresne, A.; CavaiÌlé, J. Y.; Vignon, M. R., Mechanical behavior of sheets prepared from sugar beet cellulose microfibrils. *Journal of Applied Polymer Science* **1997,** 64, (6), 1185-1194.
44. Iwamoto, S.; Nakagaito, A. N.; Yano, H., Nano-fibrillation of pulp fibers for the processing of transparent nanocomposites. *Applied Physics A* **2007,** 89.
45. Alemdar, A.; Sain, M., Isolation and characterization of nanofibers from agricultural residues – Wheat straw and soy hulls. *Bioresource Technology* **2008,** 99, (6), 1664-1671.
46. Turbak, A. F.; Snyder, F. W.; Sandberg, K. R., Microfibrillated Cellulose, A New Cellulose Product: Properties, Uses and Commercial Potential. *J. Appl. Polym. Sci. : Appl. Polym. Symp.* **1983,** 37, 815-827.
47. Zimmermann, T.; Pöhler, E.; Geiger, T., Cellulose Fibrils for Polymer Reinforcement. *Advanced Engineering Materials* **2004,** 6.
48. Gardner, D. J.; Oporto, G. S.; Mills, R.; Samir, M. A. S. A., Adhesion and surface issues in cellulose and nanocellulose. *Journal of Adhesion Science and Technology* **2008,** 22, (5-6), 545-567.
49. Saito, T.; Kimura, S.; Nishiyama, Y.; Isogai, A., Cellulose nanofibers prepared by TEMPO-mediated oxidation of native cellulose. *Biomacromolecules* **2007,** 8, (8), 2485-2491.
50. Fukuzumi, H.; Saito, T.; Iwata, T.; Kumamoto, Y.; Isogai, A., Transparent and high gas barrier films of cellulose nanofibers prepared by TEMPO-mediated oxidation. *Biomacromolecules* **2009,** 10, (1), 162-165.
51. Montanari, S.; Roumani, M.; Heux, L.; Vignon, M. R., Topochemistry of carboxylated cellulose nanocrystals resulting from TEMPO-mediated oxidation. *Macromolecules* **2005,** 38, (5), 1665-1671.
52. Lasseuguette, E.; Roux, D.; Nishiyama, Y., Rheological properties of microfibrillar suspension of TEMPO-oxidized pulp. *Cellulose* **2008,** 15, (3), 425-433.
53. Saito, T.; Hirota, M.; Tamura, N.; Kimura, S.; Fukuzumi, H.; Heux, L.; Isogai, A., Individualization of nano-sized plant cellulose fibrils by direct surface carboxylation using TEMPO catalyst under neutral conditions. *Biomacromolecules* **2009,** 10, (7), 1992-1996.

54. Aulin, C.; Varga, I.; Claesson, P. M.; Wagberg, L.; Lindstrom, T., Buildup of Polyelectrolyte Multilayers of Polyethyleneimine and Microfibrillated Cellulose Studied by in Situ Dual-Polarization Interferometry and Quartz Crystal Microbalance with Dissipation. *Langmuir* **2008,** 24, (6), 2509-2518.
55. Wagberg, L.; Decher, G.; Norgren, M.; Lindstrom, T.; Ankerfors, M.; Axnas, K., The Build-Up of Polyelectrolyte Multilayers of Microfibrillated Cellulose and Cationic Polyelectrolytes. *Langmuir* **2008,** 24, (3), 784-795.
56. Eyholzer, C.; Bordeanu, N.; Lopez-Suevos, F.; Rentsch, D.; Zimmermann, T.; Oksman, K., Preparation and characterization of water-redispersible nanofibrillated cellulose in powder form. *Cellulose* **2010,** 17, (1), 19-30.
57. Liimatainen, H.; Visanko, M.; Sirviö, J.; Hormi, O.; Niinimäki, J., Sulfonated cellulose nanofibrils obtained from wood pulp through regioselective oxidative bisulfite pre-treatment. *Cellulose* **2013,** 20, (2), 741-749.
58. Paakko, M.; Ankerfors, M.; Kosonen, H.; Nykanen, A.; Ahola, S.; Osterberg, M.; Ruokolainen, J.; Laine, J.; Larsson, P. T.; Ikkala, O.; Lindstrom, T., Enzymatic hydrolysis combined with mechanical shearing and high-pressure homogenization for nanoscale cellulose fibrils and strong gels. *Biomacromolecules* **2007,** 8, (6), 1934-1941.
59. Henriksson, M.; Berglund, L. A., Structure and properties of cellulose nanocomposite films containing melamine formaldehyde. *J. Appl. Polym. Sci.* **2007,** 106, (4), 2817-2824.
60. Janardhnan, S.; Sain, M., Isolation of cellulose microfibrils - an enzymatic approach. *BioRes.* **2006,** 1, (2), 176-188.
61. Eichhorn, S. J.; Baillie, C. A.; Zafeiropoulos, N.; Mwaikambo, L. Y.; Ansell, M. P.; Dufresne, A.; Entwistle, K. M.; Herrera-Franco, P. J.; Escamilla, G. C.; Groom, L.; Hughes, M.; Hill, C.; Rials, T. G.; Wild, P. M., Review: Current international research into cellulosic fibres and composites. *J. Mater. Sci.* **2001,** 36, (9), 2107-2131.
62. Bledzki, A. K.; Gassan, J., Composites reinforced with cellulose based fibres. *Prog. in Polym. Sci.* **1999,** 24, (2), 221-274.
63. Tanaka, F.; Iwata, T., Estimation of the elastic modulus of cellulose crystal by molecular mechanics simulation. *Cellulose* **2006,** 13, (5), 509-517.
64. Iwamoto, S.; Nakagaito, A. N.; Yano, H.; Nogi, M., Optically transparent composites reinforced with plant fiber-based nanofibers. *Applied Physics A* **2005,** 81.
65. Young, R. A., Comparison of the Properties of Chemical Cellulose Pulps. *Cellulose* **1994,** 1, (2), 107-130.
66. Hult, E. L.; Larsson, P. T.; Iversen, T., Cellulose fibril aggregation - an inherent property of kraft pulps. *Polymer* **2001,** 42, (8), 3309-3314.
67. Gibson L.J., A. M. F., *Cellular Solids: Structure and Properties*. 2 nd ed.; Cambridge Uni. Press: Cambridge, 1997.
68. Yano, H.; Sugiyama, J.; Nakagaito, A. N.; Nogi, M.; Matsuura, T.; Hikita, M.; Handa, K., Optically transparent composites reinforced with networks of bacterial nanofibers. *Adv. Mater.* **2005,** 17, (2), 153-155.
69. Ho, T. T. T.; Zimmermann, T.; Ohr, S.; Caseri, W., Composites of Cationic Nanofibrillated Cellulose and Layered Silicates: Water Vapor Barrier and Mechanical Properties. *ACS Applied Materials & Interfaces* **2012,** 4, (9), 4832-4840.
70. Syverud, K.; Stenius, P., Strength and barrier properties of MFC films. *Cellulose* **2009,** 16, (1), 75-85.
71. Zimmermann, T.; Pöhler, E.; Schwaller, P., Mechanical and Morphological Properties of Cellulose Fibril Reinforced Nanocomposites. *Advanced Engineering Materials* **2005,** 7.

72. Tingaut, P.; Zimmermann, T.; Lopez-Suevos, F., Synthesis and Characterization of Bionanocomposites with Tunable Properties from Poly(lactic acid) and Acetylated Microfibrillated Cellulose. *Biomacromolecules* **2010,** 11, (2), 454-464.
73. Iwatake, A.; Nogi, M.; Yano, H., Cellulose nanofiber-reinforced polylactic acid. *Compos. Sci. Technol.* **2008,** 68, (9), 2103-2106.
74. Suryanegara, L.; Nakagaito, A. N.; Yano, H., The effect of crystallization of PLA on the thermal and mechanical properties of microfibrillated cellulose-reinforced PLA composites. *Compos. Sci. Technol.* **2009,** 69, (7-8), 1187-1192.
75. Berglund, L. A.; Peijs, T., Cellulose biocomposites - From bulk moldings to nanostructured systems. *MRS Bulletin* **2010,** 35, (3), 201-207.
76. Frone, A. N.; Berlioz, S.; Chailan, J. F.; Panaitescu, D. M.; Donescu, D., Cellulose fiber-reinforced polylactic acid. *Polymer Composites* **2011,** 32, (6), 976-985.
77. Park, W. I.; Kang, M.; Kim, H. S.; Jin, H. J., Electrospinning of poly(ethylene oxide) with bacterial cellulose whiskers. *Macromolecular Symposia* **2007,** 249-250, 289-294.
78. Nakagaito, A. N.; Fujimura, A.; Sakai, T.; Hama, Y.; Yano, H., Production of microfibrillated cellulose (MFC)-reinforced polylactic acid (PLA) nanocomposites from sheets obtained by a papermaking-like process. *Compos. Sci. Technol.* **2009,** 69, (7-8), 1293-1297.
79. Nyström, G.; Mihranyan, A.; Razaq, A.; Lindström, T.; Nyholm, L.; Strømme, M., A nanocellulose polypyrrole composite based on microfibrillated cellulose from wood. *The Journal of Physical Chemistry B* **2010,** 114, (12), 4178-4182.
80. Nakagaito, A. N.; Yano, H., Novel high-strength biocomposites based on microfibrillated cellulose having nano-order-unit web-like network structure. *Appl. Phys. A: Mater.Sci. Process.* **2005,** 80, (1), 155-159.
81. Malainine, M. E.; Mahrouz, M.; Dufresne, A., Thermoplastic nanocomposites based on cellulose microfibrils from Opuntia ficus-indica parenchyma cell. *Compos. Sci. Technol.* **2005,** 65, (10), 1520-1526.
82. Özgür Seydibeyoğlu, M.; Oksman, K., Novel nanocomposites based on polyurethane and micro fibrillated cellulose. *Compos. Sci. Technol.* **2008,** 68, (3–4), 908-914.
83. Wang, B.; Sain, M., Dispersion of soybean stock-based nanofiber in a plastic matrix. *Polym Int* **2007,** 56, (4), 538-546.
84. Wang, B.; Sain, M., Isolation of nanofibers from soybean source and their reinforcing capability on synthetic polymers. *Composites Science and Technology* **2007,** 67, (11-12), 2521-2527.
85. Okubo, K.; Fujii, T.; Yamashita, N., Improvement of interfacial adhesion in bamboo polymer composite enhanced with micro-fibrillated cellulose. *JSME International Journal, Series A: Solid Mechanics and Material Engineering* **2006,** 48, (4), 199-204.
86. Chakraborty, A.; Sain, M.; Kortschot, M.; Cutler, S., Dispersion of Wood Microfibers in a Matrix of Thermoplastic Starch and StarchPolylactic Acid Blend. *Journal of Biobased Materials and Bioenergy* **2007,** 1, (1), 71-77.
87. Mathew, A. P.; Chakraborty, A.; Oksman, K.; Sain, M., The structure and mechanical properties of cellulose nanocomposites prepared by twin screw extrusion. In *Acs Sym Ser*, Amer Chemical Soc: Washington, 2006; Vol. 938, pp 114-131.
88. Larsson, K.; Berglund, L. A.; Ankerfors, M.; Lindström, T., Polylactide latex/nanofibrillated cellulose bionanocomposites of high nanofibrillated cellulose content and nanopaper network structure prepared by a papermaking route. *Journal of Applied Polymer Science* **2012,** 125, (3), 2460-2466.
89. Suryanegara, L.; Nakagaito, A. N.; Yano, H., The effect of crystallization of PLA on the thermal and mechanical properties of microfibrillated cellulose-reinforced PLA composites. *Composites Science and Technology* **2009,** 69.

90. Lu, J.; Drzal, L. T., Microfibrillated cellulose/cellulose acetate composites: Effect of surface treatment. *Journal of Polymer Science Part B: Polymer Physics* **2010,** 48, (2), 153-161.
91. Svagan, A. J.; Azizi Samir, M. A. S.; Berglund, L. A., Biomimetic polysaccharide nanocomposites of high cellulose content and high toughness. *Biomacromolecules* **2007,** 8, (8), 2556-2563.
92. Nakagaito, A. N.; Nogi, M.; Yano, H., Displays from transparent films of natural nanofibers. *MRS Bulletin* **2010,** 35, (03), 214-218.
93. Rampinelli, G.; Di Landro, L.; Fujii, T., Characterization of biomaterials based on microfibrillated cellulose with different modifications. *Journal of Reinforced Plastics and Composites* **2010,** 29, (12), 1793-1803.
94. Plackett, D.; Anturi, H.; Hedenqvist, M.; Ankerfors, M.; Gällstedt, M.; Lindström, T.; Siró, I., Physical properties and morphology of films prepared from microfibrillated cellulose and microfibrillated cellulose in combination with amylopectin. *Journal of Applied Polymer Science* **2010,** 117, (6), 3601-3609.
95. Svagan, A. J.; Hedenqvist, M. S.; Berglund, L., Reduced water vapour sorption in cellulose nanocomposites with starch matrix. *Compos. Sci. Technol.* **2009,** 69, (3-4), 500-506.
96. Dufresne, A.; Dupeyre, D.; Vignon, M. R., Cellulose microfibrils from potato tuber cells: Processing and characterization of starch-cellulose microfibril composites. *J. Appl. Polym. Sci.* **2000,** 76, (14), 2080-2092.
97. Avella, M.; Cocca, M.; Errico, M. E.; Gentile, G., Polyvinyl alcohol biodegradable foams containing cellulose fibres. *J Cell Plast* **2012,** 48, (5), 459-470.
98. Liu, A.; Walther, A.; Ikkala, O.; Belova, L.; Berglund, L. A., Clay Nanopaper with Tough Cellulose Nanofiber Matrix for Fire Retardancy and Gas Barrier Functions. *Biomacromolecules* **2011,** 12, (3), 633-641.
99. Spence, K. L.; Venditti, R. A.; Rojas, O. J.; Pawlak, J. J.; Hubbe, M. A., Water vapor barrier properties of coated and filled microfibrillated cellulose composite films. *BioResources* **2011,** 6, (4), 4370-4388.
100. Hüsing, N.; Schubert, U., Aerogels—Airy Materials: Chemistry, Structure, and Properties. *Angewandte Chemie International Edition* **1998,** 37, (1-2), 22-45.
101. Kistler, S. S., Coherent expanded aerogels and jellies. *Nature* **1931,** 127, (3211), 741.
102. Pierre, A. C.; Pajonk, G. M., Chemistry of Aerogels and Their Applications. *Chem. Rev.* **2002,** 102, (11), 4243-4266.
103. Gesser, H. D.; Goswami, P. C., Aerogels and related porous materials. *Chem. Rev.* **1989,** 89, (4), 765-788.
104. Sehaqui, H.; Zhou, Q.; Berglund, L. A., High-porosity aerogels of high specific surface area prepared from nanofibrillated cellulose (NFC). *Compos. Sci. Technol.* **2011,** 71, (13), 1593-1599.
105. Ali, Z. M.; Gibson, L. J., The structure and mechanics of nanofibrillar cellulose foams. *Soft Matter* **2013,** 9, (5), 1580-1588.
106. Sehaqui, H.; Salajková, M.; Zhou, Q.; Berglund, L. A., Mechanical performance tailoring of tough ultra-high porosity foams prepared from cellulose i nanofiber suspensions. *Soft Matter* **2010,** 6, (8), 1824-1832.
107. Gebald, C.; Wurzbacher, J. A.; Tingaut, P.; Zimmermann, T.; Steinfeld, A., Amine-based nanofibrillated cellulose as adsorbent for CO2 capture from air. *Environmental Science and Technology* **2011,** 45, (20), 9101-9108.
108. Jin, H.; Nishiyama, Y.; Wada, M.; Kuga, S., Nanofibrillar cellulose aerogels. *Colloids and Surfaces A: Physicochemical and Engineering Aspects* **2004,** 240, (1-3), 63-67.

109. Paakko, M.; Vapaavuori, J.; Silvennoinen, R.; Kosonen, H.; Ankerfors, M.; Lindstrom, T.; Berglund, L. A.; Ikkala, O., Long and entangled native cellulose I nanofibers allow flexible aerogels and hierarchically porous templates for functionalities. *Soft Matter* **2008,** 4, (12), 2492-2499.
110. Korhonen, J. T.; Hiekkataipale, P.; Malm, J.; Karppinen, M.; Ikkala, O.; Ras, R. H. A., Inorganic Hollow Nanotube Aerogels by Atomic Layer Deposition onto Native Nanocellulose Templates. *ACS Nano* **2011,** 5, (3), 1967-1974.
111. Sehaqui, H.; Salajkova, M.; Zhou, Q.; Berglund, L. A., Mechanical performance tailoring of tough ultra-high porosity foams prepared from cellulose I nanofiber suspensions. *Soft Matter* **2010,** 6, (8), 1824-1832.
112. Svagan, A. J.; Samir, M. A. S. A.; Berglund, L. A., Biomimetic foams of high mechanical performance based on nanostructured cell walls reinforced by native cellulose nanofibrils. *Advanced Materials* **2008,** 20, (7), 1263-1269.
113. Sehaqui, H.; Zhou, Q.; Ikkala, O.; Berglund, L. A., Strong and tough cellulose nanopaper with high specific surface area and porosity. *Biomacromolecules* **2011,** 12, (10), 3638-3644.
114. Kettunen, M.; Silvennoinen, R. J.; Houbenov, N.; Nykänen, A.; Ruokolainen, J.; Sainio, J.; Pore, V.; Kemell, M.; Ankerfors, M.; Lindström, T.; Ritala, M.; Ras, R. H. A.; Ikkala, O., Photoswitchable superabsorbency based on nanocellulose aerogels. *Adv. Funct. Mater.* **2011,** 21, (3), 510-517.
115. Olsson, R. T.; Azizi Samir, M. A. S.; Salazar-Alvarez, G.; Belova, L.; Ström, V.; Berglund, L. A.; Ikkala, O.; Nogués, J.; Gedde, U. W., Making flexible magnetic aerogels and stiff magnetic nanopaper using cellulose nanofibrils as templates. *Nature Nanotechnology* **2010,** 5, (8), 584-588.
116. Klemm, D.; Heublein, B.; Fink, H. P.; Bohn, A., Cellulose: Fascinating Biopolymer and Sustainable Raw Material. *Angewandte Chemie International Edition* **2005,** 44, (22), 3358-3393.
117. Fox, S.; Li, B.; Xu, D.; Edgar, K., Regioselective esterification and etherification of cellulose: a review. *Biomacromolecules* **2011,** 12, (6), 1956-1972.
118. Saito, T.; Uematsu, T.; Kimura, S.; Enomae, T.; Isogai, A., Self-aligned integration of native cellulose nanofibrils towards producing diverse bulk materials. *Soft Matter* **2011,** 7, (19), 8804-8809.
119. Melone, L.; Altomare, L.; Alfieri, I.; Lorenzi, A.; De Nardo, L.; Punta, C., Ceramic aerogels from TEMPO-oxidized cellulose nanofibre templates. Synthesis, characterization, and photocatalytic properties. *Journal of Photochemistry and Photobiology A: Chemistry*, (0).
120. Stenstad, P.; Andresen, M.; Tanem, B. S.; Stenius, P., Chemical surface modifications of microfibrillated cellulose. *Cellulose* **2008,** 15, (1), 35-45.
121. Okahisa, Y.; Yoshida, A.; Miyaguchi, S.; Yano, H., Optically transparent wood-cellulose nanocomposite as a base substrate for flexible organic light-emitting diode displays. *Composites Science and Technology* **2009,** 69, (11-12), 1958-1961.
122. Dlouhá, J.; Suryanegara, L.; Yano, H., The role of cellulose nanofibres in supercritical foaming of polylactic acid and their effect on the foam morphology. *Soft Matter* **2012,** 8, (33), 8704-8713.
123. Jonoobi, M.; Mathew, A.; Abdi, M.; Makinejad, M. D.; Oksman, K., A Comparison of Modified and Unmodified Cellulose Nanofiber Reinforced Polylactic Acid (PLA) Prepared by Twin Screw Extrusion. *Journal of Polymers and the Environment* **2012**, 1-7.

124. Nogi, M.; Abe, K.; Handa, K.; Nakatsubo, F.; Ifuku, S.; Yano, H., Property enhancement of optically transparent bionanofiber composites by acetylation. *Appl. Phys. Lett.* **2006,** 89, (23).
125. Ifuku, S.; Nogi, M.; Abe, K.; Handa, K.; Nakatsubo, F.; Yano, H., Surface Modification of Bacterial Cellulose Nanofibers for Property Enhancement of Optically Transparent Composites: Dependence on Acetyl-Group DS. *Biomacromolecules* **2007,** 8, (6), 1973-1978.
126. Rodionova, G.; Lenes, M.; Eriksen, Ø.; Gregersen, Ø., Surface chemical modification of microfibrillated cellulose: Improvement of barrier properties for packaging applications. *Cellulose* **2011,** 18, (1), 127-134.
127. Rodionova, G.; Hoff, B.; Lenes, M.; Eriksen, O.; Gregersen, O., Gas-phase esterification of microfibrillated cellulose (MFC) films. *Cellulose* **2013**, 1-8.
128. Eyholzer, C.; Lopez-Suevos, F.; Tingaut, P.; Zimmermann, T.; Oksman, K., Reinforcing effect of carboxymethylated nanofibrillated cellulose powder on hydroxypropyl cellulose. *Cellulose* **2010,** 17, (4), 793-802.
129. Aulin, C.; Gällstedt, M.; Lindström, T., Oxygen and oil barrier properties of microfibrillated cellulose films and coatings. *Cellulose* **2010,** 17, (3), 559-574.
130. Henriksson, M.; Berglund, L. A.; Isaksson, P.; Lindstrom, T.; Nishino, T., Cellulose nanopaper structures of high toughness. *Biomacromolecules* **2008,** 9, (6), 1579-1585.
131. Aulin C.; Netrval J.; Wågberg, L.; Lindström T., Aerogels from nanofibrillated cellulose with tunable oleophobicity. *Soft Matter* **2010,** 6.
132. Ho, T. T. T.; Zimmermann, T.; Hauert, R.; Caseri, W., Preparation and characterization of cationic nanofibrillated cellulose from etherification and high-shear disintegration processes. *Cellulose* **2011,** 18, (6), 1391-1406.
133. Pei, A.; Butchosa, N.; Berglund, L. A.; Zhou, Q., Surface quaternized cellulose nanofibrils with high water absorbency and adsorption capacity for anionic dyes. *Soft Matter* **2013,** 9, (6), 2047-2055.
134. Pahimanolis, N.; Hippi, U.; Johansson, L. S.; Saarinen, T.; Houbenov, N.; Ruokolainen, J.; Seppälä, J., Surface functionalization of nanofibrillated cellulose using click-chemistry approach in aqueous media. *Cellulose* **2011,** 18, (5), 1201-1212.
135. Siqueira, G.; Bras, J.; Dufresne, A., Cellulose Whiskers versus Microfibrils: Influence of the Nature of the Nanoparticle and its Surface Functionalization on the Thermal and Mechanical Properties of Nanocomposites. *Biomacromolecules* **2009,** 10, (2), 425-432.
136. Siqueira, G.; Bras, J.; Dufresne, A., New process of chemical grafting of cellulose nanoparticles with a long chain isocyanate. *Langmuir* **2010,** 26, (1), 402-411.
137. Missoum, K.; Bras, J.; Belgacem, M. N., Organization of aliphatic chains grafted on nanofibrillated cellulose and influence on final properties. *Cellulose* **2012,** 19, (6), 1957-1973.
138. Gousse, C.; Chanzy, H.; Cerrada, M. L.; Fleury, E., Surface silylation of cellulose microfibrils: preparation and rheological properties. *Polymer* **2004,** 45, (5), 1569-1575.
139. Ladouce, L.; Fleury, E.; Gousse, C.; Cantiani, R.; Chanzy, H.; Excoffier, G. Cellulose microfibrils with modified surface, preparation method and use therof. 2004.
140. Andresen, M.; Johansson, L. S.; Tanem, B. S.; Stenius, P., Properties and characterization of hydrophobized microfibrillated cellulose. *Cellulose* **2006,** 13, (6), 665-677.
141. Andresen, M.; Stenius, P., Water-in-oil emulsions stabilized by hydrophobized microfibrillated cellulose. *Journal of Dispersion Science and Technology* **2007,** 28, (6), 837-844.

142. Cervin, N. T.; Aulin, C.; Larsson, P. T.; Wågberg, L., Ultra porous nanocellulose aerogels as separation medium for mixtures of oil/water liquids. *Cellulose* **2011,** 19, (2), 1-10.
143. Jin, H.; Kettunen, M.; Laiho, A.; Pynnönen, H.; Paltakari, J.; Marmur, A.; Ikkala, O.; Ras, R. H. A., Superhydrophobic and superoleophobic nanocellulose aerogel membranes as bioinspired cargo carriers on water and oil. *Langmuir* **2011,** 27, (5), 1930-1934.
144. Korhonen, J. T.; Kettunen, M.; Ras, R. H.; Ikkala, O., Hydrophobic nanocellulose aerogels as floating, sustainable, reusable, and recyclable oil absorbents. *ACS Appl. Mater. Interfaces* **2011,** 3, (6), 1813-1816.
145. Qu, P.; Zhou, Y.; Zhang, X.; Yao, S.; Zhang, L., Surface modification of cellulose nanofibrils for poly(lactic acid) composite application. *Journal of Applied Polymer Science* **2012,** 125, (4), 3084-3091.
146. Andresen, M.; Stenstad, P.; Moretro, T.; Langsrud, S.; Syverud, K.; Johansson, L. S.; Stenius, P., Nonleaching antimicrobial films prepared from surface-modified microfibrillated cellulose. *Biomacromolecules* **2007,** 8, (7), 2149-2155.
147. Tingaut, P.; Hauert, R.; Zimmermann, T., Highly efficient and straightforward functionalization of cellulose films with thiol-ene click chemistry. *J. Mater. Chem.* **2011,** 21, (40), 16066-16076.
148. Lu, J.; Askeland, P.; Drzal, L. T., Surface modification of microfibrillated cellulose for epoxy composite applications. *Polymer* **2008,** 49, (5), 1285-1296.
149. Frone, A. N.; Berlioz, S.; Chailan, J. F.; Panaitescu, D. M., Morphology and thermal properties of PLA–cellulose nanofibers composites. *Carbohydrate Polymers* **2013,** 91, (1), 377-384.
150. Qua, E. H.; Hornsby, P. R.; Sharma, H. S. S.; Lyons, G., Preparation and characterisation of cellulose nanofibres. *Journal of Materials Science* **2011,** 46, (18), 6029-6045.
151. Kolb, H. C.; Finn, M. G.; Sharpless, K. B., Click chemistry: Diverse chemical function from a few good reactions. *Angew. Chem.-Int. Edit.* **2001,** 40, (11), 2004-2021.
152. Nielsen, L. J.; Eyley, S.; Thielemans, W.; Aylott, J. W., Dual fluorescent labelling of cellulose nanocrystals for pH sensing. *Chem. Commun.* **2010,** 46, (47), 8929-8931.
153. Lönnberg, H.; Fogelström, L.; Berglund, L.; Malmström, E.; Hult, A., Surface grafting of microfibrillated cellulose with poly(ε-caprolactone) - Synthesis and characterization. *European Polymer Journal* **2008,** 44, (9), 2991-2997.
154. Lönnberg, H.; Fogelström, L.; Zhou, Q.; Hult, A.; Berglund, L.; Malmström, E., Investigation of the graft length impact on the interfacial toughness in a cellulose/poly(ε-caprolactone) bilayer laminate. *Composites Science and Technology* **2011,** 71, (1), 9-12.
155. Abdelmouleh, M.; Boufi, S.; Belgacem, M. N.; Duarte, A. P.; Ben Salah, A.; Gandini, A., Modification of cellulosic fibres with functionalised silanes: development of surface properties. *International Journal of Adhesion and Adhesives* **2004,** 24.
156. Abdelmouleh, M.; Boufi, S.; ben Salah, A.; Belgacem, M.; Gandini, A., Interaction of silane coupling agents with cellulose. *Langmuir* **2002**.
157. Brochier Salon, M. C.; Abdelmouleh, M.; Boufi, S.; Belgacem, M.; Gandini, A., Silane adsorption onto cellulose fibers: hydrolysis and condensation reactions. *Journal of colloid and interface science* **2005,** 289, (1), 249-261.
158. Castellano, M.; Gandini, A.; Fabbri, P.; Belgacem, M. N., Modification of cellulose fibres with organosilanes: Under what conditions does coupling occur? *J. Colloid Interface Sci.* **2004,** 273, (2), 505-511.

159. Ly, B.; Thielemans, W.; Dufresne, A.; Chaussy, D.; Belgacem, M. N., Surface functionalization of cellulose fibres and their incorporation in renewable polymeric matrices. *Compos. Sci. Technol.* **2008,** 68, (15-16), 3193-3201.
160. Brinker C. Jeffrey , S. G. W., *Sol-gel science: the physics and chemistry of sol-gel processing*. Academic Press, Inc.: 1990; p 141.
161. White, L. D.; Tripp, C. P., An infrared study of the amine-catalyzed reaction of methoxymethyasilanes with silica. *Journal of Colloid and Interface Science* **2000,** 227, (1), 237-243.
162. White, L. D.; Tripp, C. P., A low-frequency infrared study of the reaction of methoxymethylsilanes with silica. *Journal of Colloid and Interface Science* **2000,** 224, (2), 417-424.
163. White, L. D.; Tripp, C. P., Reaction of (3-aminopropyl)dimethylethoxysilane with amine catalysts on silica surfaces. *Journal of Colloid and Interface Science* **2000,** 232, (2), 400-407.
164. Osterholtz, F. D.; Pohl, E. R., Kinetics of the hydrolysis and condensation of organofunctional alkoxysilanes: a review. *Journal of Adhesion Science and Technology* **1992,** 6, (1), 127-149.
165. Pohl, E. R.; Osterholtz, F. D., *Kinetics and mechanism of aqueous hydrolysis and condensation of alkyltrialkoxysilanes*. Plenum New York: 1985; p 157-170.
166. Brand, M.; Frings, A.; Jenkner, P.; Lehnert, R.; Metternich, H. J.; Monkiewicz, J.; Schram, J., NMR-spectroscopic investigations on the hydrolysis of functional trialkoxysilanes. *Zeitung für Naturforschung* **1999,** 54b, (2), 155-164.
167. Beari, F.; Brand, M.; Jenkner, P.; Lehnert, R.; Metternich, H. J.; Monkiewicz, J.; Siesler, H. W., Organofunctional alkoxysilanes in dilute aqueous solution: new accounts on the dynamic structural mutability. *Journal of Organometallic Chemistry* **2001,** 625, (2), 208-216.
168. Brochier Salon, M. C.; Gerbaud, G.; Abdelmouleh, M.; Bruzzese, C.; Boufi, S.; Belgacem, M. N., Studies of interactions between silane coupling agents and cellulose fibers with liquid and solid-state NMR. *Magnetic Resonance in Chemistry* **2007,** 45, (6), 473-483.
169. Loy, D. A.; Baugher, B. M.; Baugher, C. R.; Schneider, D. A.; Rahimian, K., Substituent effects on the sol-gel chemistry of organotrialkoxysilanes. *Chem. Mat.* **2000,** 12, (12), 3624-3632.
170. Li, G.; Wang, L.; Ni, H.; Pittman Jr, C. U., Polyhedral oligomeric silsesquioxane (POSS) polymers and copolymers: A review. *Journal of Inorganic and Organometallic Polymers* **2001,** 11, (3), 123-154.
171. Torry, S. A.; Campbell, A.; Cunliffe, A. V.; Tod, D. A., Kinetic analysis of organosilane hydrolysis and condensation. *International Journal of Adhesion and Adhesives* **2006,** 26, (1-2), 40-49.
172. Brochier Salon, M. C.; Bayle, P. A.; Abdelmouleh, M.; Boufi, S.; Belgacem, M. N., Kinetics of hydrolysis and self condensation reactions of silanes by NMR spectroscopy. *Colloids and Surfaces A: Physicochemical and Engineering Aspects* **2008,** 312, (2-3), 83-91.
173. Smith, K. A., A study of the hydrolysis of methoxysilanes in a two-phase system. *Journal of Organic Chemistry* **1986,** 51, (20), 3827-3830.
174. Tan, B.; Rankin, S., Study of the effects of progressive changes in alkoxysilane structure on sol-gel reactivity. *The journal of physical chemistry. B* **2006,** 110, (45), 22353-22364.

175. Arkles, B.; Steinmetz, J. R.; Zazyczny, J.; Mehta, P., Factors contributing to the stability of alkoxysilanes in aqueous solution. *Journal of Adhesion Science and Technology* **1992,** 6, (1), 193-206.
176. Jitianu, A.; Britchi, A.; Badescu, V.; Deleanu, C.; Zaharescu, M., Influence of the alkoxy group of the Si-alkoxides on the sol-gel process and on the structure of the obtained gels. *Revue Roumaine de Chimie* **2007,** 52, (1-2), 93-99.
177. Pohl, E. R., Kinetics and Mechanisms of Acid and Base-Catalyzed Hydrolysis of Alkyltrialkoxysilanes in Aqueous Solution. In *Proc. 38th Annu. Tech. Conf., Reinforced Plastics/Composites Inst. Section 4-B*, 1983.
178. G., V. M.; Mileshkevich, V. P.; Yuzhelevskii, Y. A., *The Siloxane Bond*. Consultants Bureau: New York and London, 1978.
179. Smith, K. A., Polycondensation of methyltrimethoxysilane. *Macromolecules* **1987,** 20.
180. Ly, B.; Belgacem, M. N.; Bras, J.; Brochier Salon, M. C., Grafting of cellulose by fluorine-bearing silane coupling agents. *Materials Science and Engineering: C* **2010,** 30, (3), 343-347.
181. Hassan, C. M.; Peppas, N. A., Structure and applications of poly(vinyl alcohol) hydrogels produced by conventional crosslinking or by freezing/thawing methods. In 2000; Vol. 153, pp 37-65.
182. Tsuboi, M., Infrared spectrum and crystal structure of cellulose. *J. Polym. Sci.* **1957,** 25, (109), 159-171.
183. Casserly, T. B.; Gleason, K. K., Chemical vapor deposition of organosilicon thin films from methylmethoxysilanes. *Plasma Process. Polym.* **2005,** 2, (9), 679-687.
184. Tingaut, P.; Weigenand, O.; Militz, H.; Jéso, B.; Sèbe, G., Functionalisation of wood by reaction with 3-isocyanatopropyltriethoxysilane: Grafting and hydrolysis of the triethoxysilane end groups. *Holzforschung* **2005,** 59, (4), 397-404.
185. Hook, R. J., A 29Si NMR study of the sol-gel polymerisation rates of substituted ethoxysilanes. *Journal of Non-Crystalline Solids* **1996,** 195, (1-2), 1-15.
186. Douskey, M. C.; Gebhard, M. S.; McCormick, A. V.; Lange, B. C.; Whitman, D. W.; Schure, M. R.; Beshah, K., Spectroscopic studies of a novel cyclic oligomer with pendant alkoxysilane groups. *Progress in Organic Coatings* **2002,** 45, (2-3), 145-157.
187. Heuzer, T., *The chemistry of cellulose*. John Wiley & Sons: New York, 1944; p 133-135.
188. Rånby, B. G., The Mercerisation of Cellulose. II. A Phase Transition Study with X-Ray Diffraction. *Acta Chemica Scandinavica* **1952,** 6, 116-127.
189. Sèbe, G.; Ham-Pichavant, F.; Ibarboure, E.; Koffi, A. L. C.; Tingaut, P., Supramolecular structure characterization of cellulose II nanowhiskers produced by acid hydrolysis of cellulose i substrates. *Biomacromolecules* **2012,** 13, (2), 570-578.
190. Bel-Hassen, R.; S., B.; Brochier Salon, M. C.; Abdelmouleh, M.; Belgacem, M. N., Adsorption of silane onto cellulose fibers. II. The effect of pH on silane hydrolysis, condensation, and adsorption behavior. *Journal of Applied Polymer Science* **2008,** 108.
191. Banik, G.; Brückle, I., Principles of water absorption and desorption in cellulosic materials. *Restaurator* **2010,** 31, (3-4), 164-177.
192. Corrêa, A.; de Morais Teixeira, E.; Pessan, L.; Mattoso, L., Cellulose nanofibers from curaua fibers. *Cellulose* **2010,** 17, (6), 1183-1192.
193. Yang, H.; Yan, R.; Chen, H.; Lee, D. H.; Zheng, C., Characteristics of hemicellulose, cellulose and lignin pyrolysis. *Fuel* **2007,** 86, (12–13), 1781-1788.
194. Morán, J. I.; Alvarez, V. A.; Cyras, V. P.; Vázquez, A., Extraction of cellulose and preparation of nanocellulose from sisal fibers. *Cellulose* **2008,** 15, (1), 149-159.

195. Quiévy, N.; Jacquet, N.; Sclavons, M.; Deroanne, C.; Paquot, M.; Devaux, J., Influence of homogenization and drying on the thermal stability of microfibrillated cellulose. *Polymer Degradation and Stability* **2010,** 95, (3), 306-314.
196. Rachini, A.; Le Troedec, M.; Peyratout, C.; Smith, A., Comparison of the thermal degradation of natural, alkali-treated and silane-treated hemp fibers under air and an inert atmosphere. *Journal of Applied Polymer Science* **2009,** 112, (1), 226-234.
197. Bhagat, S. D.; Oh, C. S.; Kim, Y. H.; Ahn, Y. S.; Yeo, J. G., Methyltrimethoxysilane based monolithic silica aerogels via ambient pressure drying. *Microporous and Mesoporous Materials* **2007,** 100, (1–3), 350-355.
198. Rao, A. V.; Kulkarni, M. M.; Amalnerkar, D. P.; Seth, T., Superhydrophobic silica aerogels based on methyltrimethoxysilane precursor. *Journal of Non-Crystalline Solids* **2003,** 330, (1–3), 187-195.
199. Ma, W. S.; Zhang, D. Q.; Duan, Y.; Wan, Z. R.; Wang, H.; Xu, Y. B., Preparation and characterization of polysilsesquioxane microspheres with different organofunctional groups. *Gongneng Cailiao/Journal of Functional Materials* **2012,** 43, (18), 2568-2572.
200. Lewicki, J. P.; Liggat, J. J.; Patel, M., The thermal degradation behaviour of polydimethylsiloxane/montmorillonite nanocomposites. *Polymer Degradation and Stability* **2009,** 94, (9), 1548-1557.
201. Plastics - Determination of dynamic mechanical properties - Part 2: Torsion-pendulum method In 1996-12; Vol. DIN EN ISO 6721-2.
202. Davis, W. M.; Macosko, C. W., A forced torsional oscillator for dynamic mechanical measurements. *Polymer Engineering & Science* **1977,** 17, (1), 32-37.
203. Boiko, A. V.; Kulik, V. M.; Seoudi, B. M.; Chun, H. H.; Lee, I., Measurement method of complex viscoelastic material properties. *International Journal of Solids and Structures* **2010,** 47, (3–4), 374-382.
204. Wolf, A. T.; Descamps, P. In *Determination of Poisson's ratio of silicone sealants from ultrasonic and tensile measurements*, 2002; 2002; pp 132-142.
205. Alexandru, M.; Cristea, M.; Cazacu, M.; Ioanid, A.; Simionescu, B. C., Composite materials based on polydimethylsiloxane and in situ generated silica by using the sol–gel technique. *Polymer Composites* **2009,** 30, (6), 751-759.
206. Herrera-Franco, P. J.; Valadez-González, A., A study of the mechanical properties of short natural-fiber reinforced composites. *Composites Part B: Engineering* **2005,** 36, (8), 597-608.
207. Alexandru, M.; Cazacu, M.; Nistor, A.; Musteata, V. E.; Stoica, I.; Grigoras, C.; Simionescu, B. C., Polydimethylsiloxane/silica/titania composites prepared by solvent-free sol–gel technique. *Journal of Sol-Gel Science and Technology* **2010,** 56, (3), 310-319.
208. Panou, A. I.; Papadokostaki, K. G.; Tarantili, P. A.; Sanopoulou, M., Effect of hydrophilic inclusions on PDMS crosslinking reaction and its interrelation with mechanical and water sorption properties of cured films. *European Polymer Journal* **2013,** 49, (7), 1803-1810.
209. Suryanegara, L.; Nakagaito, A. N.; Yano, H., Thermo-mechanical properties of microfibrillated cellulose-reinforced partially crystallized PLA composites. *Cellulose* **2010,** 17, (4), 771-778.
210. Tokoro, R.; Vu, D. M.; Okubo, K.; Tanaka, T.; Fujii, T.; Fujiura, T., How to improve mechanical properties of polylactic acid with bamboo fibers. *Journal of Materials Science* **2008,** 43, (2), 775-787.
211. Dufresne, A.; Vignon, M. R., Improvement of starch film performances using cellulose microfibrils. *Macromolecules* **1998,** 31, (8), 2693-2696.

212. Huda, M. S.; Drzal, L. T.; Misra, M.; Mohanty, A. K.; Williams, K.; Mielewski, D. F., A study on biocomposites from recycled newspaper fiber and poly(lactic acid). *Industrial and Engineering Chemistry Research* **2005,** 44, (15), 5593-5601.
213. Pandey, J. K.; Lee, C. S.; Ahn, S. H., Preparation and properties of bio-nanoreinforced composites from biodegradable polymer matrix and cellulose whiskers. *Journal of Applied Polymer Science* **2010,** 115, (4), 2493-2501.
214. Huda, M.; Drzal, L.; Mohanty, A.; Misra, M., Chopped glass and recycled newspaper as reinforcement fibers in injection molded poly(lactic acid) (PLA) composites: A comparative study. *Composites Science and Technology* **2006,** 66, (11-12), 1813-1824.
215. Ho, K. L. G.; Pometto, A. L.; Hinz, P. N., Effects of temperature and relative humidity on polylactic acid plastic degradation. *J. Environ. Polym. Degrad.* **1999,** 7, (2), 83-92.
216. Rao, A. V.; Bhagat, S. D.; Hirashima, H.; Pajonk, G. M., Synthesis of flexible silica aerogels using methyltrimethoxysilane (MTMS) precursor. *Journal of Colloid and Interface Science* **2006,** 300, (1), 279-285.
217. Kanamori, K.; Aizawa, M.; Nakanishi, K.; Hanada, T., New Transparent Methylsilsesquioxane Aerogels and Xerogels with Improved Mechanical Properties. *Adv. Mater.* **2007,** 19, (12), 1589-1593.
218. Xia, F.; Jiang, L., Bio-inspired, smart, multiscale interfacial materials. *Adv. Mater.* **2008,** 20, (15), 2842-2858.
219. Yamane, C.; Aoyagi, T.; Ago, M.; Sato, K.; Okajima, K.; Takahashi, T., Two different surface properties of regenerated cellulose due to structural anisotropy. *Polym. J.* **2006,** 38, (8), 819-826.
220. Lindman, B.; Karlström, G.; Stigsson, L., On the mechanism of dissolution of cellulose. *Journal of Molecular Liquids* **2010,** 156, (1), 76-81.
221. Rein, D. M.; Khalfin, R.; Cohen, Y., Cellulose as a novel amphiphilic coating for oil-in-water and water-in-oil dispersions. *Journal of Colloid and Interface Science* **2012,** 386, (1), 456-463.
222. Gui, X.; Wei, J.; Wang, K.; Cao, A.; Zhu, H.; Jia, Y.; Shu, Q.; Wu, D., Carbon nanotube sponges. *Advanced Materials* **2010,** 22, (5), 617-621.
223. Choi, S. J.; Kwon, T. H.; Im, H.; Moon, D. I.; Baek, D. J.; Seol, M. L.; Duarte, J. P.; Choi, Y. K., A polydimethylsiloxane (PDMS) sponge for the selective absorption of oil from water. *ACS Applied Materials and Interfaces* **2011,** 3, (12), 4552-4556.
224. Terinte, N.; Ibbett, R.; Schuster, K. C., Overview on native cellulose and microcrystalline cellulose I structure studied by X-ray diffraction (WAXD): Comparison between measurement techniques. *Lenzinger Berichte* **2011,** 89, 118-131.
225. Sichina, W. J., Measurement of Tg by DSC. In PerkinElmer, Application note.
226. Sehaqui, H.; Zhou, Q.; Berglund, L. A., Nanostructured biocomposites of high toughness - A wood cellulose nanofiber network in ductile hydroxyethylcellulose matrix. *Soft Matter* **2011,** 7, (16), 7342-7350.
227. Stahl, T.; Brunner, S.; Zimmermann, M.; Ghazi Wakili, K., Thermo-hygric properties of a newly developed aerogel based insulation rendering for both exterior and interior applications. *Energy and Buildings* **2012,** 44, (0), 114-117.

RESUMÉ :

Au cours de ce travail de thèse, la cellulose nanofibrillée (CNF) a été isolée à partir de fibres de paille d'avoine puis modifiée chimiquement par des alcoxysilanes en milieu aqueux. La CNF silylée a ensuite été utilisée pour élaborer de nouveaux matériaux composites et mousses biosourcés.

Le chapitre I présente quelques aspects généraux concernant les nanocelluloses, en particulier la NFC et ses applications dans le domaine des matériaux composites et des mousses.
Le chapitre II est consacré à la fonctionnalisation de la CNF par le méthyltriméthoxysilane - choisi comme alcoxysilane modèle - ainsi qu'à la caractérisation du matériau silylé. Plusieurs paramètres réactionnels (pH, temps de réaction, concentration initiale en silane) ont été étudiés et optimisés, à partir de deux protocoles expérimentaux distincts. Les modifications ont été caractérisées à l'échelle moléculaire par différentes techniques physico-chimiques. Les propriétés des nanofibrilles silylées, comme la morphologie, cristallinité, mouillabilité, hygrocopicité et stabilité thermique, ont ensuite été évaluées.
Dans le chapitre III, l'impact de la silylation sur les propriétés mécaniques et hygroscopiques de composites à matrice acide poly(lactique) ou matrice polydiméthylsiloxane chargés en NFC a été évalué.
Pour finir, l'impact de la silylation sur les propriétés de mousses élaborées à partir de NFC lyophilisées a été étudié dans le chapitre IV (porosité, propriétés en compression, conductivité thermique, mouillabilité, hygroscopicité et oléophilicité).

Mots-clé : Cellulose nanofibrillée, alcoxysilanes, composites, mousses.

ABSTRACT:

In this thesis, nanofibrillated cellulse (NFC) has been isolated from oat straw and chemically modified by alkoxysilanes in water medium. Silylated NFC has been subsequently used to elaborate novel biobased composite materials and foams

Chapter I presents some general aspects about nanocelluloses, in particular NFC and its use in composite materials and foams.
Chapter II is dedicated to the functionalization of NFC by methyltrimethoxysilane - chosen as a model silane - and to the comprehensive examination of the silylated material. Reaction conditions such as pH, reaction time and initial silane concentration have been particularly investigated and optimized using two distinct experimental protocols. The modifications have been characterized at the molecular level by various physicochemical techniques. The properties of the silylated nanofibrils i.e. the morphology, crystallinity, wettability, hygroscopicity and thermal stability, have been subsequently examined.
Chapter III investigates the impact of silylation on the mechanical and hygroscopic properties of NFC-reinforced composites prepared with two distinct polymeric matrices: poly(lactic acid) (PLA) and polydimethylsiloxane (PDMS).
Chapter IV examines the impact of silylation on the properties of NFC-foams prepared by freeze drying, in particular on the porosity, compressive properties, thermal conductivity, wettability, hygroscopicity and oleophilicity.

Keywords: Nanofibrillated cellulose, alkoxysilanes, composites, foams.